Master of Science Thesis

Comprehensive assessment of NEK5000 DNS capabilities

Turbulent Channel Flow and Conjugate Heat transfer

Pradyumna M. K. Prasad

21st December 2016

Faculty of Aerospace Engineering · Delft University of Technology

Comprehensive assessment of NEK5000 DNS capabilities

Turbulent Channel Flow and Conjugate Heat transfer

Master of Science Thesis

For obtaining the degree of Master of Science in Aerospace Engineering at Delft University of Technology

Pradyumna M. K. Prasad

21st December 2016

Faculty of Aerospace Engineering · Delft University of Technology

Delft University Of Technology
Department Of
Aerodynamics

The undersigned hereby certify that they have read and recommend to the Faculty of Aerospace Engineering for acceptance a thesis entitled **"Comprehensive assessment of NEK5000 DNS capabilities "** by **Pradyumna M. K. Prasad** in partial fulfillment of the requirements for the degree of **Master of Science**.

Dated: 21st December 2016

Thesis supervisors:

Dr.ir. M. Gerritsma

Dr.ir. A. Shams

Dr.ir. C. Lettieri

Dr. S. J. Hulshoff

Acknowledgements

This project, like any worthwhile endeavor, would not have been possible without the support and guidance of many people. I wish to take this opportunity to express my gratitude to them. First of all, I would like to thank Nuclear Research Group (NRG), Petten, for giving me an opportunity to work at the company and conduct this project. The advice, guidance and patience of my supervisors at the company, Ir. Ed Komen and Dr. Ir. Afaque Shams has been crucial to its succeas. I would also like to thank my supervisor at the university, Dr. Ir. Marc Gerritsma, for his valuable inputs and support. This page on acknowledgements however would be incomplete without thanking my parents, friends and family. Their emotional support in this time has been invaluable, and it wouldn't have been possible without them.

Delft, The Netherlands
21st December 2016

Pradyumna M. K. Prasad

Contents

List of Figures

List of Tables

Chapter 1

Introduction

Energy is the key to the future. It is the most vital aspect of civilization, needed to maintain and improve the quality of life for human beings. Indeed the demand for energy, throughout the world, and especially in the developing countries, is growing at a breakneck pace. It is estimated that by 2040, the demand for energy will have grown by 33% of its present value [6]. This, especially in the background of the eventual exhaustion of the fossil fuels makes the sustainable sources of energy extremely important. The energy production of the future has to be secure, economical and sustainable. This is where nuclear energy establishes itself as a critical source of energy.

Even today, nuclear energy is one of the chief sources of power in the world. In 2012, about 10.9% of the world's total energy production was from Nuclear sources. As of today, there are 444 nuclear reactors throughout the world and more than 13 countries rely on nuclear energy supply for more than a quarter of their total energy needs [3]. There are around 73 nuclear reactors under construction currently and expected to operate by 2030 (29: China, 10: Russia, 6: India, 5: South Korea and 5: USA) and there are some 172 ordered or planned in the world. [5] With such stupendous growth predicted in the production of Nuclear Energy throughout the world, it is of tremendous importance to increase the safety margins in the design and maintenance of Nuclear Power Plants (NPPs).

NPPs can be schematically understood to be loops of pipes carrying fluids, using which the heat from a source (the nuclear reactor core) is transferred to the fluid and then to the final heat sink (where it can be converted to electrical energy). Essential to this heat transfer, is the thermal interaction between the involved fluids (coolants, working fluids etc.) and the various solid walls. The nature of the flow that drives these heat interactions is, almost as a rule, a turbulent flow. This makes the accurate analysis of these thermal phenomenon a very complex process, since turbulent flows are essentially chaotic in nature. However, on the other hand, these phenomenon cannot be totally ignored, as they have a profound impact on the structural life of the Nuclear Power Plants (NPPs).

These can be further elaborated. For the determination and extension of the NPP lifetime, the integrity assessment of the Reactor Pressure Vessel (RPV) is an important issue. The

importance of this, derives from the fact that the RPV represents the last barrier against the release of fission products into containment, and there are no feasible countermeasures to mitigate the effects of a catastrophic rupture of the RPV. One of the chief reasons that can compromise the integrity of the RPV is occurence of reactor transients such as Pressurized Thermal Shocks (PTS). Transients, also called Anticipated Operational Occurrences (AOOs), are events likely to occur one or more times during a reactors operating lifetime, and yet are events that are desired to be avoided [4]. A PTS consists of a rapid cooling of the RPV wall under pressurized conditions that may induce the criticality of existing or postulated defects inside the vessel wall. The most severe PTS event has been identified by Emergency Core Cooling (ECC) injection during a Loss-of-Coolant Accident (LOCA). The injected cold water mixes with hot water present in the cold leg, and flows towards the downcomer, causing further thermal mixing and, therefore, large temperature gradients. The core barrel and the reactor vessel wall form a cylindrical shell, which is referred to as the downcomer. This sudden change in temperature may induce high stresses in the RPV wall, leading to the propagation of flaws inside the vessel wall, especially in the embrittled region adjacent to the core. A proper knowledge of these loads is important for the RPV remnant lifetime assessment.

Traditional one-dimensional thermal-hydraulic system codes like RELAP-5 or CATHARE, often used in the nuclear industry, fail to reliably predict the complex three-dimensional thermal mixing phenomena in the downcomer occurring during the ECC injection [7]. Hence, CFD can bring real benefits in terms of more realistic and more predictive results. However, to gain confidence in the application of CFD modelling for PTS, a comprehensive validation programme is necessary. Experiments have been utilized to assess the performance of CFD codes for PTS in the past. For instance, a series of CFD simulations carried out by Rohde et. al. [20] were validated with the ROCOM experiments [16]. However, due to limitations of the data from the experiments, measurements are not always sufficient to describe all the involved phenomena. For example, the vessel of the ROCOM facility is made of acrylic glass and, therefore, no wall heat transfer data is obtained from ROCOM experiments. Another limitation of the experiments is that the spatial resolution of measurements in the wall-vicinity is limited and therefore not sufficient to produce accurate data on velocity and temperature fluctuations in that region. This data, however, is necessary to reliably obtain the wall heat flux etc. Therefore, in such scenarios, high fidelity Direct Numerical Simulations (DNS) can play an important role in the validation of the CFD results [7]. Due to the computing expenses of performing a full DNS simulation of a realistic PTS scenario, it is unfeasible in the near future. However, a DNS of a simplified PTS case can throw light on the many complex phenomenon involved in the transient and be utilized reliably in a validation program of modelled CFD analyses such as RANS, LES etc.

Towards this end, at NRG, an extensive research project is under execution to perform such a simplified PTS DNS. To accomplish this, the spectral element solver NEK5000 has been chosen, owing to its reliability and scalability. However before, the solver is utilized to conduct a full DNS of the PTS case, its capabilities need to be assessed and validated with relevant references, in order to ensure that the final results are reliable. The main goal of this thesis work is, therefore, to perform this assessment.

1.1 Research objectives

In order to evaluate the DNS results generated by NEK5000, a configuration with highly reliable reference data is needed. The incompressible turbulent channel, is one such domain where high precision data is available for validation. The wall bounded fully turbulent flow also involves viscous layers in the wall vicinity, which are ideal to evaluate the high accuracy predictions of DNS computations. However since the turbulent channel is a very simplistic domain, there is a need to be able predict the reliability of the solver to more practical cases, involving skewed meshes and elements. Moreover, in order to be able to extend the computation of the flow variables towards the end application, thermal parameters are calculated by simulating conjugate heat transfer for the turbulent channel. To accomplish all these tasks comprehensively, the following set of goals have been established for the research:

1. Assess the capabilities of NEK5000 to reliably perform DNS on a planar incompressible turbulent channel.
2. Assess the capability of NEK5000 to reliably perform DNS on distorted domains and mesh elements.
3. Assess the capabilities of NEK5000 to reliably perform conjugate heat transfer analysis on the turbulent channel flow configuration.

Chapter 2

Turbulence

Chaos from order, order in chaos.

Turbulence is the state of fluid motion which is characterised by random and chaotic three dimensional vorticity. Turbulent flow dominates all other flow phenomena by completely changing its nature and results in increase of energy dissipation, mixing, heat transfer etc. It is a fact that the most fluid flows are turbulent in nature, starting from circulation, respiratory system in the body to macro world of geophysical, atmospheric and planetary flows. Due to its primordial importance in nature, it has been widely studied over the centuries. However, like for most fundamental entities, there is no good definition, as such, for the phenomenon of turbulence. However it can be described by a few fundamental characteristics that turbulent flow possess. Some of these characteristics of turbulent flows are [1]

1. **Irregularity** Or as it is often termed, the *chaos* of turbulence. This describes the nature of the flow parameters, such as velocity, pressure, etc., that are seemingly indeterministic in such flows. thus a completely deterministic approach to turbulence is practically impossible, and statistical methods are employed.

2. **Diffusivity** The characteristic of turbulence that causes rapid mixing and increased rates of momentum, heat and mass transfer. It is termed as the single most important characteristic of turbulence [1]. Any flow that might seem random and yet is not dissipative, is not turbulent.

3. **Large Reynolds numbers** Turbulent flows always occur at large Reynolds numbers. Turbulence originates as a consequence of instabilities in laminar flow. These instabilities are fue to the interaction of the viscous terms and nonlinear inertia

terms in the equations of motion. Due to the nonlinearity and randomness of turbulence, it is extremely challenging to understand turbulence in its entirety. It has been one of the principal unsolved problems in Physics.

4. **Three-dimensional vorticity fluctuations** Turbulence is rotational and three dimensional. The random vorticity fluctuations that characterize turbulence need the vortex stretching mechanism, which can exist only in three dimensions. Thus turbulence would not sustain itself in two-dimensional flows. Random waves in the ocean, for instance, which are not rotational, would not qualify as turbulent flows themselves.

5. **Dissipation** Turbulent flows are always dissipative. Viscous shear stresses increase the internal energy of the fluid at the expense of the kinetic energy of turbulence. Thus turbulence flows need a continuous supply of energy for dissipation, else they decay.

6. **Sensitivity to initial conditions** The Navier-Stokes equations for most boundary conditions are ill-posed. This implies that the solution is extremely sensitive to initial conditions.

7. **Large range of time and length scales**

2.1 Statistical analysis of turbulent flows

A given turbulent parameter (Velocity) can be decomposed into two components, mean part and the fluctuating part, which enables analysis of these components separately with the available tools of statistics. This is shown in figure 2.1. This process is called Reynolds decomposition.

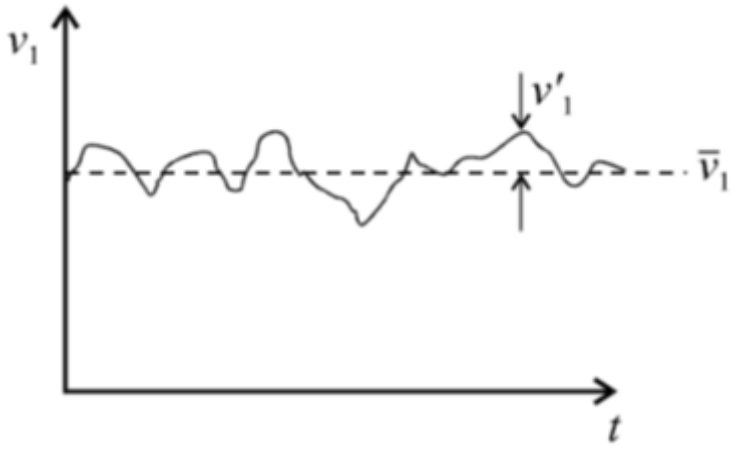

Figure 2.1: Reynolds decomposition

x = X + x'

where,

x denotes a complete turbulent parameter, eg: Velocity

X denotes the mean part

x' denotes the fluctuating part

Statistical analysis of turbulent flow is carried out using different tools like, ensemble average, different order of moments, Probability density function, Correlation function etc. These tools are shortly defined in the following paragraphs.

2.1.1 Ensemble average

The concept of an ensemble average is based upon the existence of independent statistical events. Suppose, consider a random variable, x. The nth realisation of x is x_n. Then, the ensemble average is calculated as

$$< x >= \lim_{N\to\infty} \frac{1}{N} \sum_{n=1}^{N} x_n \ . \tag{2.1}$$

From the above definition, it is understood that the true ensemble average is unobtainable since it needs infinite independent realisations. But the idea is very much useful and the arithmetic mean is calculated which will serve as ensemble average in limited sense.

2.1.2 Probability density function and moments

A complete description of a turbulent variable v, at given space and time is given by probability density function (PDF), P(v). P(v)dv is the probability of the variable v taking a value between v and v+dv, mathematically written as below

$$\int_{-\infty}^{\infty} P\left(v\right) dv = 1. \tag{2.2}$$

PDF is obtained by constructing a histogram of all ensemble values of v at fixed location at different times (repeating the same experiment time and time again). If an experiment is repeated many times, ensemble will be large and therefore histogram will be close to PDF.

The moments of the variable v is derived from the PDF as given below

$$< v^n >= \int_{-\infty}^{\infty} v^n P(v) dv.$$

The first moment $< v >$ is the mean:$< v >= \int_{-\infty}^{\infty} vP(v)dv$

The second moment is the variance of the variable v'

$$< v'^2 >= \int_{-\infty}^{\infty} (v - < v >)^2 P(v) dv.$$

Variance describes the level of variability of the mean

Skewness is the third moment of v' which is normalised by variance. It reveals the information about the asymmetry of the PDF. PDF which is symmetric about the mean has zero skewness. Positive skewness indicates that the PDF has a longer tail. Hence a positive skewness reveals that the variable v' is more likely to take positive values than negative values.

Skewness = $\frac{<v'^3>}{(<v'^2>)^{3/2}}$

Kurtosis is the fourth order moment normalised with the variance and denotes the flatness, ie. PDF with longer tails have a larger kurtosis than a PDF with narrower tails.

Kurtosis = $\frac{<v'^4>}{(<v'^2>)^2}$

2.1.3 Governing equations

Conservation of mass and momentum are the two physical principles behind the following equations for a fluid flow which is viscous in nature

$$\nabla . \overrightarrow{u} = 0. \tag{2.3}$$

$$\frac{\rho D \overrightarrow{u}}{Dt} = \mu \nabla^2 \overrightarrow{u} - \nabla p + \overrightarrow{F}. \tag{2.4}$$

Where, $\overrightarrow{u}$ being the flow velocity, $\frac{D\overrightarrow{u}}{Dt}$ being the material derivative, μ is the viscosity, ρ is the fluid density, p is the pressure and $\overrightarrow{F}$ is the external force per unit volume. The complete set of above equations is called as Navier-stokes equations. Equation (2.3) is obtained by the phenomenon of conservation of mass while the second one represents the conservation of momentum. The prime motive of solving the equation is to obtain the solution in terms of velocity field $\overrightarrow{u}$.

2.1.4 Kolmogorov's phenomenology of turbulence

Mean flow motion of the flow is characterised by the largest scale eddies which carry the maximum Kinetic energy (KE). Large scale eddies generates small scale eddies via non-linear mechanism, ie. transferring the energy to smaller scale in an inviscid fashion. The generated smaller eddies generates many more eddies smaller than them and this process continues till the energy of the smallest eddies is dissipated by viscosity. This energy cascade behaviour is propagated by the Russian Physicist, Kolmogorov in 1941 and till now is widely accepted by the turbulence practitioners. In precise, he assumed that at sufficiently large Reynolds number, the flow is locally homogeneous and isotropic and to be statistically in equilibrium in this range of high wave numbers. Thus, in this range of spectrum, turbulence is uniquely determined only by two parameters, ie, kinematic viscosity and dissipation rate. So, as explained before there exist an inertial range in between the high kinetic energy and purely dissipative stage which is depicted in the below figure.

It can be seen from the above plot of energy spectrum in logarithmic scales suggested by Kolmogorov is contained in the envelope constituted of three successive lines, namely,

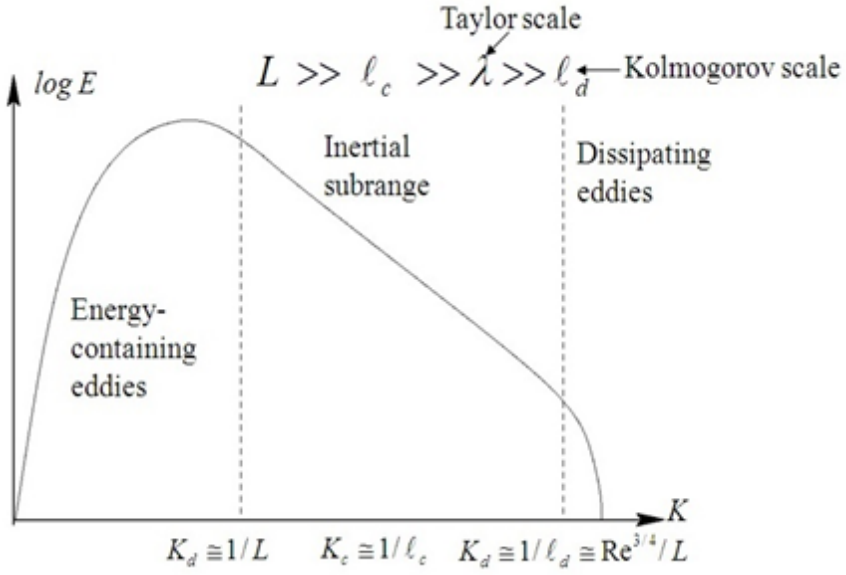

Figure 2.2: Energy spectrum

1. An horizontal line at the ordinate which denotes the maximum kinetic energy
2. Inertial range where the energy flux is constant and energy cascades as a power law with the exponent -5/3
3. A vertical line located at dissipative cut-off wave number (κ_D)

2.1.5 Turbulent scales

Turbulent flow is characterised by eddies which extends its length scale from large to small. Thus, one of the most important characteristic of turbulent flow is that it has wide range of scales. Smallest eddies are governed by two important parameters, kinematic viscosity ν and turbulent kinetic energy dissipation ε as a function of time. Length and time scales are given below.

$$\eta_k = (\nu^3/\varepsilon)^{1/4}. \tag{2.5}$$

$$\tau_k = (\nu/\varepsilon)^{1/2}. \tag{2.6}$$

Where, η_k and τ_k are referred to as Kolmogorov length and time scale of the smallest eddies.

2.1.6 Turbulent modelling and Kinetic energy

In the previous section, Navier-Stokes equations are introduced. The solution of N-S equations gives the evolution of the velocity field $\overrightarrow{u}$ as a function of space and time. But, there are no full analytical solutions to the N-S equations and hence modelling is required

to reduce it to the form, where the solutions could be sought of. In this context, different techniques like RANS, Hybrid RANS, LES are available.

RANS operates on the level that it is averaged (NS equations are averaged) and hence it provides the final solution which is not exact but acceptable from engineering point of view. In LES, filtering technique is used to eliminate the smaller eddies while only larger eddies are clearly seen. This technique is more useful in industrial research. Finally, DNS is the technique of solving the entire Navier-Stokes equations without filtering and hence will have the entire picture of the flow from the largest to smallest eddies. This is widely used among the research community who are looking at turbulent structures of all scales. But, both LES and DNS are very expensive methods and hence RANS is the most useful technique for engineering purpose.

RANS are time averaged equations of Navier-Stokes. These equations can be used with approximations based on the flow properties to give approximate time-averaged N-S equations. RANS equations are given below.

$$\frac{\partial}{\partial t}\left(\rho\overrightarrow{\overline{u}}\right) + \nabla.\left(\rho\overrightarrow{\overline{u}}\,\overrightarrow{\overline{u}}\right) = \nabla.(\overrightarrow{\overline{\tau}} - p\overrightarrow{\overline{I}}) + \rho\overrightarrow{g} - \nabla.(\rho\overrightarrow{\overline{u'}}\,\overrightarrow{\overline{u'}})$$

$\overrightarrow{I}$ being the identity matrix, $\overrightarrow{\tau}$ being the viscous stress tensor and the external force gravity $\overrightarrow{g}$

The term in the RHS, $\rho\overrightarrow{\overline{u'}}\,\overrightarrow{\overline{u'}}$ is the Reynolds stress tensor ($\overrightarrow{\tau}_{Re}$), similar to viscous stress tensor in its composition, but expresses the correlation among the velocity fluctuations. So, this is generally viewed as the component of the total stress tensor which accounts for turbulent fluctuations in momentum of the fluid. It is a 3×3 symmetric tensor with nine components as depicted below. It has six independent components, three normal stresses (diagonal terms) and three independent shear stress (off-diagonal terms).

$$\overrightarrow{\tau}_{Re} = \begin{bmatrix} \overline{u'2} & \overline{u'v'} & \overline{u'w'} \\ \overline{u'v'} & \overline{v'2} & \overline{v'w'} \\ \overline{u'w'} & \overline{v'w'} & \overline{w'2} \end{bmatrix}.$$

Equations for the components of Reynolds stress tensor are obtained by subtracting RANS with Navier-Stokes equations by decomposing the velocity into mean and fluctuating part. The resulting equations are averaged and manipulated to obtain the so called Reynolds stress transport equations. In order to denote the independent equations for all six terms of Reynolds stress tensor, Einstein's notation is used, ie. ($u_i,\ u_j,\ u_k$) means the three velocity (u, v, w), while ($x_i,\ x_j,\ x_k$) means the three spatial directions (x, y, z).

$$\begin{aligned}\frac{\partial}{\partial t}\left(\overline{u_i{}'u_j{}'}\right) + \overline{u_k}\frac{\partial}{\partial x_k}\left(\overline{u_i{}'u_j{}'}\right) =& \frac{1}{\rho}\left(\overline{u_j{}'\frac{\partial p'}{\partial x_i}} + \overline{u_i{}'\frac{\partial p'}{\partial x_j}}\right) - 2\nu\overline{\frac{\partial u_i{}'}{\partial x_k}\frac{\partial u_j{}'}{\partial x_k}} + \\ & \overline{\frac{\partial u_i{}'u_j{}'u_k{}'}{\partial x_k}} - \left(\overline{u_j{}'u_k{}'}\frac{\partial\overline{u_i{}'}}{\partial x_k} + \overline{u_i{}'u_k{}'}\frac{\partial\overline{u_j{}'}}{\partial x_k}\right) + \nu\nabla^2(\overline{u_i{}'u_j{}'})\end{aligned} \tag{2.7}$$

On a similar note, dynamic equation for turbulent Kinetic energy can be derived, which is given below

$$\frac{\partial k}{\partial t} + \overline{u_k}\frac{\partial k}{\partial x_k} = -\frac{1}{\rho}\overline{\frac{\partial u_i' p'}{\partial x_i}} - \nu\overline{\frac{\partial u_i'}{\partial x_k}\frac{\partial u_i'}{\partial x_k}} - \frac{1}{2}\frac{\partial u_i' u_i' u_k'}{\partial x_k} + \overline{u_i' u_k'}\frac{\partial \overline{u_i'}}{\partial x_k} + \nu\nabla^2 k/ \tag{2.8}$$

In the above equation, the first term in the LHS denotes the local rate of change of turbulent kinetic energy (KE), while the second one is a convection term representing the turbulent kinetic energy due to mean fluid motion. Referring to the terms in the RHS, the first term gives the pressure diffusion which is obtained by the correlation of pressure and velocity fluctuations. This term does not contribute to the production or destruction of Kinetic energy, rather involves itself in the redistribution of Kinetic energy. The second term of the RHS denotes the dissipation rate of kinetic energy. Technically, it denotes the rate at which it converts the Kinetic energy into thermal dissipation (heating) due to viscous process. It can be noted that the sign of this term is negative which implies that it is dissipating the energy.The third term is called as turbulent transport term, which represents the contribution of velocity fluctuations to the global kinetic energy transport. This is just an another term which just redistributes the Kinetic energy without producing or dissipating it. The fourth term describes the energy transfer rate from the mean flow. This is the term which represents the energy cascading from largest to smaller eddies. The last term denotes the molecular diffusion term which represents the diffusive transport of Kinetic energy due to molecular viscosity.

Chapter 3

Turbulent channel flow and Conjugate Heat Transfer: a review

3.1 Turbulent channel flow

As discussed earlier, in most of the Nuclear Reactor Safety (NRS) applications, it is important, not only to resolve the mean flow and the heat transfer characteristics, but also the flow and the temperature fluctuations [11]. To understand the behavior of these parameters, CFD codes (LES, URANS etc) are used. The validation of these codes requires the use of DNS data to serve as a reference. This generation of DNS data has been planned at NRG to be conducted on the spectral element code NEK5000. However, prior to the actual utilization of the code to produce the necessary results, a thorough assessment of the capabilities and the accuracy of the code is necessary. For the purposes of this assessment, which forms the main part of this thesis, the Turbulent Channel Flow domain (or similar sheared versions) has been chosen.

Turbulent channel flows have been widely studied since the early 1930s to investigate the mechanisms in a wall-bounded turbulent flow. The simplicity of the domain makes it very attractive to study and understand the flow, through the use of theoretical, experimental and numerical techniques, and yet can offer deep insights into the complex turbulent phenomenon, especially in the near-wall region. [15]

3.1.1 Domain geometry

The Turbulent Channel is a flow domain consisting of two infinitely large parallel plates which are at a finite distance of 2δ apart. However in practice this is represented by a finite flow channel sub-domain with a rectangular cross section. Periodic boundary conditions are applied in the streamwise (x-axis) and spanwise (z-axis) directions respectively (see figure 3.1. This essentially means that the last element faces in the x and z directions are connected to the first element faces, thereby creating a continuity in the flow. In

the wall-normal direction (y-axis), no-slip and no-penetration boundary conditions are applied on both the walls. Once the flow is fully developed, it is homogeneous in the streamwise and the spanwise directions.

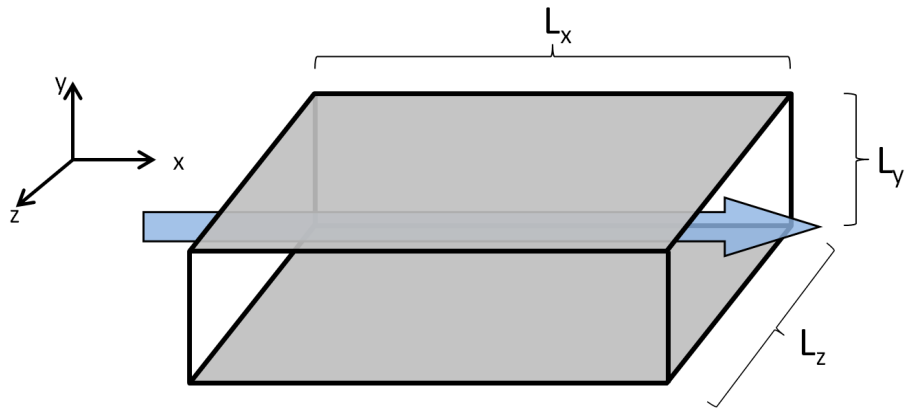

Figure 3.1: Turbulent channel flow configuration

The lengths L_x and L_z are chosen so as to ensure that the largest turbulent structures in the flow are encompassed within the dimensions of the channel. These lengths were initially designed using measurements of two-point correlations and the domains were then adjusted, if necessary, to ensure that the turbulence fluctuations are uncorrelated at a separation of at least one half-period in homogeneous directions. [15]

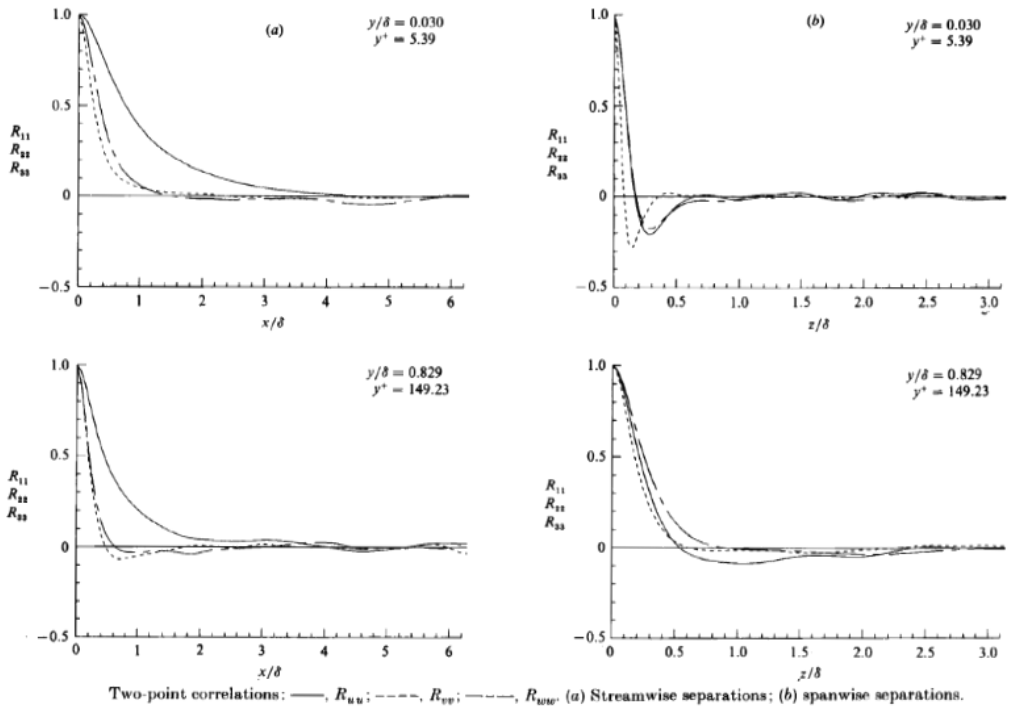

Figure 3.2: Two point correlations, adopted from [15]

To represent symbolically, the turbulent channel is a three-dimensional box represented in cartesian by:

$$x \in [0, L_x] \qquad y \in [-\delta, \delta] \qquad z \in [0, L_z]. \tag{3.1}$$

The boundary conditions can be defined by:

$$\begin{aligned} &\overrightarrow{V}(0, y, z) = \overrightarrow{V}(L_x, y, z), \\ &\overrightarrow{V}(x, -\delta, z) = \overrightarrow{V}(x, \delta, z) = \overrightarrow{0}, \\ &\overrightarrow{V}(x, y, 0) = \overrightarrow{V}(x, y, L_z). \end{aligned} \tag{3.2}$$

The flow in these channels is set up with suitable initial conditions that favors induction and growth of instabilities leading to turbulence. The flow is maintained at a constant mass flow rate, usually through the application of a pressure gradient in the domain. The developed turbulent channel flow is characterized by only one defining parameter, the turbulent Reynolds number Re_τ, which is defined as:

$$Re_\tau = \frac{u_\tau \delta}{\nu} \tag{3.3}$$

where, u_τ is the wall friction velocity. It is given by:

$$u_\tau = \sqrt{\frac{\tau_w}{\rho_f}} \tag{3.4}$$

here, $\tau_w \rightarrow$ wall shear stress, calculated as $(\partial u/\partial y)_{y=0}$
and, $\rho_f \rightarrow$ is the fluid density.

3.1.2 Early turbulent channel flow experiments

Before the advent of dependable DNS results for this set-up, the data available was through experiments. Some of the earliest known investigations of fully developed turbulent channel flow was by Nikuradse and Reichardt in the 1920s and 1930s. Both of these works were limited to the measurement of mean flows only (though the latter reported fluctuations). Laufer was the first to document detailed turbulent statistics, which he did at three Reynolds numbers (12300, 30800 and 61600) [15]. However Eckelmann (1974) [10] and Eckelmann (1970) for the first time conducted experiments in very low Reynolds numbers ($Re_b = 2800$, $Re_\tau = 142$). They used oil channel, leading to a thick viscous sublayer, facilitating near-wall measurements. Hot-film anemometer was used to take the measurements in this experiment. However inspite of the simplicity of the domain, and the significant amount of resources dedicated to this flow, poor agreement was reported amongst the results, even in the lower-order statistics. It is suspected that this is mainly due to the difficulty in measuring turbulence quantities near the wall, though the vast variety of Reynolds numbers used in the experiments would also have played a part.

3.1.3 Kim, Moin and Moser, 1987

The first Direct Numerical Simulation (DNS) on an incompressible turbulent channel flow was performed by Kim, Moin and Moser [15] (abbreviated from now as KMM), where they resolved all the essential scales of motion of the flow. They used a rectangular cross section domain with periodic boundary conditions in the streamwise and spanwise directions, and no-slip in the wall normal direction, as described above. The domain dimensions for this simulation were: $L_x = 4\pi\delta$, $L_y = 2\delta$ and $L_z = 2\pi\delta$. A uniformly distributed mesh in the streamwise and spanwise directions is adopted, with $\Delta x^+ = 11.8$ and $\Delta z^+ = 7.1$. However the distribution in the wall normal direction is non-uniform to account for better resolution of scales in the near-wall region. The $\Delta y^+ \approx 0.05$ at the first grid position from the wall, at the centerline it is $\Delta y^+ = 4.4$. There are 192, 129 and 160 elements in the streamwise, wall-normal and spanwise directions respectively, forming a grid with four million points.

It is to be noted that some of the dimensions used above (eg. Δx^+ and Δz^+ etc.) are non-dimensionalized. The expressions used for normalization of length, time and velocity quantities are given below:

$$L^+ = \frac{Lu_\tau}{\nu}. \tag{3.5}$$

$$V^+ = \frac{V}{u_\tau}. \tag{3.6}$$

$$t^+ = \frac{tu_\tau^2}{\nu}. \tag{3.7}$$

However for the wall-normal coordinate y^+, a slightly different normalization is used, which gives $y^+ = 0$ at the wall and $y^+ = Re_\tau$ at the centerline.

$$y^+ = \frac{(\delta - |y|)u_\tau}{\nu}. \tag{3.8}$$

These conventions will be adopted throughout the rest of this document, unless otherwise specified.

In the DNS simulation by KMM, a $Re_\tau = 180$ (at a $Re_b = 3000$, based on centerline velocity and channel half-width δ), is used to characterize the flow. Even though there can be a significant effect of the Reynolds number on the flow characteristics [22], a very low Re_τ is used. This is because a lower Reynolds number requires lesser number of grid points to resolve the essential scales, making it more affordable for simulation. No sub-grid scale modelling is used in this simulation, since it was learnt from previous simulations, and confirmed *a posteriori* that the grid resolution is sufficiently small enough to resolve all the essential turbulent scales, even though it is coarser than the Kolmogorov scales [15]. Spectral methods are used to solve the PDEs. Fourier series in the streamwise and spanwise directions and Chebyshev polynomial expansion in the normal direction are used for the spatial derivatives. Time advancement is carried out using Crank-Nicolson for the viscous terms and Adams-Bashforth for the nonlinear terms.

The statistics for the velocity and other variables must be collected only once the flow has reached a statistically stationary state. To identify this, KMM use a linear profile of the total shear stress, and also the quasi-periodic total kinetic energy in the entire domain. After the flow is statistically stationary, the integration over time of the turbulence statistics is conducted. KMM also perform spectral analysis and confirm that the results adhere to the 5/3 power law of Kolmogorov. Overall the results of the mean and the standard deviation (RMS of fluctuations) of the velocity show excellent agreement with the experimental results renormalized with corrected values of u_τ. A reasonable agreement with experiments is also obtained for the turbulence intensities and Reynolds shear stress. The discrepancies in the results with respect to experiments occur specially in the near-wall region, indicating sources of possible errors in the experimental data. The DNS data of this simulation is later on confirmed by many other numerical experiments.

3.1.4 Moser, Kim and Mansour, 1999

This is the most cited article in literature on turbulent channel flows. The database of results of this simulation is available publicly and widely used as a reference to validate work on turbulent channel flows and others. The work described in this thesis will also utilize Moser, Kim and Mansour (MKM) as one of the references for the assessment of the capabilities of NEK5000.

MKM performed a DNS pseudo-spectral simulation of the turbulent channel flow with a turbulent Reynolds number of 180 [19]. This simulation was a refinement of the study performed by KMM in 1987 [15] with a few key comparisons presented here:

- KMM and MKM both use a pseudo-spectral code with the spatial derivatives Fourier transformed in the streamwise and apanwise directions, and through the use of Chebyshev polynomials in the wall-normal direction.
- Crank-Nicholson scheme is used for the time-stepping of the viscous terms in both the simulations. On the other hand, while KMM uses Adam-Bashforth for the nonlinear terms, MKM uses third-order Runge-Kutta.
- The domains for the two simulations slightly differ. The domain in KMM has already been described. However MKM uses the same length $4\pi\delta$ in the streamwise direction, but a length of $4/3\pi\delta$ for the spanwise.
- The mesh is slightly coarser in the x-direction with a $\Delta x^+ = 17.7$ and a finer spanwise $\Delta z^+ = 5.9$. The distribution for the y-direction remains the same.
- The mesh consists of 2 million grid points with 128, 129 and 128 points in the x, y and z directions respectively.
- The original KMM simulations were carried out on only $Re_\tau = 180$, but in this expensive investigations on $Re_\tau = 590$ and $Re_\tau = 395$ have been carried out. This also gives an insight into the behavior of channel flows with significantly less influence of low Reynolds number effects.

3.1.5 del Alamo and Jimenez, 2003

In order to investigate the effect of large turbulent structures in the flow, del Alamo and Jimenez [9], performed simulations on a very large domain spanning $12\pi\delta$ in the streamwise direction and $2\pi\delta$ in the spanwise direction. The wall-normal direction and the numerical methods for computations were maintained the same as by MKM in [**?**]. The grid spacing in the x-direction was $\Delta x^+ = 8.9$ and in the z-direction $\Delta z^+ = 4.5$. The first grid point in the wall-normal direction has a spacing of $\Delta y^+_{wall} = 0.1$ and at the centerline, $\Delta y^+_{center} = 6.1$ The results of this investigation was intended for a spectral study of the structures at the very large scales. The Reynolds number Re_τ was maintained at 186.3 and the total grid consisted of 26 million grid points. This data obtained, at a later time was further investigated and statistically elaborated by Hoyas and Jimenez [13] This data is used in the present thesis work as a reference database to understand the influence of various factors in the flow characteristics.

3.1.6 Vreman and Kuerten, 2014

There have been a number of different DNS investigations of the incompressible turbulent channel with similar (but not the exact same) parameters for the simulations. The results of these investigations agreed with each other reasonably well, but the discrepancies necessitated research to understand and compare these results, in order to better understand the effect that various factors had on the turbulent statistics.

In 2014, Vreman and Kuerten [22], conducted four new simulations and compoared the results with the results of four different DNS databases with $Re_\tau \approx 180$. They investigated the role of the following factors as a source of disturbance in the computation of statistics: (1) statistical errors, (2) discretization errors, (3) programming errors, (4) non-uniqueness of a statistically stationary state, and (5) forcing method [22]. Vreman et. al. performed simulations through the use of two different codes: Finite difference (FD) and Spectral at a $Re_\tau = 180$. The FD method uses a fourth order discretization in the streamwise and spanwise directions, and second order in the y-direction. The spectral simulation uses the same numerical method as described by MKM [19]. The domain size was taken to be $L_x = 4\pi\delta$, $L_y = 2\delta$, $L_z = (4/3)\pi\delta$. Some of the other relevant parameters of the mesh are,

$\Delta x^+ = 5.9$ $\Delta y^+_{center} = 2.9$
$\Delta y^+_{wall} = 0.02$ $\Delta z^+ = 3.9$
Number of grid points = 14 million
Integration time, $t^+ = 36000$

In all the simulations discussed till now, the flow rate in the channel was maintained a constant using a forcing term in the equations, to ensure that the Re_τ is maintained a constant. However in this simulation, Vreman et. al. use a constant pressure gradient that fixes the Re_τ to a particular value. However, to account for the differences due to this, a simulation is also run in this work with a forcing term, and it is established that as long as the Re_τ is maintained a constant, significant differences cannot be observed due to this distinction alone.

It is clear from the grid size and resolution that it's very highly refined. Due to this and the very large integration time, the results of this simulation are expected to be most

accurate. Indeed, in the comparison with the other databases, it is seen that, although there is excellent agreement in the mean velocities among all the databases, MKM shows a certain oscillating behavior in the higher order profiles. This might be due to the insufficiency of averaging time. The spectral analysis conducted indicates that a more highly resolved grid needs to be utilized to resolve the lowest scales of turbulence and accurately represent the higher order statistics. However a coarser grid is still effective in predicting the lower order statistics.

3.2 Conjugate Heat Transfer

The turbulent transport mechanism is of great engineering and scientific importance. From the nuclear applications which have been mentioned in the first chapter of this document, to governing mechanisms in reentry systems, the study of heat transfer from a wall to a fluid is of fundamental importance. This phenomenon is strongly dependent on turbulent mechanisms especially in the near-wall region. The DNS of Conjugate Heat transfer, for the turbulent channel flow domain, is a basic coupled simulation of heat transfer, and serves as a powerful workbench in the investigation and understanding of the basic mechanisms in the heat transfer between the wall and the fluid.

The conjugate heat transfer simulation for a turbulent channel flow configuration, consists of a similar domain. There are two heated walls which are infinite in dimension (in the streamwise and spanwise directions) and are separated from each other by a distance of 2δ (see figure 3.3. They are of a finite thickness themselves, which is usually taken to be the half-channel height δ. In order to reduce this to a practical problem, this configuration is represented by a finite sub-domain of length L_x and L_z in the x (streamwise) and z(spanwise) directions, and periodic boundary conditions are applied for both the velocity and thermal fields. In the wall-normal direction, no-slip and no-penetration condition is applied for the fluid at the walls. For the temperature/ other transport scalars, the walls at the are isolated (no-flux) at the outer boundary. At the wall-fluid interface, the temperature and the heat flux are taken to be equal.

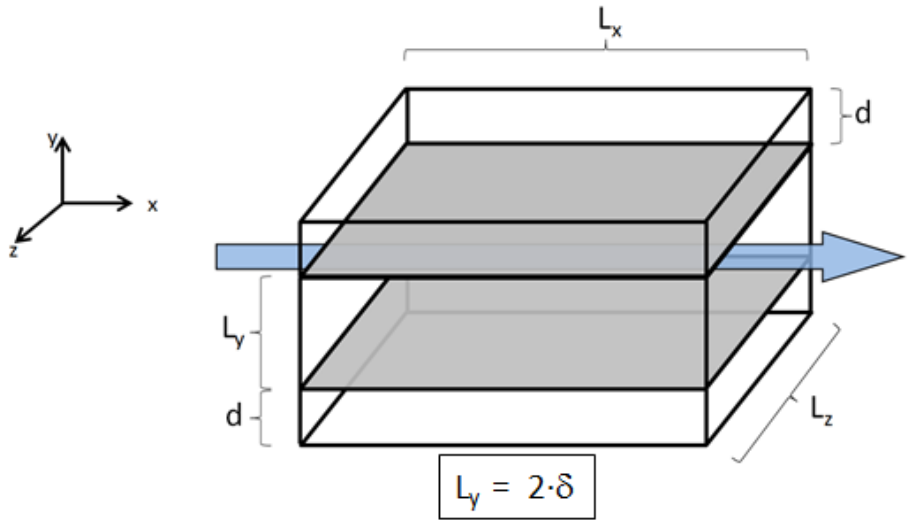

Figure 3.3: Conjugate Heat Transfer configuration

It is to be noted here, that the temperature and other transport scalars used here are *passive* scalars. This means that they do not affect the velocity or the pressure fields, and can be their governing equations can therefore be solved separately and is not coupled to the momentum equation. A separate equation for these temperature/passive scalars is used for the wall-solid and the fluid domains. Such an exercise reduces the computational effort, and also allows multiple such passive scalars to be simulated. Hence multiple temperature/ transport quantities can be computed in a given simulation.

Therefore symbolically:

$$\begin{aligned}\overrightarrow{V}(0,y,z) &= \overrightarrow{V}(L_x,y,z,)\\ \overrightarrow{V}(x,-\delta,z) &= \overrightarrow{V}(x,\delta,z) = \overrightarrow{0},\\ \overrightarrow{V}(x,y,0) &= \overrightarrow{V}(x,y,L_z).\end{aligned} \tag{3.9}$$

while for the temperature and other passive scalars, it is:

$$\begin{aligned}T(0,y,z) &= T(L_x,y,z),\\ T_f(x,\pm\delta,z) &= T_w(x,\pm\delta,z),\\ \lambda_f\left(\frac{\partial T_f}{\partial y}\right)_{(x,\pm\delta,z)} &= \lambda_w\left(\frac{\partial T_w}{\partial y}\right)_{(x,\pm\delta,z)},\\ \left(\frac{\partial T}{\partial y}\right)_{y=-\delta-d} &= \left(\frac{\partial T}{\partial y}\right)_{y=\delta+d} = 0\\ T(x,y,0) &= T(x,y,L_z).\end{aligned} \tag{3.10}$$

where,

$$x \in [0, L_x] \qquad y \in [-\delta - d, \delta + d] \qquad z \in [0, L_z]. \tag{3.11}$$

The governing equations for the velocity and the passive scalar are given below:

$$\nabla.\overrightarrow{V} = 0. \tag{3.12}$$

$$\frac{\partial \overrightarrow{V}}{\partial t} = -\overrightarrow{V}.\nabla(\overrightarrow{V}) + \nu\nabla^2\overrightarrow{V} - \frac{1}{\rho}\nabla p + \overrightarrow{F}. \tag{3.13}$$

$$\frac{\partial T}{\partial t} = -\overrightarrow{V}.\nabla T + \alpha_f\nabla^2 T + S_f\frac{u}{u_b}. \tag{3.14}$$

$$\frac{\partial T}{\partial t} = \alpha_s\nabla^2 T - S_s. \tag{3.15}$$

These are the Navier-stokes equations 3.12 and 3.13, and the energy equations re-written for the passive scalars in the fluid and the solid domains respectively (3.14 and 3.15). The heat transfer in these domains is driven because of a temperature difference between the fluid and the solid. The reason for this temperature difference is clearly seen in the thermal equations (3.14 and 3.15). There is a sink/source term in the fluid (S_f) and the solid(S_s). These terms are volumetric; it is dependent on the x-velocity in the fluid and constant in the solid. The terms are so set (S_f is scaled by u/u_b, where u/u_b is the bulk velocity) that the total enthalpy in the entire domain remains constant in time.

Since there is continuity between the solid and fluid domsins, the heat flux at the interface must be the same for both the domains, given by q_w. The source terms can be accordingly derived from this as

$$\begin{aligned} S_f &= \frac{q_w}{\delta \rho_f c_{p,f}}, \\ S_s &= \frac{q_w}{\delta \rho_s c_{p,s}}. \end{aligned} \tag{3.16}$$

The (wall) friction temperature (used for the subsequent non-dimensionalization) is defined by:

$$T_\tau = \frac{q_w}{u_\tau \rho_f c_{p,f}}. \tag{3.17}$$

Some solvers employ these above equations 3.12 to 3.15 in their non-dimensional form. Thus, for the sake of completeness, these equations will be specified here. These equations have been obtained by normalizing each of the terms using the parameters u_τ, T_τ and δ [18]:

$$\nabla^+ . \overrightarrow{V^+} = 0. \tag{3.18}$$

$$\frac{\partial \overrightarrow{V^+}}{\partial t^+} = -\overrightarrow{V^+} . \nabla^+ (\overrightarrow{V^+}) + \frac{1}{Re_\tau} \nabla^{+^2} \overrightarrow{V^+} - \nabla^+ p^+ + \overrightarrow{F^+}. \tag{3.19}$$

$$\frac{\partial T^+}{\partial t^+} = -\overrightarrow{V^+} . \nabla^+ T^+ + \frac{1}{Re_\tau Pr} \nabla^{+^2} T^+ + \frac{u^+}{u_b^+}. \tag{3.20}$$

$$\frac{\partial T^+}{\partial t^+} = \frac{1}{G Re_\tau Pr} \nabla^{+^2} T^+ - \frac{K}{d^+ \sqrt{G}}. \tag{3.21}$$

In the above equations,

$$K = \frac{\sqrt{\lambda_f \rho_f c_{p,f}}}{\sqrt{\lambda_s \rho_s c_{p,s}}},$$

the ratio of thermal effusivities of the fluid and the solid,

$$G = \frac{\alpha_f}{\alpha_s},$$

the ratio of thermal diffusivities of the fluid and the solid,

$$d^+ = \frac{d}{\delta}.$$

3.2.1 Tiselj and Cizelj, 2012

Although many previous DNS with heat transfer had simulated the behavior of thermal variables in the flow with an imposed isothermal (Dirichlet) or isoflux (Neumann) boundary conditions, Tiselj et. al. were the first to perform a conjugate heat transfer simulation in 2001 [14]. DNS of fully developed temperature and velocity fields in a turbulent channel were carried out, coupling unsteady conduction of heat in the solid with turbulent heat transfer in the fluid domain. These simulations were performed at a Re_τ of 150 and Prandtl numbers between 0.71 and 7. These simulations pointed to the inadequacies in the previous (isoheat and isoflux) simulations which underestimated the the values of the wall temperature fluctuations, and thus demonstrated the need for studying more realistically, the behavior of fluid-solid systems through the use of conjugate heat tranfer.

Tiselj et. al. in 2012 [21], studied the conjugate heat transfer in a turbulent channel flow domain with a Prandtl number of 0.01. They performed the computations at turbulent Reynolds numbers of 180, 395 and 590. The Navier-stokes equations for the fluid are resolved using the method utilized by KMM [15] in their work in 1987, and discussed in section 3.1.3. To restate, the spatial derivatives in the x and z directions are resolved using Fourier series and using the Chebychev polynomial expansion in the y-direction. For the heat conduction equations, a spectral method is used in the homogenous streamwise and spanwise directions, and a finite difference method in the wall-normal direction. For the time derivatives, a second order temporal scheme with Cranck-Nicolson scheme for the diffusive terms and the Adam-Bashfort scheme for the other terms is utilized, and a maximum CFL ≈ 0.1 is achieved. The computational domain is the one utilized by MKM [19] and has been discussed in section 3.1.4

Fifteen passive scalars are simulated for a single velocity field with a given Reynolds number. The averaging of the thermal fluctuations were started only after the thermal fluctuations in the wall reached a statistically steady state. The first temperature field is always a reference field with ideal isoflux boundary conditions. The other fourteen fields are computed for different values of the wall thickness and different values of the fluid-solid thermal activity ratios. For this present thesis work, the thermal diffusivity ratio, G = 1, and three thermal effusivity ratios, K = 1, 0.01 and 10 are relevant. The case of 0.01 nears isothermal conditions, while K = 10, approximates isoflux boundary conditions. It is worth mentioning here that the ratio of thermal effusivities is important in understanding the overall thermal characteristics of the flow-wall interaction, such as the distribution of the mean temperature, the temperature of the fluid-solid interface etc, while the thermal diffusivity ratio affects the damping of thermal fluctuations in the solid. A thick wall with a low thermal effusivity ratio (the solid thermal capacity dominates over the fluid), the thermal fluctuations inside the wall tend to zero, and this is therefore similar to the isotemperature case. On the other end of the spectrum, when the fluid thermal activity dominates over the solid, the fluctuations are almost freely transmitted into the solid, making the case an isoflux scenario (ideally isoflux at $K \to \infty$).

It is seen, in the analysis of the results, that even for the highest Reynolds number used in the simulation, the temperature profile in the fluid does not exhibit log-law region, and the near-wall RMS fluctuations show Reynolds number dependence. The simulations also indicate that in a liquid sodium-steel system, there is a relatively intensive penetration of turbulent temperature fluctuations into the heated wall.

3.2.2 Komen, Shams, Camilo and Koren, 2014

In 2013, Komen et. al. [11] have performed quasi-DNS simulations of the conjugate heat transfer for the turbulent channel case. They have employed a finite-volume approach on the open-source solver OpenFoam with structured hexahedral meshes and unstructured polyhedral meshes with an intent to evaluate the possibilities of carrying out DNS for more conventional and complex geometries. Since they use the finite volume method, and a coarse grid on the edge of the limit for DNS, lower accuracy can be expected for this simulation than a highly resolved DNS [11]. Therefore they term this simulation as a q-DNS, rather than a DNS.

This method of solution has been applied at two turbulent Reynolds number values of 180 and 395, for three passive scalar fields of K = 1, 0.01 and 10 at a Pr = 0.01. The hexahedral mesh consists of homogeneous grid spacing in the x and z-directions, with $\Delta x^+ = 6.0$ and $\Delta z^+ = 4.5$, and a linear stretching ratio of 1.05 is employed in the y-direction, resulting in a $\Delta y^+_{wall} = 0.8$ and $\Delta y^+_{centerline} = 4.5$. The mesh spacing in the solid domain is generated so that it is symmetric about the wall-fluid interface. The final grid consists of 3.8 million points. A second-order implicit backward differencing scheme is used for the temporal discretization with a maximum CFL of about 0.5. The results report a good agreement of the q-DNS results with other DNS databases for conjugate heat transfer in a turbulent channel flow.

Chapter 4

Spectral element methods

4.1 Spectral Element Codes

DNS computations require robust algorithms that have maximum efficiency. This in turn necessitates the need for highly accurate discretizations per degree of freedom [2]. Spectral element methods, which work like a combination of both spectral methods and finite element methods, when used for spatial discretization, have been shown to possess very favourable properties for high level discretization.

Spectral element methods essentially involve the incorporation of the spectral method on discrete finite elements. Both finite element and spectral methods work on the process of *approximating the solution* using a combination of prespecified basis functions. The solution to the governing equations can be expressed as

$$u_{approx} = \sum_{i=1}^{N} a_i \phi_i. \tag{4.1}$$

where u_{approx} is the approximation of the exact solution, expressed as an expansion of N basis functions ϕ_i having amplitudes a_i respectively. These N basis functions are usually selected from a family of functions that form an orthonormal basis. The amplitudes a_i are the **discrete unknowns** and the numerical approach involves calculating these amplitudes.
Spectral methods use global basis functions as the ϕ_i, which span the entire domain of the problem, where as in the finite element methods the basis functions are confined to one or more elements. Hence finite element methods use local basis functions. The numerical method employed consists of multiplying the governing partial differential equations with a *trial* or *weighting* function and then integrating over the domain, thereby reducing the order of the differential equation. The weak form of the equations is then solved, wherein the dependent variable is substituted by series of basis functions, analogous to the equation above and the resulting system of equations are solved to find the unknown amplitudes at all the grid points.

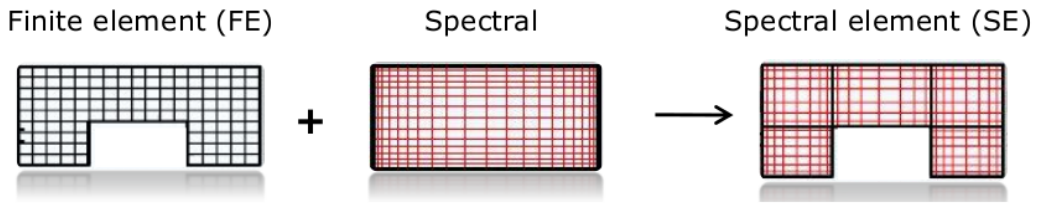

Figure 4.1: Spectral "finite" element methods

Since spectral methods use global polynomials (which are usually orthogonal), the obtained solutions are globally smooth. Another important characteristic of these methods is that they possess the property of exponential convergence. This implies that the truncation error decreases exponentially with the number of polynomials. The solutions obtained represent very high order of accuracy. The advantage of this that the number of grid points can be reduced , because a high order method requires less grid points for its discretization. Also, if certain types of polynomials such as Chebyshev, Legendre or if Fourier modes are used as the orthonormal basis functions, the efficiency of the method can be increased by incorporating Fast Fourier Transforms [17]. However, spectral methods although, prove to be excellent for simulating flows over simple geometries, with simple boundary conditions, they are not suitable for simulation over complex geometries. Nonperiodic boundary conditions especially pose a problem when using spectral methods.

In finite element methods (FEM), the domain is divided into finite elements, and local piecewise polynomials are used to approximate the solution, locally over one or more of these elements. The simplest of the local basis functions ϕ_i that can be chosen are piecewise linear functions.The generic ϕ_i is chosen to be 1 at the $i-th$ node and is zero everywhere else. The equations that model these finite elements are then assembled into a larger system of equations that models the entire problem. Thus the process results in a system of N equations (for N-1 elements) with N unknowns, which can be assembled into a global matrix and solved using an iterative procedure. Finite element methods can be employed on any kind of geometry and their accuracy depends upon element size, the approximation function and the number of elements used to represent the geometry. The order of accuracy of FEM, is however, margin lower than Spectral methods.

Spectral element methods (SEM) thus, reap the benefits of both - spectral and FEM numerical schemes, by using high order expansion basis functions locally on each element. Spectral methods usually use Legendre, Chebyshev or Lagrange polynomials because they are orthogonal functions and have high order of accuracy. SEM can be used on any kind of geometry as is typical of finite element methods and at the same time, has exponential convergence in space, which guarantees accurate discretization.

In NEK5000, the Lagrange polynomials are used as the local basis functions, computed on the N-th order Gauss-Lobatto-Legendre (GLL) point distribution inside each element. GLL grids are formed by the N+1 zeros of the corresponding orthogonal polynomials of order N, especially the first derivatives of Legendre polynomials. Such grids are used for the interpolation of the Lagrange polynomials. GLL point distribution ensures a stable and smooth quadrature (minimum negative quadrature) for the interpolation of

the Lagrange polynomials.

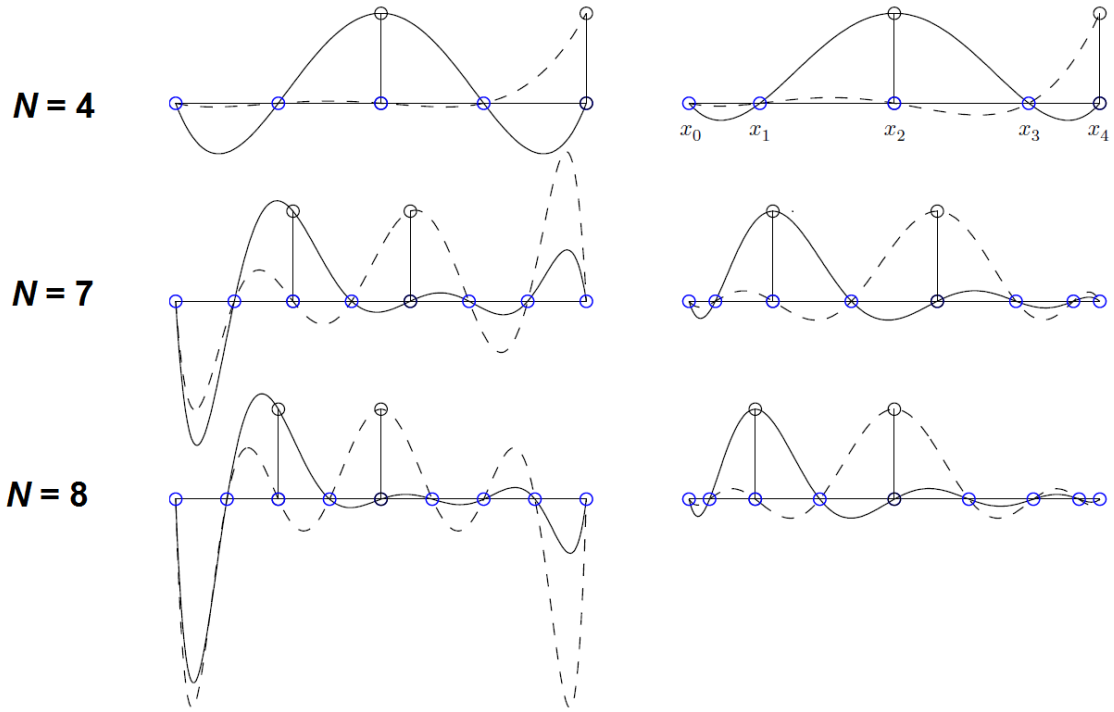

Figure 4.2: Lagrange polynomial basis functions for uniform distributions of points (left) and GLL distributions (right) [12]

Chapter 5

Assessment of NEK5000 DNS capabilities for turbulent channel flow

In the integrity assessment of RPVs in NPPs, due to the influence of PTS and other severe transients, use of CFD analyses in order to study the behavior of the thermal interaction between the fluid and the solid walls is of prime importance. Such CFD models require a DNS database to serve as a reference in order to gain confidence in the accuracy of the simulations. This has been discussed in more detail in chapter 1. To prepare such a DNS database for the case of a simplified PTS, the spectral element solver NEK5000 has been chosen at NRG. However, before utilizing NEK5000 to compute DNS on the PTS case, a thorough assessment of the capabilities of the solver is needed to gain confidence in the accuracy and reliability of the results. As a first step towards this, turbulent channel flow simulations have been carried out on NEK5000, and the results have been compared to the wealth of data already available for this configuration. The current chapter and those to follow, detail the intensive process that has been carried out towards this end.

5.1 Objective

The assessment of the flow field solution capabilities, especially in a turbulent channel flow, is the first step in its evaluation. Towards this, the use of a fully developed incompressible turbulent channel flow domain is highly convenient due to the large amount of literature already available for this configuration, which could serve as a reference. Therefore, the objective of the first part of the thesis research is to carry out a flow-field-only Direct Numerical Solution (DNS) of the incompressible turbulent channel using NEK5000, and the comparison of the obtained results with those available in literature to assess the agreement of the same.

5.2 Procedure of numerical experiment

The characteristics of the configuration for a turbulent channel flow were discussed in detail in chapter 3. However, for the sake of completeness, figure 3.1 has been reproduced here.

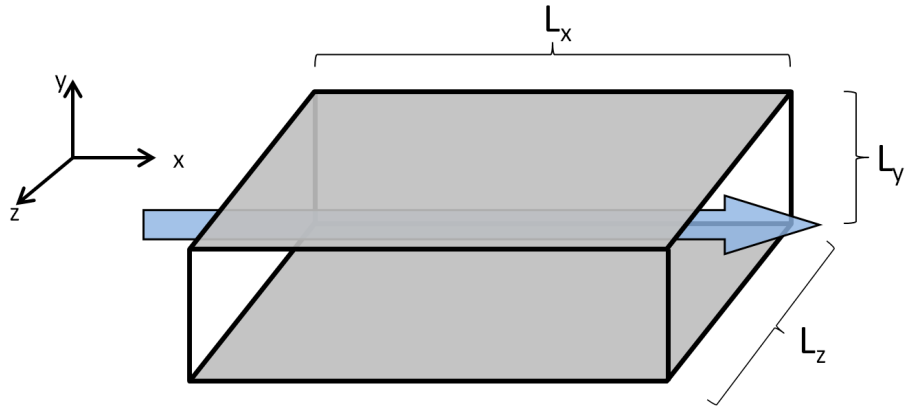

Figure 5.1: Turbulent channel flow configuration

To restate, the turbulent channel flow domain consists of two flat plates/walls. Periodic conditions are imposed in the streamwise (x) and spanwise (z) directions, with an intent to extrapolate the finite sub-domain into an infinite one, in these directions. The wall-normal direction consists of no-slip, no-penetration conditions at the walls. The procedure undertaken for the assessment of the capabilities of NEK5000 to simulate the turbulent channel flow will now be described.

5.2.1 Preliminary set-up

One of the most important parameters characterizing the turbulent channel flow is the turbulent Reynolds number (Re_τ). Since it was expected that multiple simulations of various kinds would have to be run to thoroughly analyze the capabilities of NEK5000, and keeping in mind that a smaller Re_τ would require smaller computational effort, a $Re_\tau = 180$ was chosen for the simulations. The Re_τ for a given flow is given by:

$$Re_\tau = \frac{u_\tau \delta}{\nu}. \tag{5.1}$$

where u_τ is $\sqrt{\tau_w/\rho}$, and δ is the channel half-width. From this, it may be noted that the value of Re_τ from this definition might only be computed *a posteriori*. Thus it is necessary to perform some iterations with the flow conditions in order to calibrate the Re_τ to 180. Dean's formula [8], given by:

$$Re_\tau = 0.175 \left(\frac{Re_b}{2} \right)^{\frac{7}{8}}. \tag{5.2}$$

presents a first estimate on how this Re_τ might be achieved through the use of the bulk Reynolds number. In the simulations carried out, the bulk velocity u_b is fixed to 1, the hydraulic diameter $D = 2\delta$, with δ taken as 1. Now to set the value of the Re_b in order to set the value of Re_τ from eqn. 5.2, an appropriate value of the kinematic viscosity ν was to be chosen. Dean's formula predicts that a value of $Re_b = 5540$ corroborates to a $Re_\tau = 180$. However through the performance of multiple calibration simulations, it was found that this values is slightly underestimated and that a value of $Re_b \approx 5626$ corresponds better to the required value of Re_τ. With this exercise, the value of Re_τ was set equal to 180 within an error of less 0.5%.

Many further preliminary simulations were needed in order to test the FORTRAN routines developed in order to compute the Turbulent Kinetic Energy budgets and the velocity statistics from the output of the NEK solver. In fact, the NEK solver only provides values of the instantaneous velocity, pressure and (if present) temperature or passive scalar values. Extensive routines were written to process this data, by averaging it over time and space, calculating gradients etc. These routines were all written taking care to extract information from all the multiple processors involved in the simulations.

NEK5000, being a spectral solver, is capable of using multiple points (or order of polynomials) within each super-element. As a result of multiple simulations, the polynomial order was fixed to nine for the final simulations. Mesh-grid spacing distributions for polynomial orders of N = 5 and N = 9 are shown in the figure 5.2.

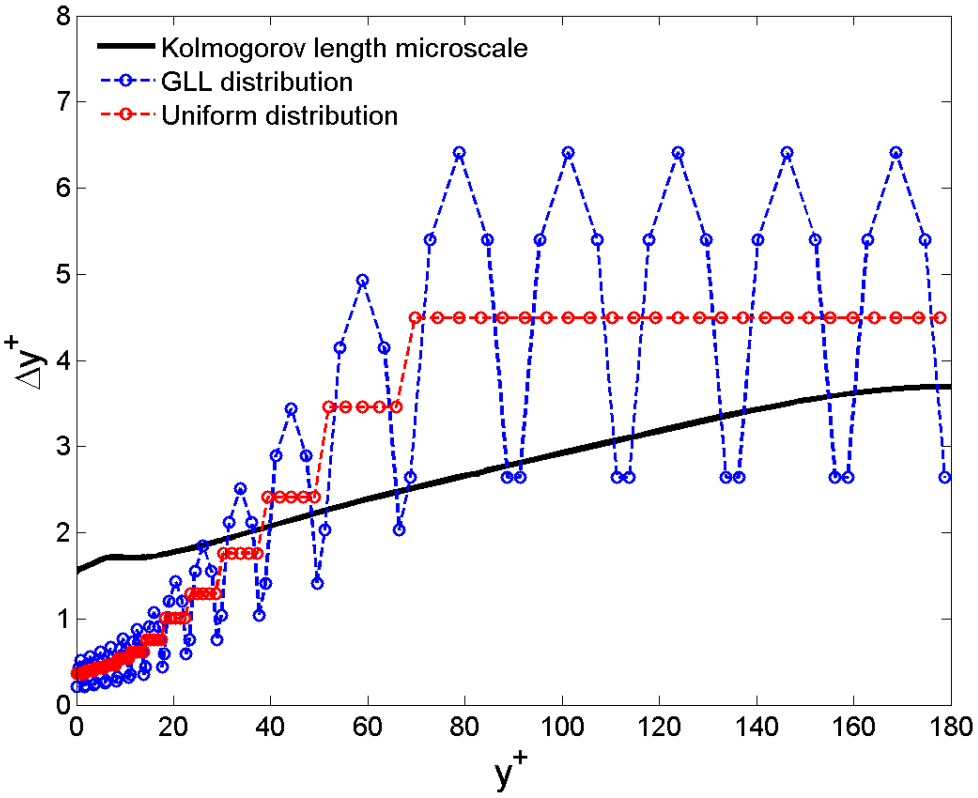

(a) N = 5

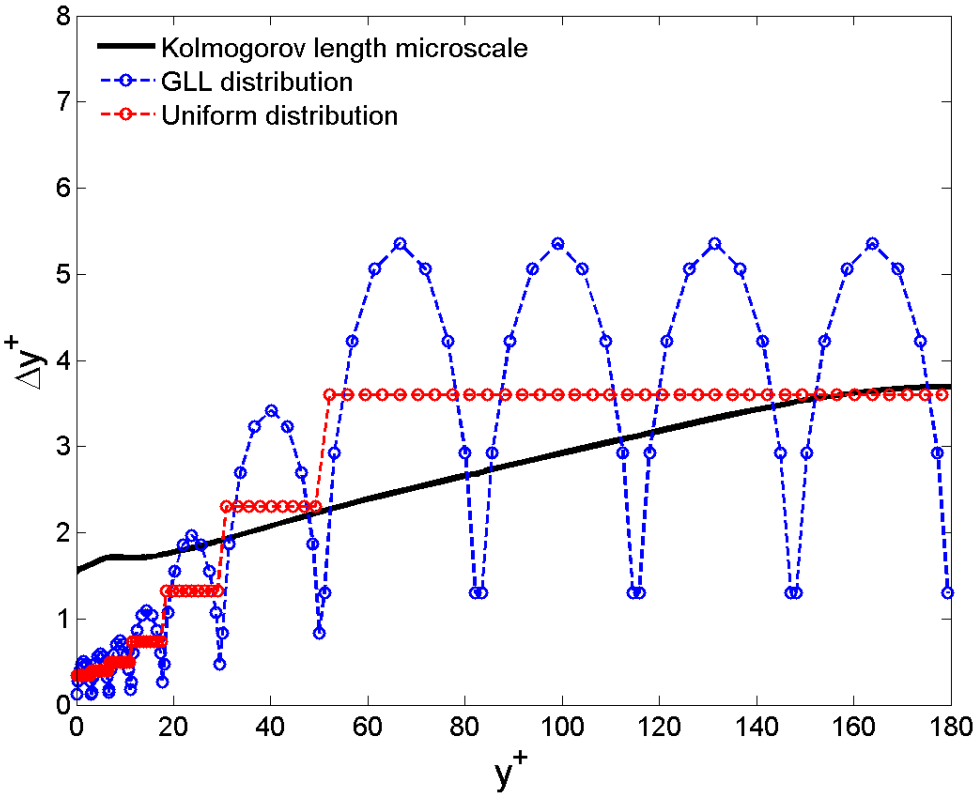

(b) N = 9

Figure 5.2: Grid spacing distribution vs wall normal distance, as compared to the Kolmogorov length scales

5.2.2 Definition of simulations

Domain and mesh

The requirement of the minimum size of the domain, on the basis of the minimum uncorrelated distance, was discussed in section 3.1.1. As was seen from figure 3.2, this distance is around 2π for the streamwise direction and π for the spanwise directions (with $\delta = 1$)), and they correspond to the sizes of the largest eddies in the configuration. A channel with these dimensions for the L_x and L_z, the so called *small domain*, would therefore correspond to the minimum possible dimensions to justify the use of periodic boundary conditions reliably. Another choice for a standard domain size would be with $L_x = 4\pi\delta$ and $L_z = (4/3)\pi\delta$, the so called *normal domain*. Both of these domains are used for the assessment conducted in this thesis work. However for the present chapter, the *normal domain* will be first employed owing to the large amount of literature available with this configuration.

A homogeneous mesh size is adopted in the streamwise and spanwise directions with a $(\Delta x^+, \Delta z^+) = (9.0, 4.5)$. For the wall-normal direction, a personalized distribution of the elements is developed, with highly refined mesh elements near the wall to a coarser mesh near the centerline. This distribution was developed to ensure grid-point spacing of the same order as the local Kolmogorov and Batchelor length scales. This implies that the involved GLL distribution of the points within the super-elements also was also taken into account. From literature it is known that a $\Delta y^+_{wall} < 0.5$ is necessary in the vicinity of the wall, even though the local Kolmogorov scales indicates that $\Delta y^+_{wall} \approx 1.5$ would be sufficient. Thus the mesh is made denser in the wall vicinity beyond the Kolmogorov scale requirement [22]. On the other hand, it has been shown from previous simulations that a mesh somewhat coarser than the Kolmogorov scales in the bulk does not significantly impact on the quality of the results. Incorporating all these considerations, a mesh distribution as shown in the figure 5.2 was generated. A uniform distribution of points within the super-elements was first assumed, and then the grid-point spacing within these fictional elements was made to follow the trend of the Kolmogorov scales, keeping a few additional considerations as stated above in mind. The resultant mesh yields a distribution in the y-direction varying from $\Delta y^+_{wall} = 0.28$ to $\Delta y^+_{centerline} = 5.0$. For the polynomial order of N = 9, a total of 7.58 million points are present in the grid, and a total averaging time of $t^+ = 16140$ is used.

Temporal discretization

NEK5000 uses a third-order backward difference method for time advancement, along with third order extrapolation for the explicit evaluation of non-linear and pressure terms. The Kolmogorov time scale given by 2.6 is the smallest time step required to capture all the scales of turbulence. However for numerical stability of the simulations, usually a smaller time step needs to be employed. This is measured through the CFL (Courant-Friedrichs-Lewy) number. This is defined by

$$C = \frac{u\Delta t}{\Delta x}. \tag{5.3}$$

for the one dimensional case. The condition for stabillty is that this quantity must be maintained underneath a certain limit C_{max}. This can be extended to the n-dimensional case as:

$$C = \Delta t \sum_{i=1}^{n} \frac{u_{x_i}}{\Delta x_i} \leq C_{max}. \tag{5.4}$$

Preliminary analyses were performed on coarser meshes to understand the effect of CFL upto 0.5. A value of CFL = 0.2 was decided for the final simulation. The value of time step dt necessary to maintain such a CFL in the developed flow was calibrated, and the final simulations were done with this constant time step dt.

Other parameters

Testing simulations were conducted on the NRG clusters in Petten, with a maximum of 32 processors per simulations. However due to the greater demands of computing for the final simulation, it was performed at the Narodowe Centrum Badan Jadrowych (NCBJ-National Center for Nuclear Research) in Otwock, Poland using about 500 processors. The simulation ran for 14 days.

The averaging procedure for the flow variables has been started only once the statistically stationary state of the flow has been reached. This state, it has been confirmed by many numerical simulations, for every value of Re_τ is unique [22]. In order to confirm that this statistically stationary state has been reached for the current flow, the Re_τ has been used as the defining criterion. The flow is taken to be converged once the value of Re_τ has converged to the target value of 180. FORTRAN routines have been written that average the Re_τ over small periods of time, and once these successive averages are within a certain limit of each other, the stationary state is taken to have reached, and the averaging is started. A plot showing the evolution of Re_τ with time is shown in figure.

5.3 Results and analysis

The results of the ninth order simulation are compared in this section to various databases amongst those mentioned in the section 3.1. MKM [19], which is an improvement over the simulation in KMM [15], Vreman [22], which might be the most accurate available database for the $Re_\tau = 180$ case, Hoyas and Jimenez [13] and [9], conducted on the largest domain, and Tiselj and Ciselj [21], which is a database that will be employed to analyze the results of conjugate heat transfer, are the references that will be used for the analysis of the results here. Lower-order statistics (mean and standard deviation) and higher-order statistics (skewness and flatness) of the velocity, terms and the balance of the turbulent kinetic energy, and the Reynolds shear stress terms in the streamwise-wall normal direction are all compared and analyzed.

The channel has a periodic boundary condition in the x and z directions. Once the flow is fully converged, these two directions are homogeneous. This implies that the partial derivative of the (mean of the) flow quantities with respect to these spatial coordinates is going to be zero. Therefore for the purposes of the analysis of the turbulent plane channel flow, only the wall normal profiles of the velocity and other quantities are important. In

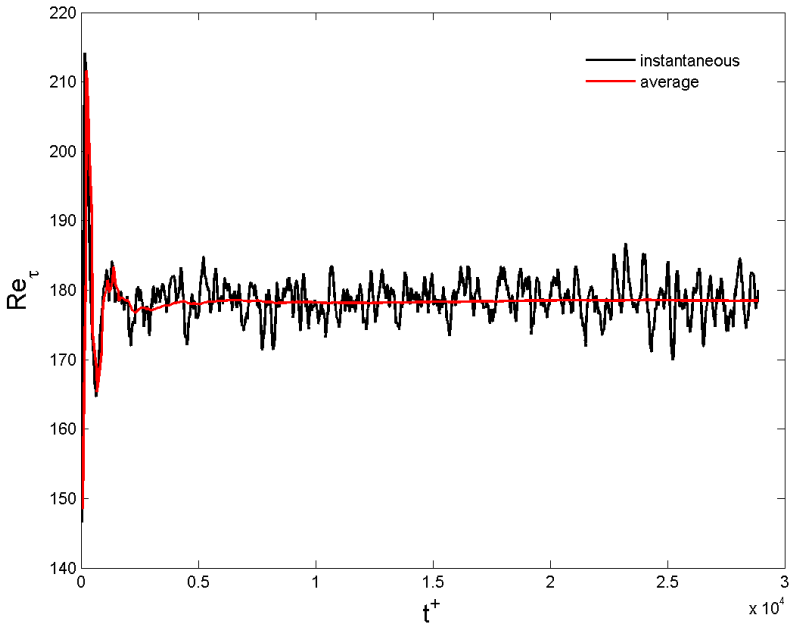

Figure 5.3: Evolution of averaged and instantaneous turbulent Reynolds number

addition, the flow configuration, owing to the symmetry of the boundary conditions in the wall-normal direction, is also expected to be statistically symmetric about the center plane of the channel. Hence, for the statistics of the variables, the averaging is conducted over time, the homogeneous planes in the x and z directions, and the centerline of the channel, in that order. This will be denoted by $\overline{c}$ for the quantity c, and c' is the deviation or fluctuation about this average. The non-dimensionalization of the quantities is done as indicated in section 3.1.3, through the use of u_τ. Since all the reference data used here is for the same value of Re_τ (and hence u_τ), this scaling is not expected to generate any differences in the results, as compared to the scaled values of the reference results.

Characterization of discrepancies

Since the goal of the entire research is to assess the performance of NEK5000 relative to the reliable databases found in literature, it is necessary to quantify the errors systematically to enhance the understanding of the discrepancies. All the errors in this particular experiment, along with those of the reference databases, are compared to the data by Vreman et.al. [22]. This data set refers to the most recently published DNS data set for $Re_\tau = 180$ and is obtained with the highest spatial resolution thus far, for this Reynolds number, using a pseudo-spectral code, together with a long statistical averaging time. The difference is quantified by relative difference in % given by:

$$\epsilon_{\Psi,database}(y^+) = \frac{\Psi(y^+)_{database} - \Psi(y^+)_{VremanDNS}}{\Psi(y^+)_{VremanDNS}} \times 100. \tag{5.5}$$

where, Ψ can represent any quantity being considered, such as the mean velocity, the

flatness or any of the terms of the Reynolds stress budget equations for the given database. The global quantification of this quantity, the mean relative difference, has been computed using the following equation , and is used to characterize the difference of that particular variable of that particular database with respect to Vreman et.al.

$$||\epsilon_\Psi(y)||_1 = \frac{1}{2h}\int_{y=0}^{y=2h} |\epsilon_\Psi(y)|dy. \tag{5.6}$$

While implementing this integral in the wall normal direction for the various quantities, points very close to the wall have been avoided, in order to avoid singularities.

Table 5.1: Relative error $||\epsilon_\Psi(y)||_1$ in % with respect to Vreman et.al.

Database	Mean U	RMS u	RMS v	RMS w	k
NEK5000	0.264	0.869	0.803	0.0425	0.484
KMM	0.004	0.15	0.52	1.624	0.8541
Tiselj et.al.	0.101	0.396	0.408	0.110	0.873
Hoyaz et.al.	0.439	0.509	1.809	0.881	1.800

Table 5.2: Relative error $||\epsilon_\Psi(y)||_1$ in % with respect to Vreman et.al.

Database	skewness(u)	skewness(v)	skewness(w)	skewness(p)
NEK5000	0.042	8.49	-	3.492
KMM	2.14	16.4	-	44.01
Tiselj et.al.	0.477	-	-	10.41

Table 5.3: Relative error $||\epsilon_\Psi(y)||_1$ in % with respect to Vreman et.al.

Database	flatness(u)	flatness(v)	flatness(w)	flatness(p)
NEK5000	0.246	2.297	0.810	3.722
KMM	0.339	0.994	1.547	6.837
Tiselj et.al.	1.125	0.759	0.632	5.388

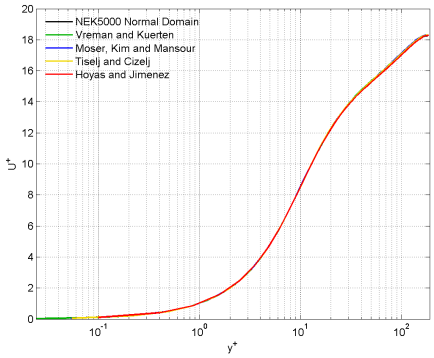

(a) Mean velocity in streamwise direction

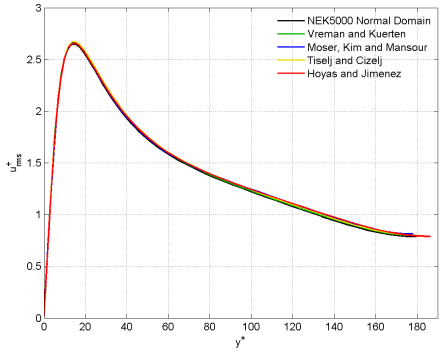

(b) RMS of velocity fluctuations in streamwise direction

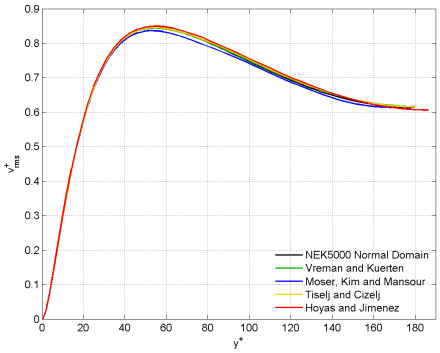

(c) RMS of velocity fluctuations in normal direction

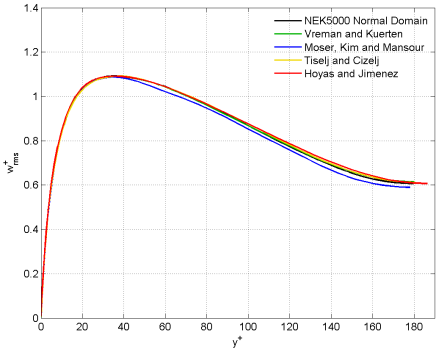

(d) RMS of velocity fluctuations in spanwise direction

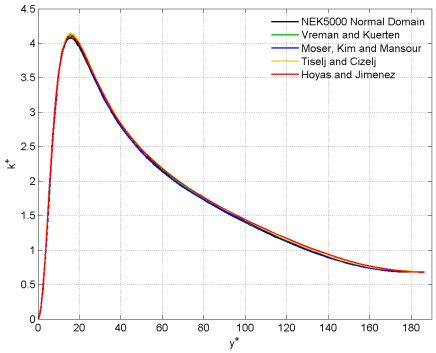

(e) Turbulent kinetic energy

Figure 5.4: Mean, RMS and turbulent kinetic energy profiles; *black:* NEK5000, *green:* Vreman et.al., *blue:* Moser et.al., *yellow:* Tiselj et.al., *red:* Hoyaz et.al.

Table 5.4: Relative error $||\epsilon_\Psi(y)||_1$ of Reynolds stress $\overline{u'u'}$ budget terms in % with respect to Vreman et.al.

Database	Production	Dissipation	Press. Diff.	Press. Strain	Turb. Trans.	Vis. Diff
NEK5000	5.522	0.291	-	0.525	0.595	0.158
KMM	1.759	0.968	-	1.677	2.54	2.175
Tiselj et.al.	-	1.196	-	0.051	0.628	0.309
Hoyaz et.al.	-	0.559	-	4.553	2.15	5.556

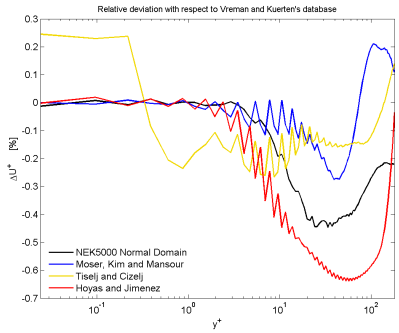

(a) Relative deviation of mean velocity in x

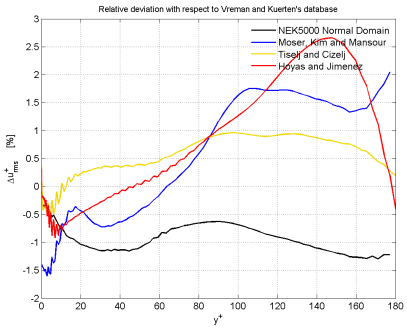

(b) Relative deviation of RMS of velocity fluctuations in x

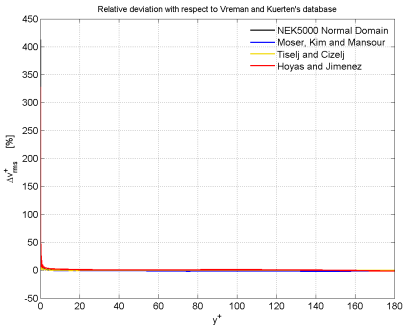

(c) Relative deviation of RMS of velocity fluctuations in y

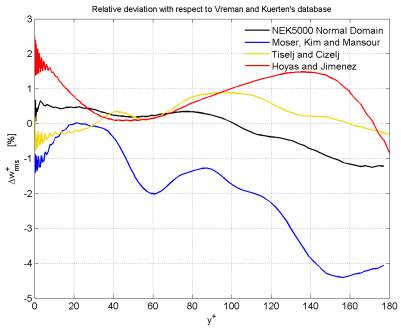

(d) Relative deviation of RMS of velocity fluctuations in z

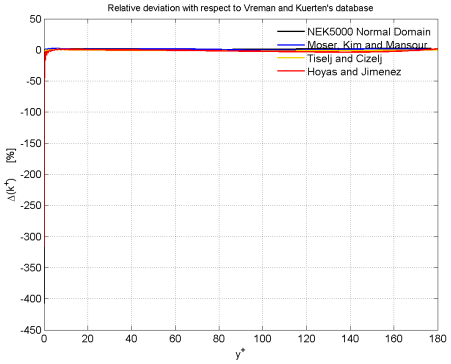

(e) Relative deviation of turbulent kinetic energy

Figure 5.5: Relative deviations of the mean velocity, RMS and turbulent kinetic energy profiles with respect to Vreman et. al.; *black:* NEK5000, *blue:* Moser et.al., *yellow:* Tiselj et.al., *red:* Hoyaz et.al.

Table 5.5: Relative error $||\epsilon_\Psi(y)||_1$ of Reynolds stress $\overline{v'v'}$ budget terms in % with respect to Vreman et.al.

Database	Production	Dissipation	Press. Diff.	Press. Strain	Turb. Trans.	Vis. Diff
NEK5000	-	1.138	8.287	0.831	2.2	0.158
KMM	9.6774	0.492	7.454	4.7	43	16.16
Tiselj et.al.	8.5	1.26	9.302	0.088	9.104	6.664
Hoyaz et.al.	8.511	2.694	7.183	4.2	14.316	7.45

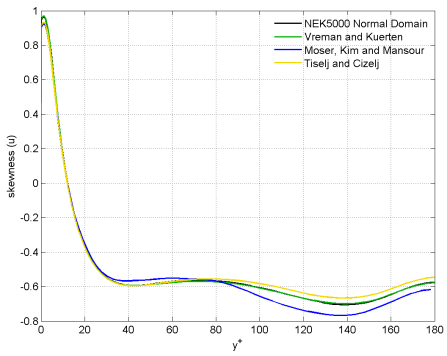

(a) Skewness in streamwise velocity fluctuations

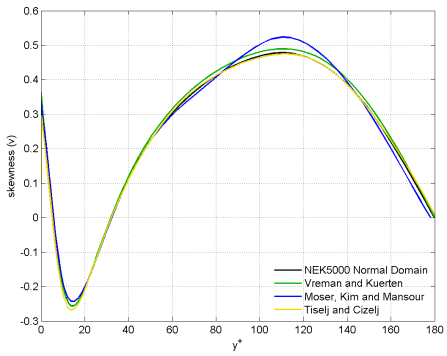

(b) Skewness in normal velocity fluctuations

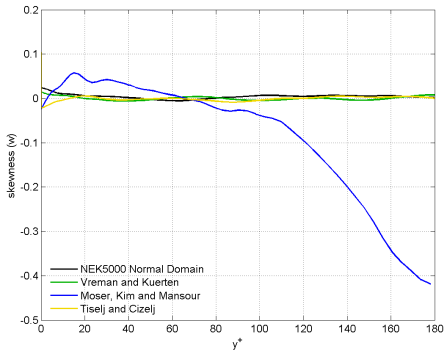

(c) Skewness in spanwise velocity fluctuations

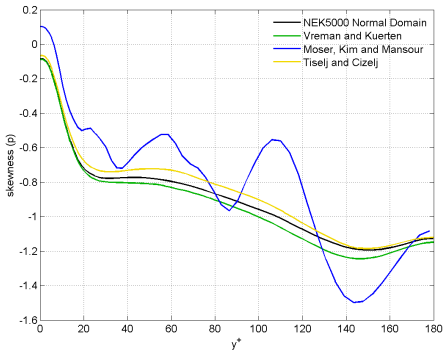

(d) Skewness in pressure fluctuations

Figure 5.6: Skewness of the velocity and pressure fluctuations; *black:* NEK5000, *green:* Vreman et.al., *blue:* Moser et.al., *yellow:* Tiselj et.al., *red:* Hoyaz et.al.

Table 5.6: Relative error $||\epsilon_\Psi(y)||_1$ of Reynolds stress $\overline{w'w'}$ budget terms in % with respect to Vreman et.al.

Database	Production	Dissipation	Press. Diff.	Press. Strain	Turb. Trans.	Vis. Diff
NEK5000	-	0.798	-	0.598	4.197	10.988
KMM	-	0.47	7.454	-	0.95	29.78
Tiselj et.al.	-	1.363	-	0.742	5.2176	26.485
Hoyaz et.al.	-	1.717	-	4.531	8.446	10.632

Mean and RMS profiles

The profiles of the mean velocity in the streamwise direction, the fluctuations of the velocity in the x, y and z directions are given in the figure 5.4. It is evident from the variation of the mean velocities that the logarithmic layer of the velocity is not yet developed, owing to the low Reynolds number. The agreement of NEK5000, and all the

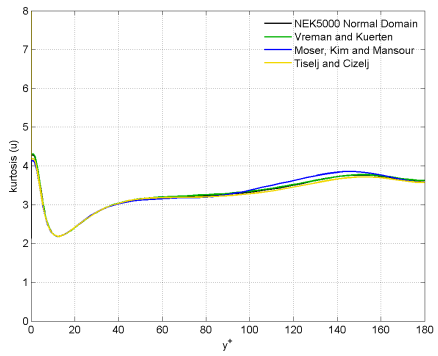

(a) Kurtosis in streamwise velocity fluctuations

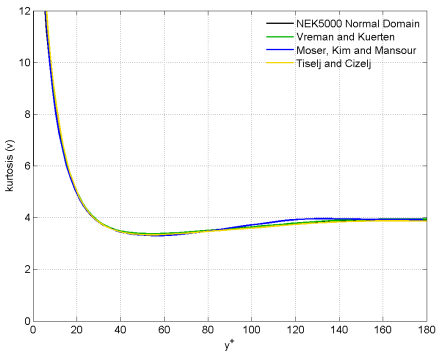

(b) Kurtosis in normal velocity fluctuations

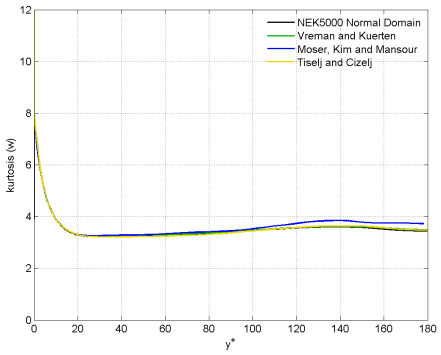

(c) Kurtosis in spanwise velocity fluctuations

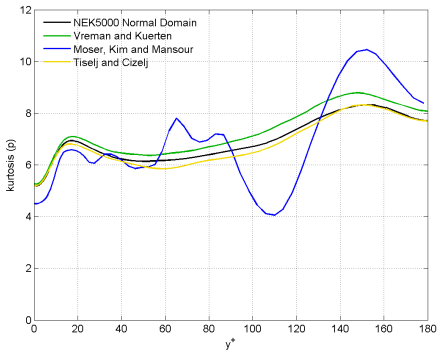

(d) Kurtosis in pressure fluctuations

Figure 5.7: Kurtosis/ flatness of the velocity and pressure fluctuations; *black:* NEK5000, *green:* Vreman et.al., *blue:* Moser et.al., *yellow:* Tiselj et.al., *red:* Hoyaz et.al.

other databases is very good with respect to Vreman et.al. This is further supported by the figures in the following page (refer fig 5.5) which contains the plots of the relative errors of the same quantities with respect to Vreman et.al. as defined by eq. 5.5. The mean of the same quantities have been quantized in table 5.1. The case is similar for the RMS of the fluctuations, although the deviations might be slightly higher than those for the mean. It is noticeable that NEK5000 underpredicts the mean and RMS values of the streamwise velocity throughout the domain, although it is somewhat closer to Vreman et. al. near the bulk of the flow than the wall. The other databases tend to underpredict in the wall vicinity but overpredict in the bulk of the flow. However it might be concluded that the performance of NEK5000 is very good, since the agreement is within 1% for all the quantities shown here. A slight difference due to the change in Re_τ and hence the normalization is visible for Hoyaz and Jimenez database.

Higher order statistics

Higher order moments are needed in order to better understand the characteristics of a turbulent flow. Skewness is a third order statistic that describes the asymmetry of the distribution about the mean value. If it is a negative value of a large magnitude, then this means that the flow is characterized by larger negative values of fluctuation than positive

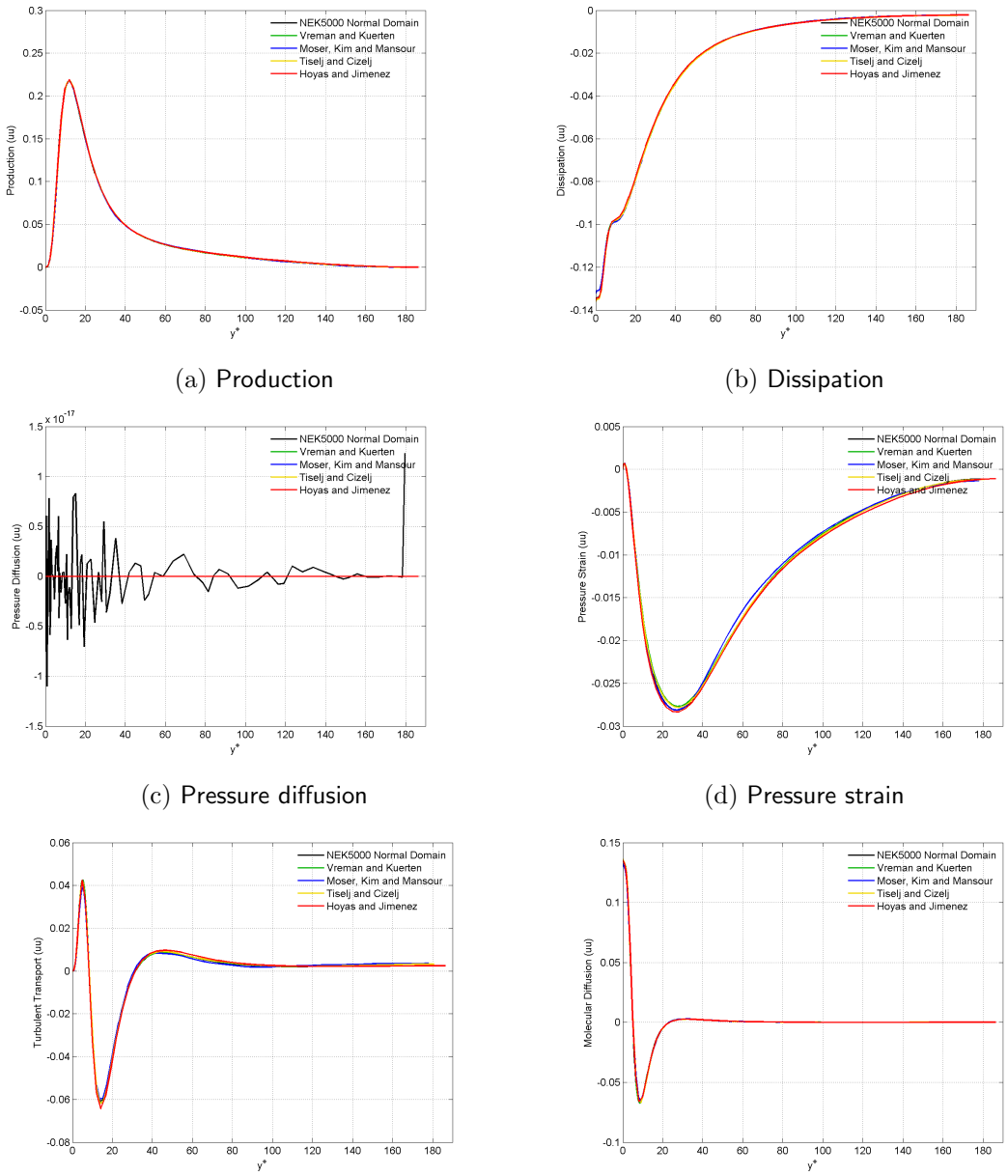

(a) Production

(b) Dissipation

(c) Pressure diffusion

(d) Pressure strain

(e) Turbulent transport

(f) Molecular diffusion

Figure 5.8: Budget quantities for the Reynolds stress term $\overline{u'u'}$; *black:* NEK5000, *green:* Vreman et.al., *blue:* Moser et.al., *yellow:* Tiselj et.al., *red:* Hoyaz et.al.

ones [22]. The skewness for the three velocity components and pressure are shown in figures 5.6. NEK results agree very well with Vreman et.al. and shows a mean relative deviation in the third order statistic of within 0.04% in the streamwise direction (see the relative deviations shown in table 5.2)! This shows excellent resolution of the flow field and the essential fields. A similar trend is seen for Tiselj et. al., however it may be said that the deviations are slightly higher of the order of 0.5%, 5% and 10% respectively for the streamwise velocity, wall normal velocity and pressure. It is to be noted here

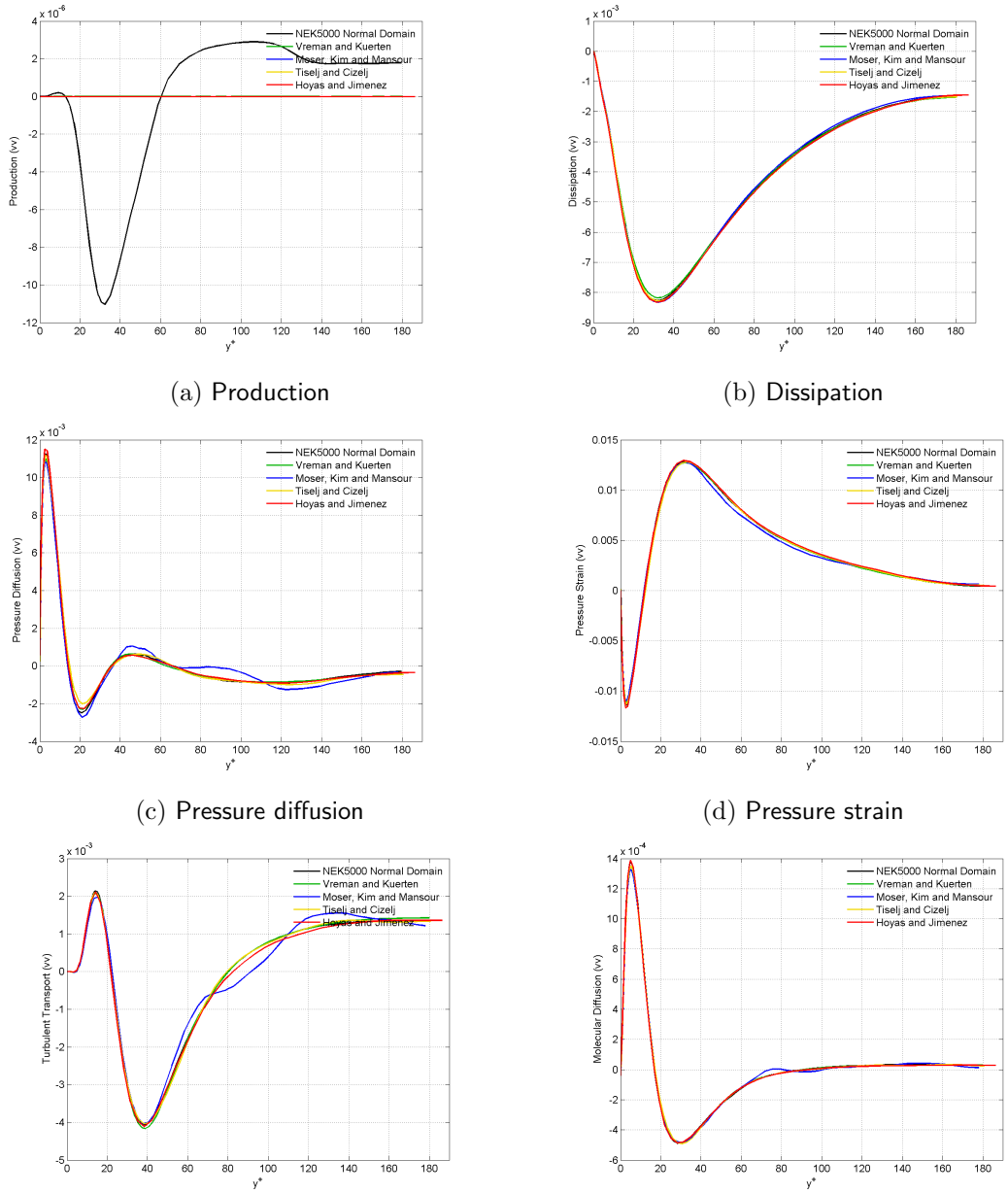

(a) Production

(b) Dissipation

(c) Pressure diffusion

(d) Pressure strain

(e) Turbulent transport

(f) Molecular diffusion

Figure 5.9: Budget quantities for the Reynolds stress term $\overline{v'v'}$; *black:* NEK5000, *green:* Vreman et.al., *blue:* Moser et.al., *yellow:* Tiselj et.al., *red:* Hoyaz et.al.

that due to the proximity of the reference values to zero, the relative error sometimes tends to very high values. Such entries are removed from the table and indicated by a '-'. MKM database shows a very large error component (order of the skewness itself) and oscillatory behavior, possibly due to inadequate averaging time. The Navier-stokes equations are reflection symmetric at the channel centerline and this causes the skewness in the z-direction to be zero, which can be observed in figure 5.6c.

The flatness measures the intermittency of a quantity. A strongly intermittent signal at

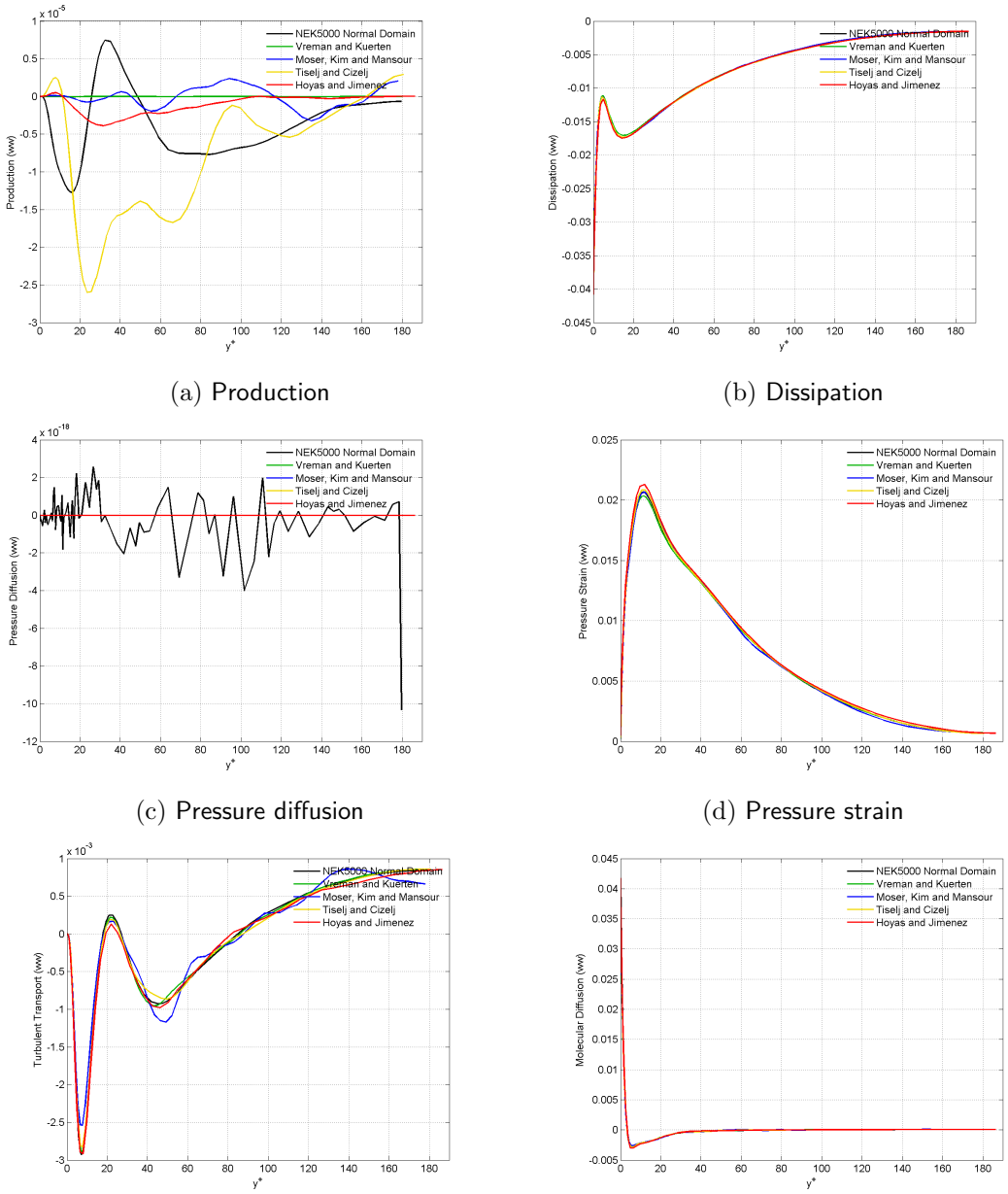

(a) Production

(b) Dissipation

(c) Pressure diffusion

(d) Pressure strain

(e) Turbulent transport

(f) Molecular diffusion

Figure 5.10: Budget quantities for the Reynolds stress term $\overline{w'w'}$; *black:* NEK5000, *green:* Vreman et.al., *blue:* Moser et.al., *yellow:* Tiselj et.al., *red:* Hoyaz et.al.

some point is dormant most of the time; there are periods with activity, but most of the time the activity is small [22]. It can be seen, surprisingly from the plots in 5.7 that the maximum value of the kurtosis occurs near the wall for the velocity, but near the bulk for the pressure. This observation is well matched by all the databases. It is very interesting to note that the fluctuations in y-direction are extremely intermittent near the wall. The deviations are small for all databases (refer table 5.3), especially near the centerline of the flow, but higher near the wall. It remains within 2.2% for velocity and around 3.7%

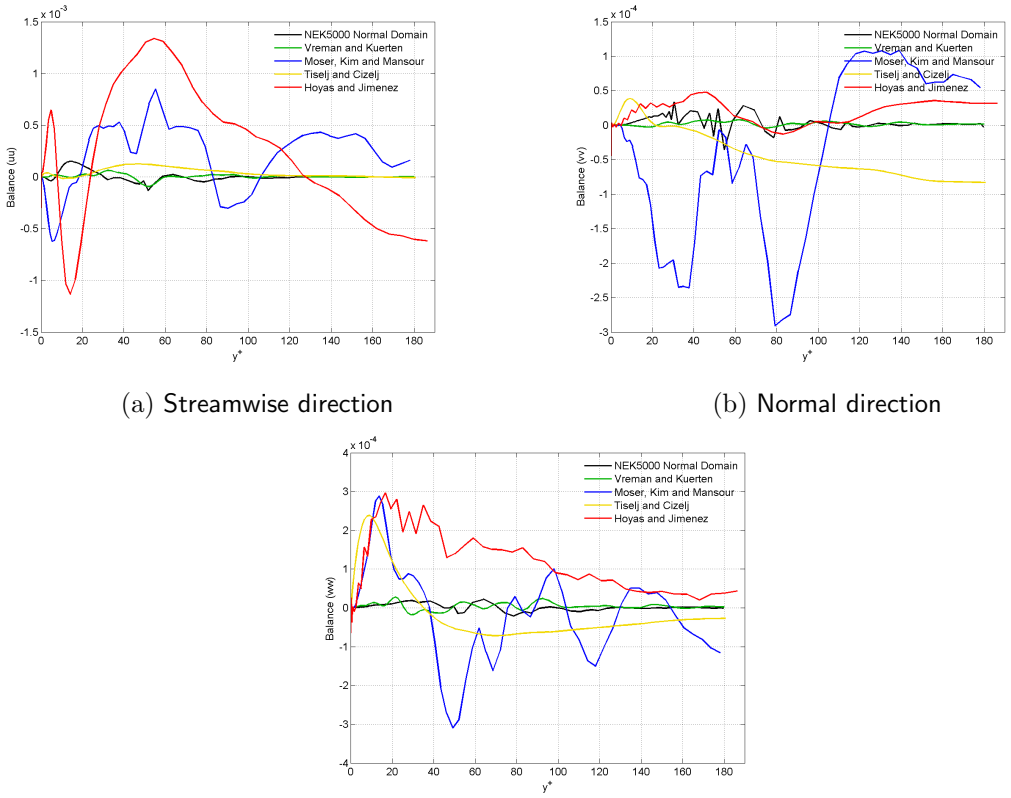

(a) Streamwise direction

(b) Normal direction

(c) Spanwise direction

Figure 5.11: Sum of the budget equation terms in the three coordinate directions; *black:* NEK5000, *green:* Vreman et.al., *blue:* Moser et.al., *yellow:* Tiselj et.al., *red:* Hoyaz et.al.

for pressure. The deviation in pressure is the largest amongst all the quantities.

5.3.1 Reynolds stress budget terms

The relevance of the Reynolds stress terms and their conservation equation was introduced in 2. These terms are plotted in the figure 5.8, 5.9 and 5.10. Along with being important parameters to the understanding of the turbulent flow, due to the higher order correlations and the derivatives involved, they serve as ideal terms for the assessment of performance of the code. The stress budget terms are themselves small in most of the domain except in the near-wall region. In the bulk region the velocity profile flattens, generating the reduction of the production term. The pressure strain is theoretically zero, and accordingly the terms here the NEK computation indicates the value of these terms to be of the order of 10^{-6}. Furthermore, even though non-zero but negligible values are expected for every numerical simulation, all the other databases report an empty array. However, NEK5000 results are shown for this term too, in order to depict its magnitude. The agreement of NEK5000 is good with Vreman et.al. This can be seen from the tables 5.4, 5.5 and 5.6. The relative error of NEK5000 is less than 6% in the streamwise direction and less than 11% overall. Even at the maximum points of these relatively low differences occur, it

can be observed from the budget plot profiles that the absolute magnitudes of these are quite low. Figure 5.11 shows the sum of the budget terms in each directions. Owing to the periodicity of the domain, the budget sum for the turbulent kinetic energy should be theoretically zero. Accordingly it is seen here that the values of the budget sum for all the three Reynolds stress terms is very small. Therefore the turbulent kinetic energy budget terms (which are represented by the sum of the normal Reynolds stress terms indicated here) must also be close to zero. Thus also their deviation from (the theoretical) zero, and the reference.

5.4 Conclusions

The DNS capabilities of NEK5000 for the flow variables on the incompressible turbulent channel flow has been thoroughly assessed and analyzed with respect to other databases available in literature. It has been found that there is excellent agreement of results as compared to the other databases for all the flow parameters considered including mean, RMS, skewness and Reynolds stress budgets. Therefore it may be concluded that NEK5000 serves as an excellent solver for flow field calculations for incompressible turbulent flows.

Chapter 6

Assessment of NEK5000: Small domain

6.1 Objective

In the assessment of NEK5000 for a PTS scenario, the evaluation of its performance on distorted domains is an important necessity. However to analyze these domains, it is anticipated that multiple simulations at various angles might be necessary. With such a requirement, to reduce the computational cost of the simulation, it is desirable to employ the so called *small* domain. However before such a small domain is used to analyze the turbulent channel flow, and also used as a reference for other similar simulations, it must be validated with respect to the results of the DNS on the *normal* domain used in the previous chapter, which has already been proved to be an excellent database for channel flow results. The objective of this part of the research is to conduct such a simulation and compare it to the results of the normal domain.

6.2 Procedure of numerical experiment

The details of the domain for a turbulent channel were discussed in chapter 5 and 3. The small domain that is used for the simulation in this chapter is a reduced version of the same domain in the streamwise and the spanwise direction. It remains *the same* in the wall-normal direction. The dimensions of the domain is given by

$$L_x, L_y, L_z = 2\pi\delta, 2\delta, \pi\delta$$

6.2.1 Preliminary setup and mesh

The small domain differs from the normal domain only in the homogeneous directions. Therefore the definitions of parameters such as Re_τ, τ_w are not expected to change since

they all depend on variations of variables in the wall normal direction. Thus for this simulation the exact same value of bulk Reynolds $Re_b = 5626$ was used as in the previous chapter.

The mesh resolution for this simulation is maintained the exact same as in the *normal* domain. Consequently, the number of mesh elements reduces to half in the x-direction and a slightly less than half in the z-direction. The number of elements in the y-direction is preserved. The element distribution becomes $(\Delta x^+, \Delta y^+_{wall} \rightarrow \Delta y^+_{centerline}, \Delta z^+) = (9.0, 0.28 \rightarrow 5.0, 4.5)$. There are a total of 2.8 million grid points in the domain, and an averaging time of $\Delta t^+_{avg} = 16000$ is used. The simulations were run at the Narodowe Centrum Badan Jadrowych (NCBJ- National Center for Nuclear Research) in Otwock, Poland using about 500 processors for about 7 days.

6.3 Results and analysis

Table 6.1: Relative error $||\epsilon_\Psi(y)||_1$ in % with respect to NEK normal domain

Database	Mean U	RMS u	RMS v	RMS w	k
NEK5000 small domain	0.1672	2.193	2.873	2.177	2.205

Table 6.2: Relative error $||\epsilon_\Psi(y)||_1$ in % with respect to NEK normal domain

Database	skew(u)	skew(v)	skew(w)	skew(p)
NEK5000 small domain	28.2	0.853	-	0.613

Table 6.3: Relative error $||\epsilon_\Psi(y)||_1$ in % with respect to NEK normal domain

Database	flatness(u)	flatness(v)	flatness(w)	flatness(p)
NEK5000 small domain	0.025	0.805	0.571	1.5

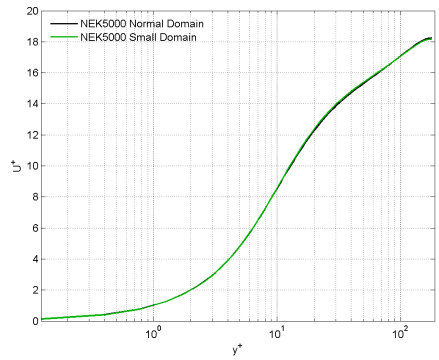

(a) Mean velocity in streamwise direction

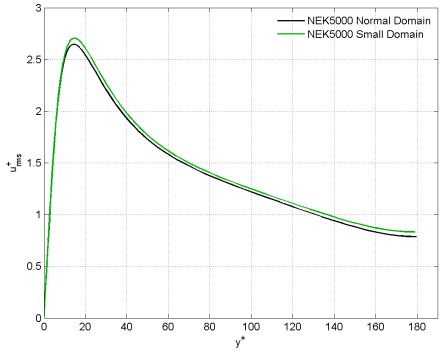

(b) RMS of velocity fluctuations in streamwise direction

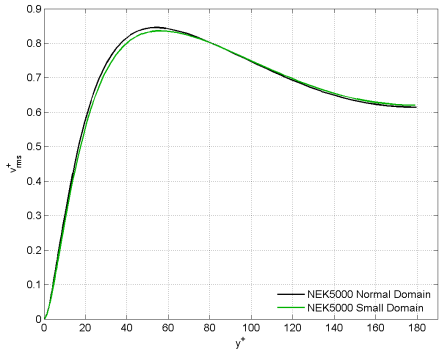

(c) RMS of velocity fluctuations in normal direction

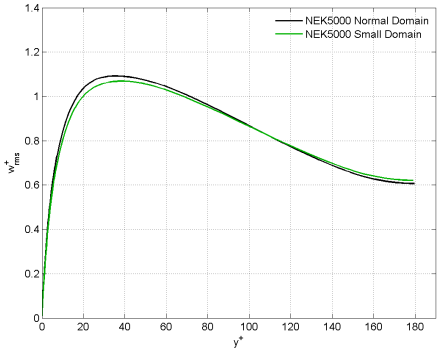

(d) RMS of velocity fluctuations in spanwise direction

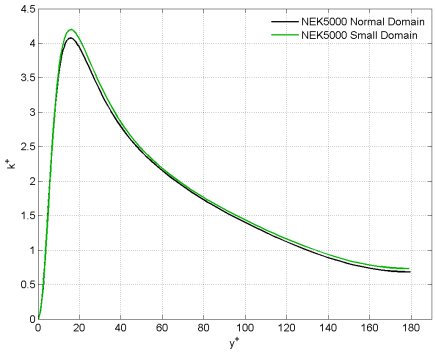

(e) Turbulent kinetic energy

Figure 6.1: Mean, RMS and turbulent kinetic energy profiles; *black:* NEK5000 normal domain, *green:* NEK5000 small domain

Table 6.4: Relative error $||\epsilon_\Psi(y)||_1$ of Reynolds stress $\overline{u'u'}$ budget terms in % with respect to NEK normal domain

Database	Production	Dissipation	Press. Diff.	Press. Strain	Turb. Trans.	Vis. Diff
NEK5000 small domain	4.15	1.12	-	1.719	0.892	2.047

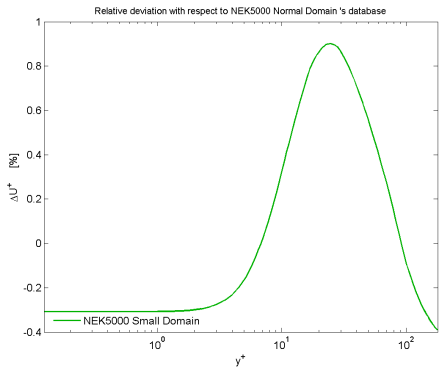

(a) Relative deviation of mean velocity in x

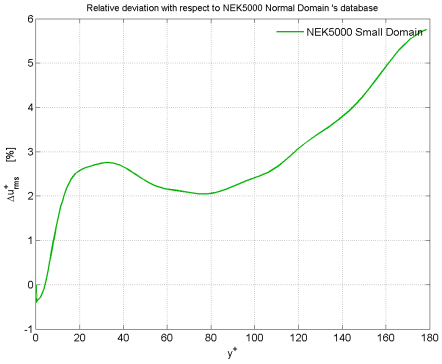

(b) Relative deviation of RMS of velocity fluctuations in x

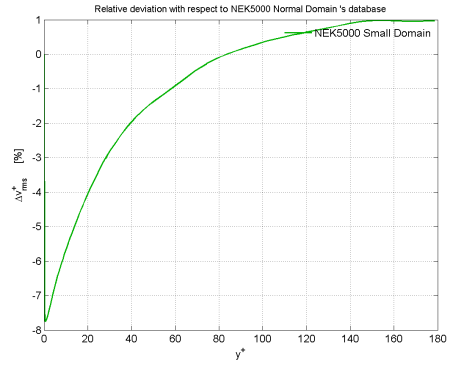

(c) Relative deviation of RMS of velocity fluctuations in y

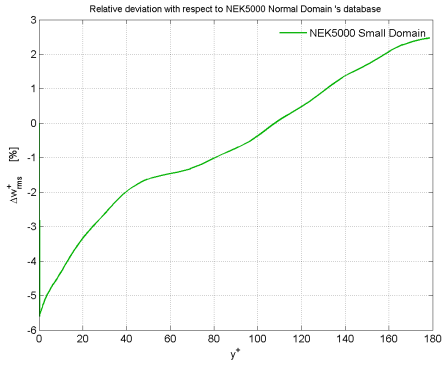

(d) Relative deviation of RMS of velocity fluctuations in z

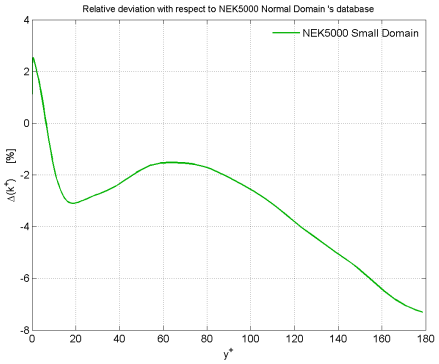

(e) Relative deviation of turbulent kinetic energy

Figure 6.2: Relative deviations of the mean velocity, RMS and turbulent kinetic energy profiles with respect to Vreman et. al.;*green:* NEK5000 small domain

Table 6.5: Relative error $||\epsilon_\Psi(y)||_1$ of Reynolds stress $\overline{v'v'}$ budget terms in % with respect to NEK normal domain

Database	Production	Dissipation	Press. Diff.	Press. Strain	Turb. Trans.	Vis. Diff
NEK5000 small domain	-	7.07	12.91	15.58	2.493	8.443

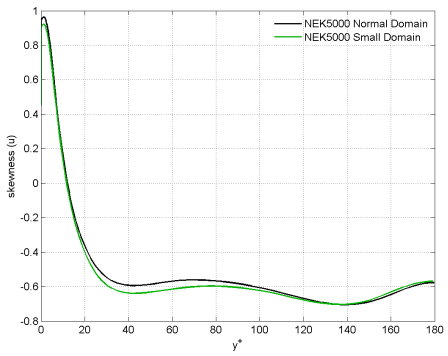

(a) Skewness in streamwise velocity fluctuations

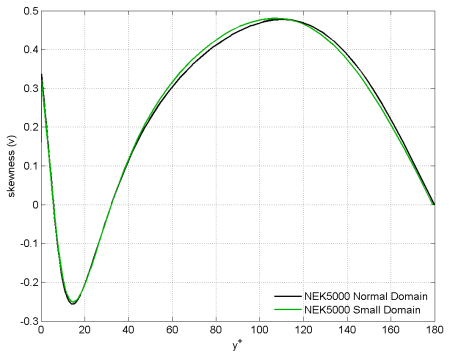

(b) Skewness in normal velocity fluctuations

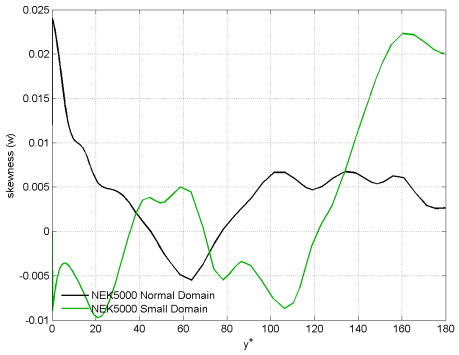

(c) Skewness in spanwise velocity fluctuations

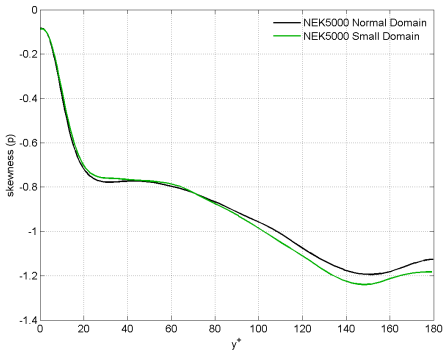

(d) Skewness in pressure fluctuations

Figure 6.3: Skewness of the velocity and pressure fluctuations; *black:* NEK5000 normal domain, *green:* NEK5000 small domain

Table 6.6: Relative error $||\epsilon_\Psi(y)||_1$ of Reynolds stress $\overline{w'w'}$ budget terms in % with respect to NEK normal domain

Database	Production	Dissipation	Press. Diff.	Press. Strain	Turb. Trans.	Vis. Diff
NEK5000 small domain	-	6.445	-	6.328	19.8	2.524

From the figures 6.1 it can be seen that the results for the normal domain and the small domain practically collapse on each other for the mean and the RMS of velocity fluctuations. There is good agreement in skewness and flatness (refer figure 6.2), except for some discrepancy in skewness in the spanwise direction. However in terms of absolute differences, this is quite small and acceptable. The kurtosis agrees very well with the values of the normal domain. The Reynolds stress (figures 6.3 through 6.8) in the most prominent direction (streamwise) has excellent agreement in the two domains. The differences for the pressure diffusion is of the order of 10^{-17} and 0.005 in pressure strain. There appear to be some *waviness* in the production terms for the y and z- directions but the magnitudes of the differences are acceptable (10^{-5}). The balance/ sum of the budget terms is quite

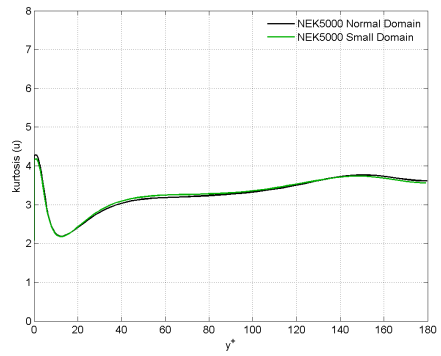

(a) Kurtosis in streamwise velocity fluctuations

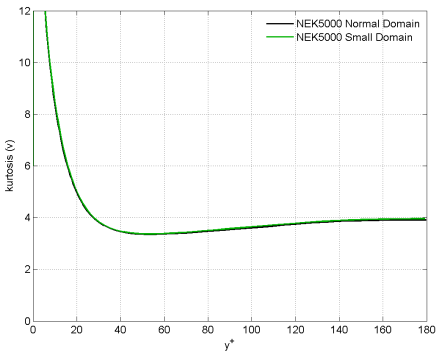

(b) Kurtosis in normal velocity fluctuations

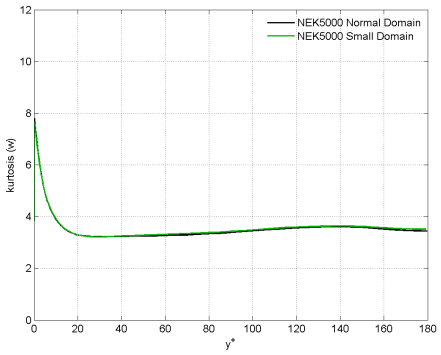

(c) Kurtosis in spanwise velocity fluctuations

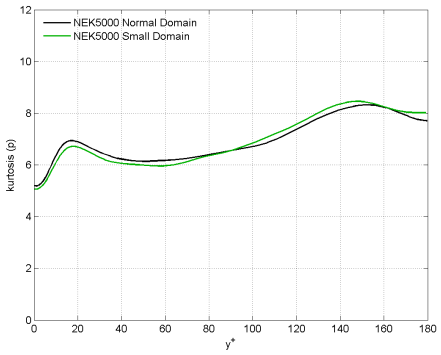

(d) Kurtosis in pressure fluctuations

Figure 6.4: Kurtosis/ flatness of the velocity and pressure fluctuations; *black:* NEK5000 normal domain, *green:* NEK5000 small domain

good, even though the normal domain is much closer to the theoretical value of zero.

6.4 Conclusions

The agreement in results between the normal and the small domain is quite good. Therefore the results of the small domain can be considered good quality DNS and can be used for references for other further investigations.

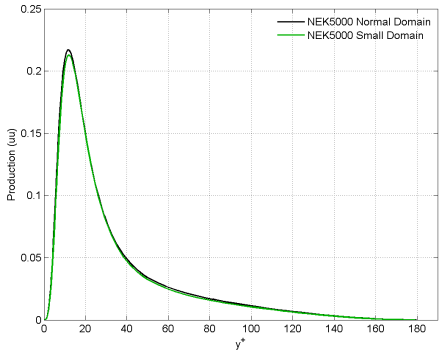

(a) Production

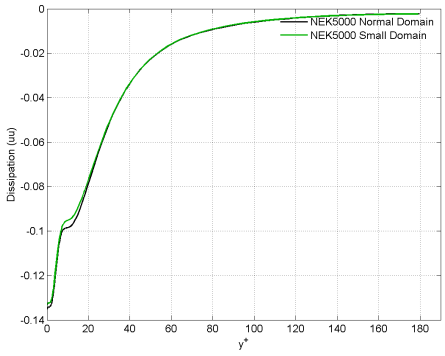

(b) Dissipation

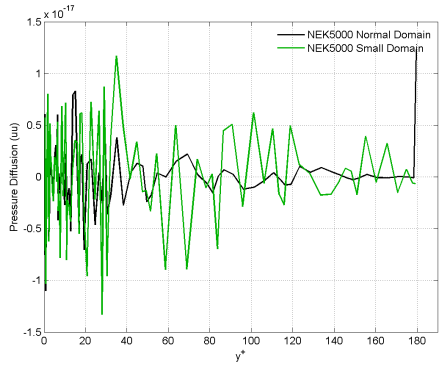

(c) Pressure diffusion

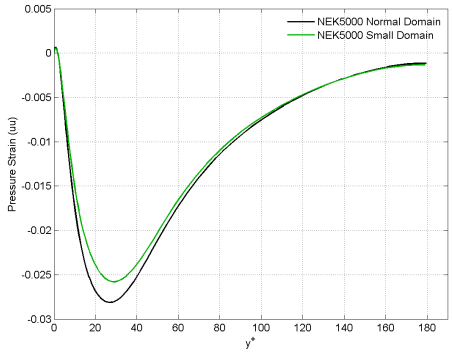

(d) Pressure strain

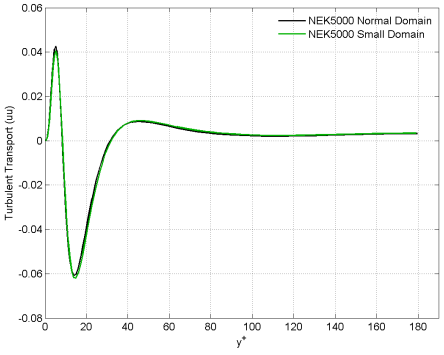

(e) Turbulent transport

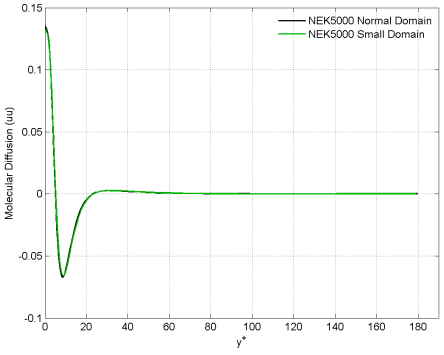

(f) Molecular diffusion

Figure 6.5: Budget quantities for the Reynolds stress term $\overline{u'u'}$; *black:* NEK5000 normal domain, *green:* NEK5000 small domain

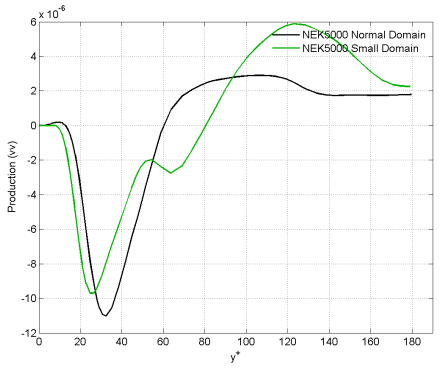

(a) Production

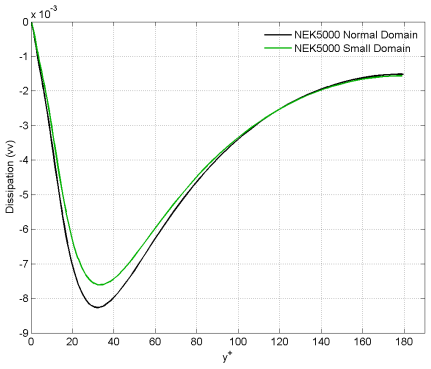

(b) Dissipation

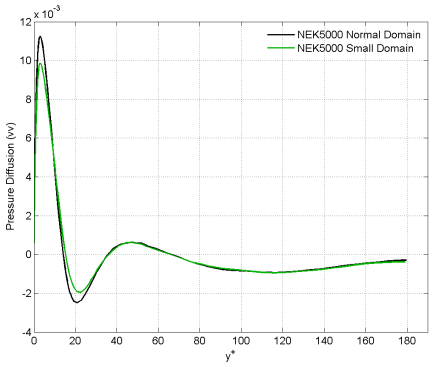

(c) Pressure diffusion

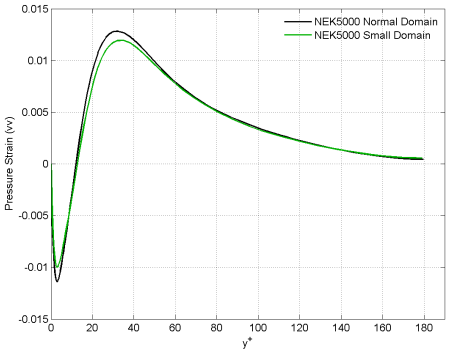

(d) Pressure strain

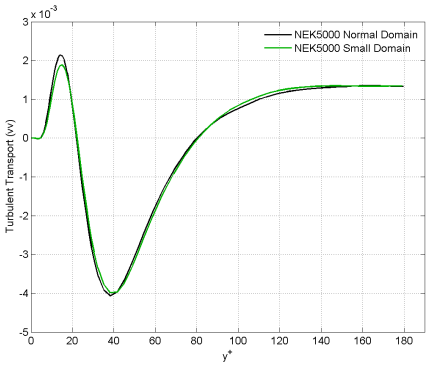

(e) Turbulent transport

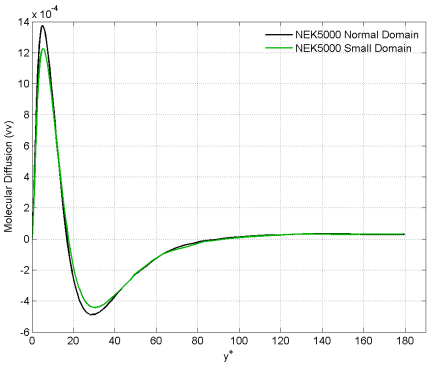

(f) Molecular diffusion

Figure 6.6: Budget quantities for the Reynolds stress term $\overline{v'v'}$; *black:* NEK5000 normal domain, *green:* NEK5000 small domain

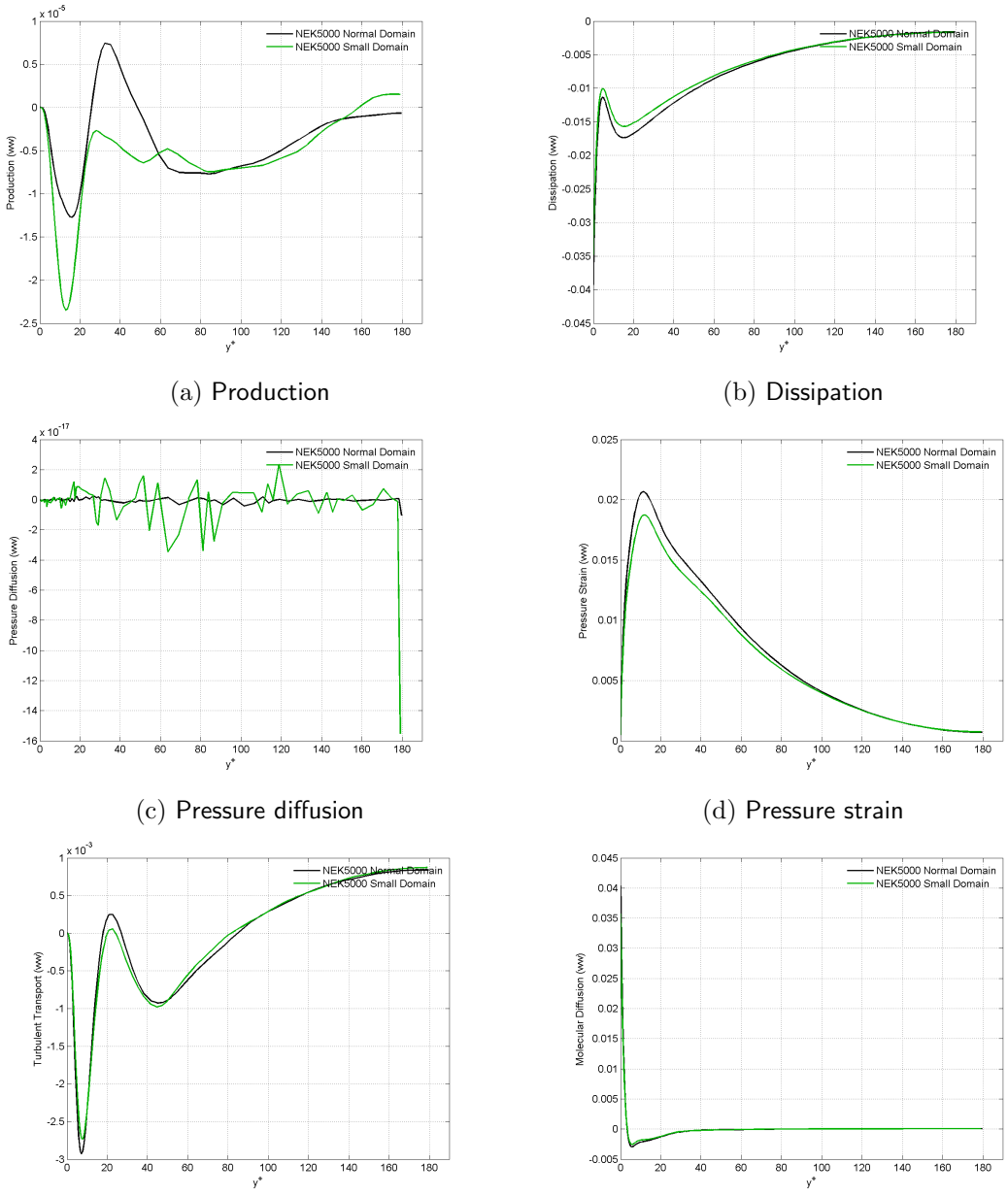

(a) Production

(b) Dissipation

(c) Pressure diffusion

(d) Pressure strain

(e) Turbulent transport

(f) Molecular diffusion

Figure 6.7: Budget quantities for the Reynolds stress term $\overline{w'w'}$; *black:* NEK5000 normal domain, *green:* NEK5000 small domain

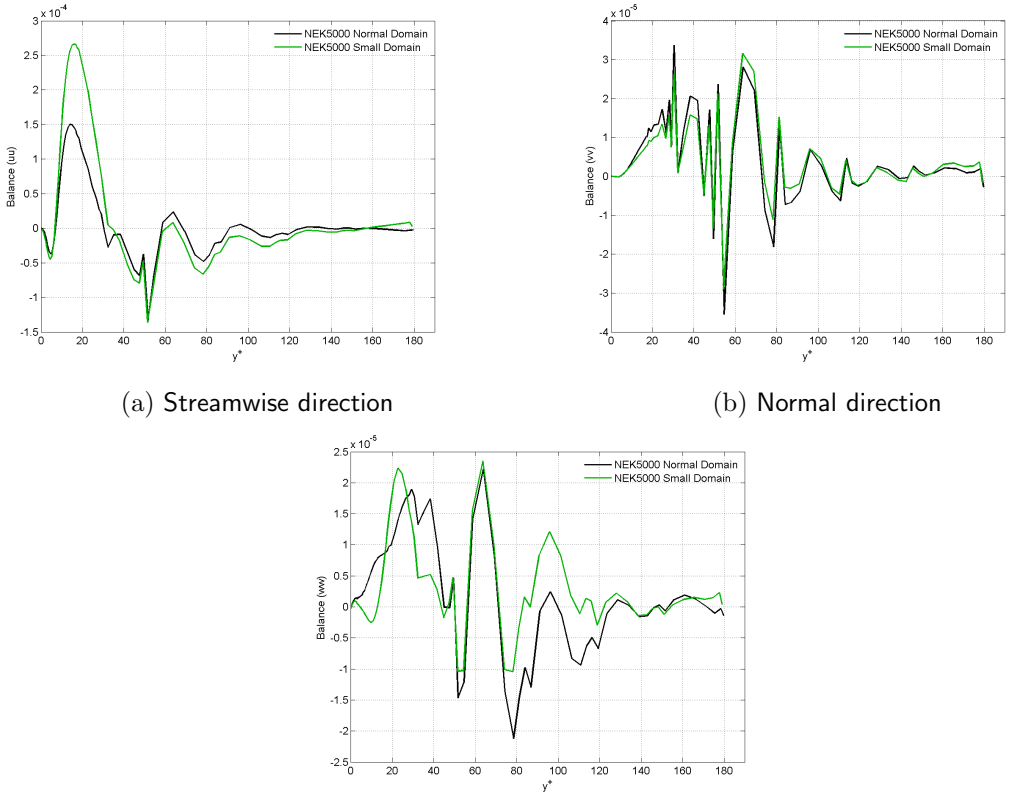

(a) Streamwise direction

(b) Normal direction

(c) Spanwise direction

Figure 6.8: Sum of the budget equation terms in the three coordinate directions; *black:* NEK5000 normal domain, *green:* NEK5000 small domain

Chapter 7

Assessment of NEK5000: Distorted domains and meshes

7.1 Objective

During the simulation of a simplified PTS scenario, owing to the geometry, it is extremely difficult, if not impossible to mesh the domain through the use of only orthogonal elements. It is inevitable that a number of distorted elements are present in the mesh. However, considering the standards of accuracy to be maintained in order to create a reference database for such crucial scenarios, it is critical that the effect of this distortion be taken into consideration before applying the selected NEK5000 solver to the PTS scenario.

Therefore the main objective of this chapter, is to use NEK5000 to compute the flow on domains obtained by shearing of the turbulent channel flow domain, and to analyze the results on the flow field with respect to the orthogonal domain.

7.2 Procedure of numerical experiment

The details of the domain for a turbulent channel were discussed in chapter 5 and 3. This domain, through the use of scripts written on MATLAB to manipulate simple meshes, is sheared about the z-axis (spanwise direction) by various values. Several lower order simulations are carried out on these sheared domains to understand the effect of shearing and obliqueness on the calculations of the flow parameters such as Re_τ. The FORTRAN routines that are used to calculate the wall shear stress and other related parameters are likewise adjusted to ensure that the calculations are relevant for angled elements. Samples of the meshes used are indicated in figure 7.1a and **??**.

For the final 9th order simulations, angles of 60^0 and 30^0 are selected based on the relevance for the application. The mesh and element parameters are maintained the same as for the small domain 6. The simulations are conducted at the Narodowe Centrum

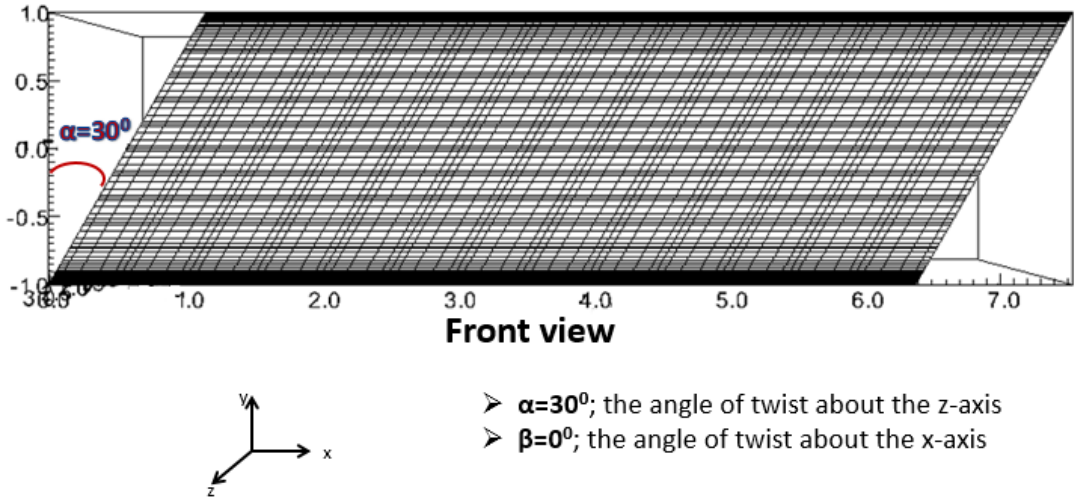

(a)

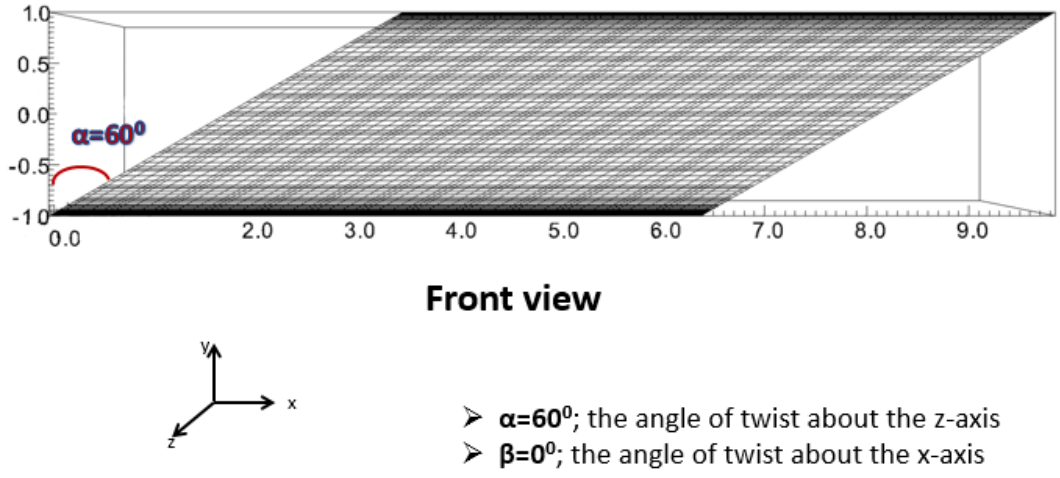

(b)

(c) Influence of sheared mesh on the simulations

Badan Jadrowych (NCBJ- National Center for Nuclear Research) in Otwock, Poland using about 500 processors for about 7 days each.

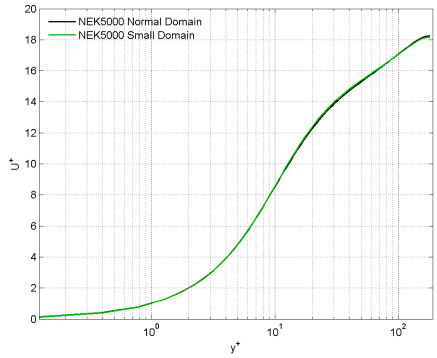

(a) Mean velocity in streamwise direction

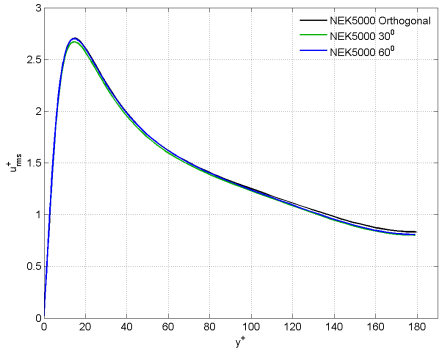

(b) RMS of velocity fluctuations in streamwise direction

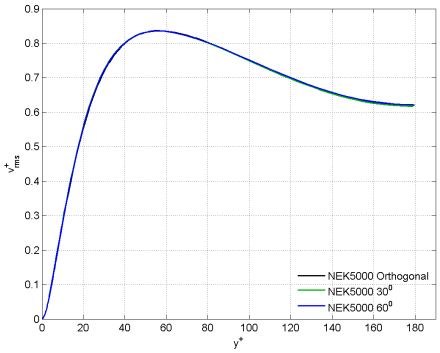

(c) RMS of velocity fluctuations in normal direction

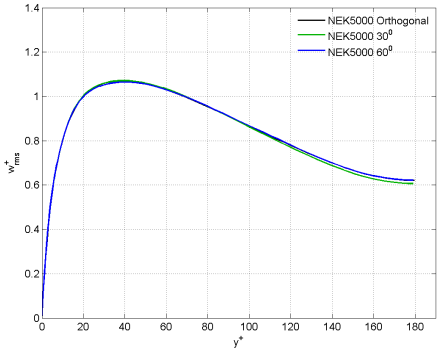

(d) RMS of velocity fluctuations in spanwise direction

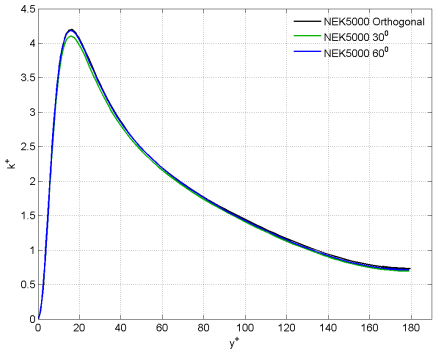

(e) Turbulent kinetic energy

Figure 7.2: Mean, RMS and turbulent kinetic energy profiles; *black:* NEK5000 normal domain, *green:* NEK5000 small domain

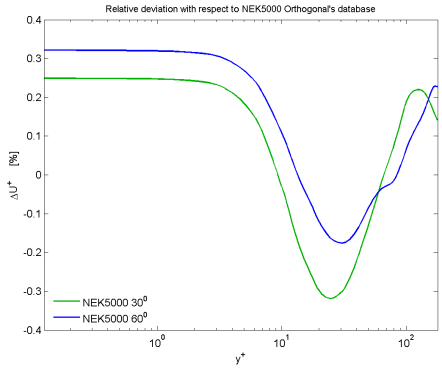

(a) Relative deviation of mean velocity in x

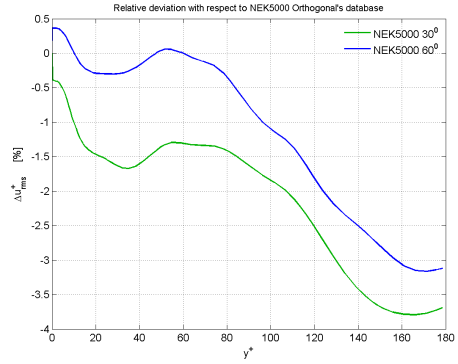

(b) Relative deviation of RMS of velocity fluctuations in x

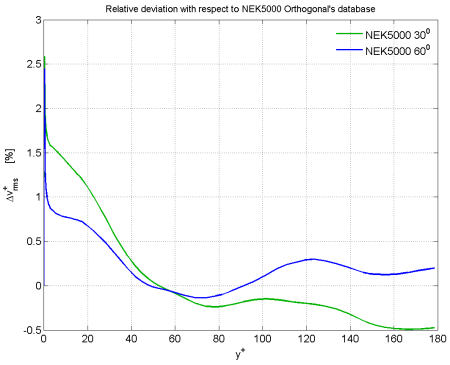

(c) Relative deviation of RMS of velocity fluctuations in y

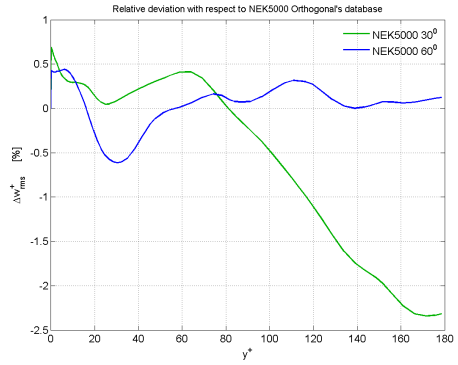

(d) Relative deviation of RMS of velocity fluctuations in z

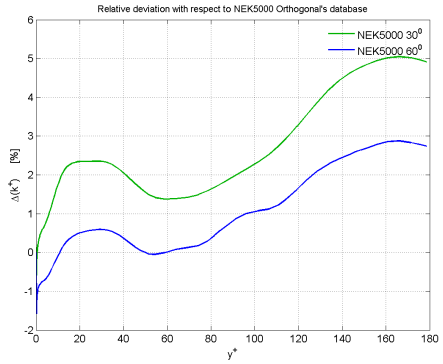

(e) Relative deviation of turbulent kinetic energy

Figure 7.3: Relative deviations of the mean velocity, RMS and turbulent kinetic energy profiles with respect to Vreman et. al.;*green:* NEK5000 small domain

7.3 Results and analysis

Table 7.1: Relative error $||\epsilon_\Psi(y)||_1$ in % with respect to NEK small domain-orthogonal

Database	Mean U	RMS u	RMS v	RMS w	k
NEK 30^0	0.1248	1.5862	0.39653	0.22275	2.2033
NEK 60^0	0.069046	0.62733	0.23995	0.081341	0.5733

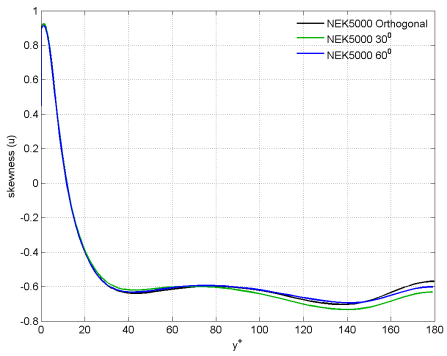

(a) Skewness in streamwise velocity fluctuations

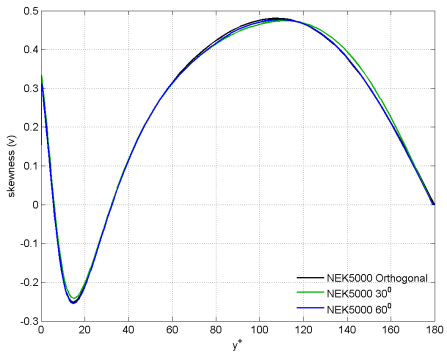

(b) Skewness in normal velocity fluctuations

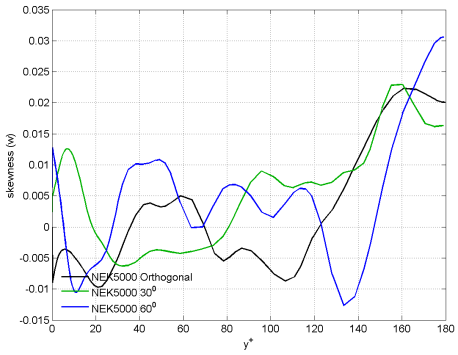

(c) Skewness in spanwise velocity fluctuations

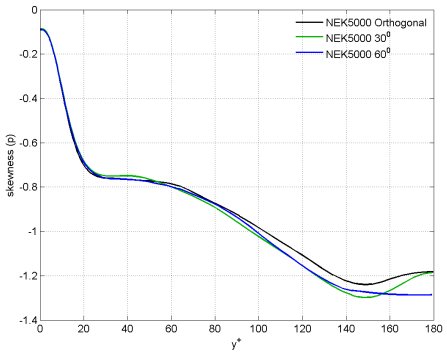

(d) Skewness in pressure fluctuations

Figure 7.4: Skewness of the velocity and pressure fluctuations; *black:* NEK5000 normal domain, *green:* NEK5000 small domain

Table 7.2: Relative error $||\epsilon_\Psi(y)||_1$ in % with respect to NEK small domain-orthogonal

Database	skew(u)	skew(v)	skew(w)	skew(p)
NEK 30^0	1.464	106.2566	116.522	0.0042598
NEK 60^0	0.098618	2.0792	94.2072	1.4041

Table 7.3: Relative error $||\epsilon_\Psi(y)||_1$ in % with respect to NEK small domain-orthogonal

Database	flatness(u)	flatness(v)	flatness(w)	flatness(p)
NEK 30^0	0.70003	1.8452	0.39198	0.96502
NEK 60^0	0.31498	0.61483	0.015522	1.131

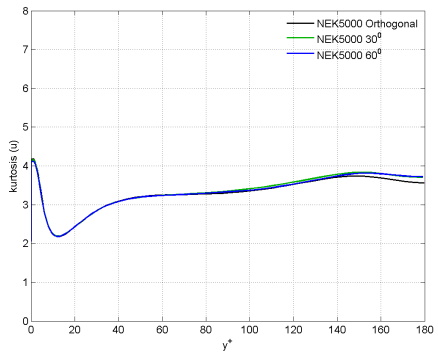

(a) Kurtosis in streamwise velocity fluctuations

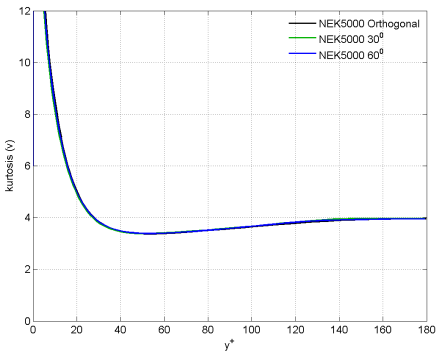

(b) Kurtosis in normal velocity fluctuations

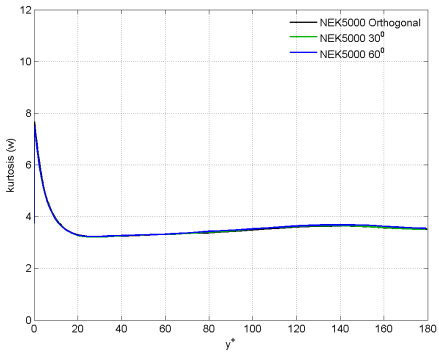

(c) Kurtosis in spanwise velocity fluctuations

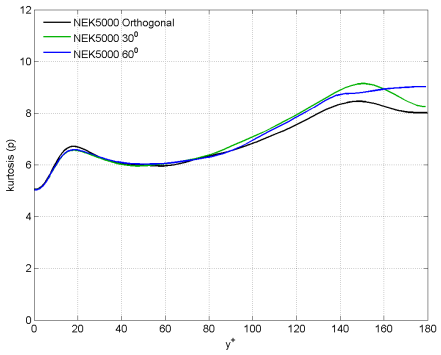

(d) Kurtosis in pressure fluctuations

Figure 7.5: Kurtosis/ flatness of the velocity and pressure fluctuations; *black:* NEK5000 normal domain, *green:* NEK5000 small domain

Table 7.4: Relative error $||\epsilon_\Psi(y)||_1$ of Reynolds stress $\overline{u'u'}$ budget terms in % with respect to NEK small domain-orthogonal

Database	Production	Dissipation	Press. Diff.	Press. Strain	Turb. Trans.	Vis. Diff
NEK 30^0	1.1469	0.066997	1.9222	0.21858	0.91794	1.9866
NEK 60^0	0.27869	0.085987	3.0061	0.050944	0.4854	0.89494

Table 7.5: Relative error $||\epsilon_\Psi(y)||_1$ of Reynolds stress $\overline{v'v'}$ budget terms in % with respect to NEK small domain-orthogonal

Database	Production	Dissipation	Press. Diff.	Press. Strain	Turb. Trans.	Vis. Diff
NEK 30^0	-	1.1734	4.4346	3.9854	11.0826	3.5027
NEK 60^0	-	0.61572	2.4208	2.8828	5.2566	9.4814

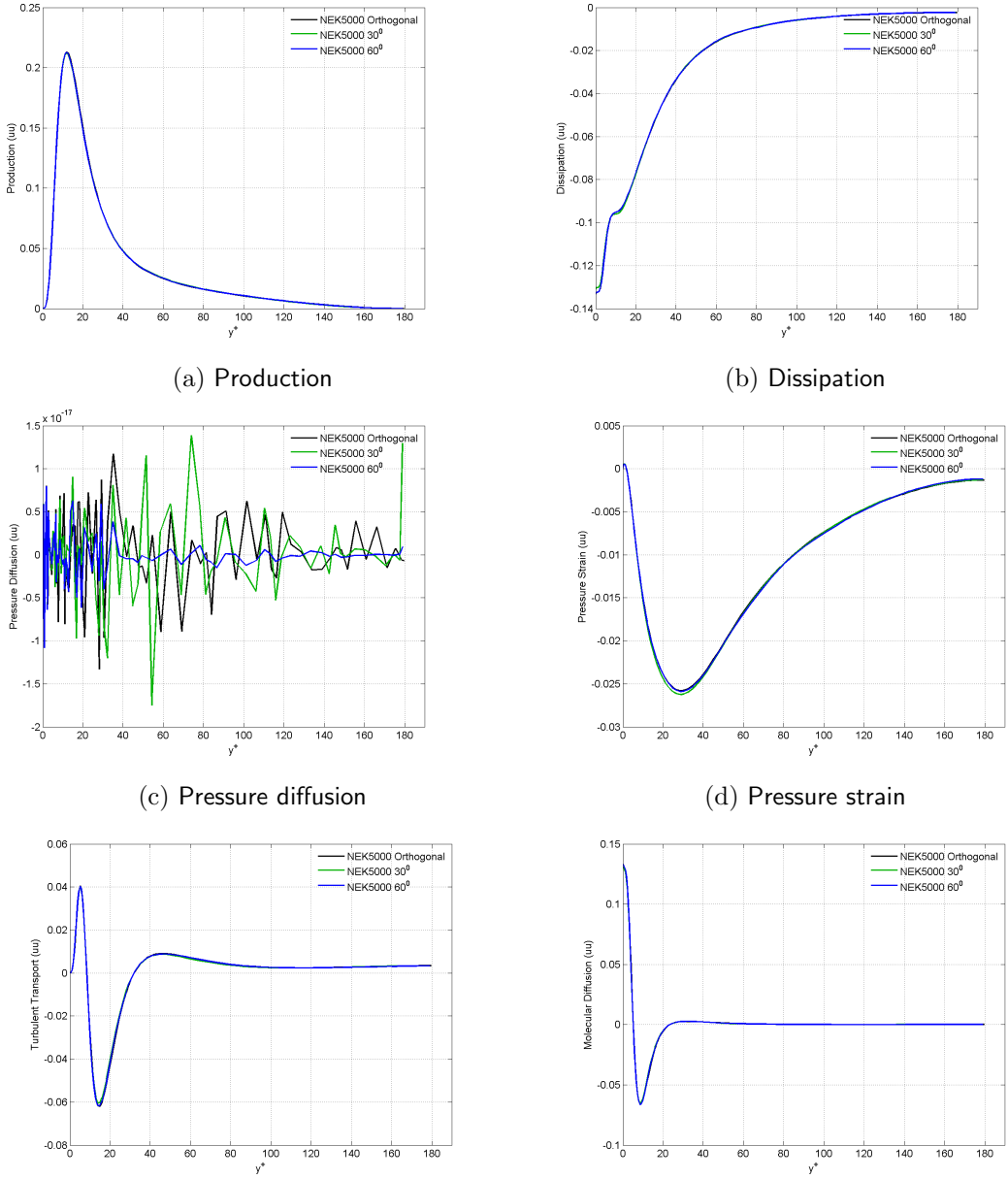

(a) Production

(b) Dissipation

(c) Pressure diffusion

(d) Pressure strain

(e) Turbulent transport

(f) Molecular diffusion

Figure 7.6: Budget quantities for the Reynolds stress term $\overline{u'u'}$; *black:* NEK5000 normal domain, *green:* NEK5000 small domain

Table 7.6: Relative error $||\epsilon_\Psi(y)||_1$ of Reynolds stress $\overline{w'w'}$ budget terms in % with respect to NEK small domain-orthogonal

Database	Production	Dissipation	Press. Diff.	Press. Strain	Turb. Trans.	Vis. Diff
NEK 30^0	29.2872	0.7476	12.7914	0.85492	13.261	9.6156
NEK 60^0	71.7801	0.73998	2.4729	0.43647	28.4029	10.9283

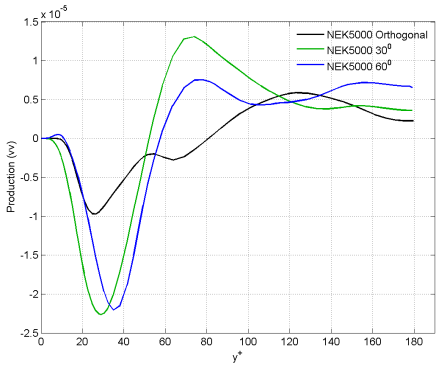

(a) Production

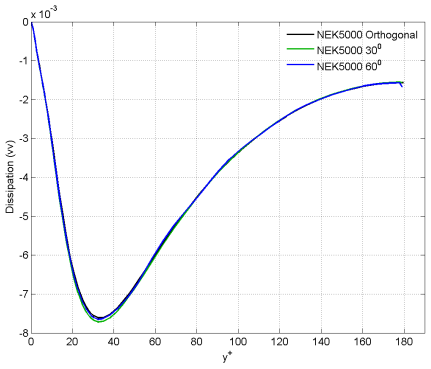

(b) Dissipation

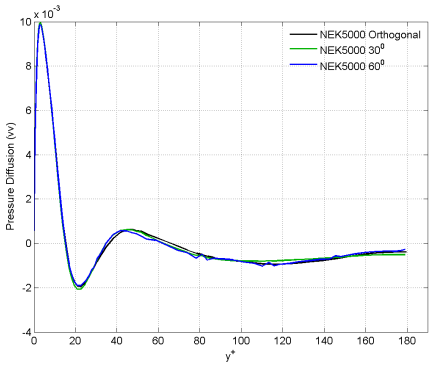

(c) Pressure diffusion

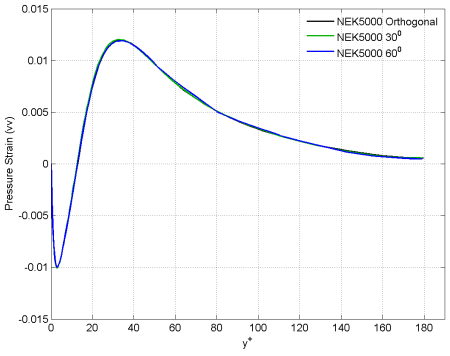

(d) Pressure strain

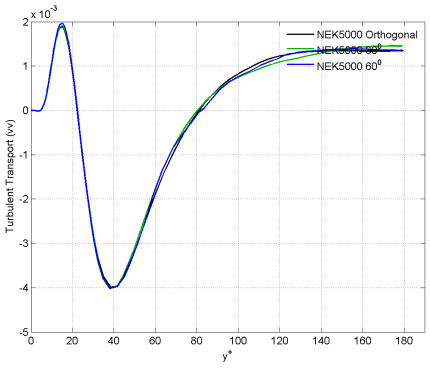

(e) Turbulent transport

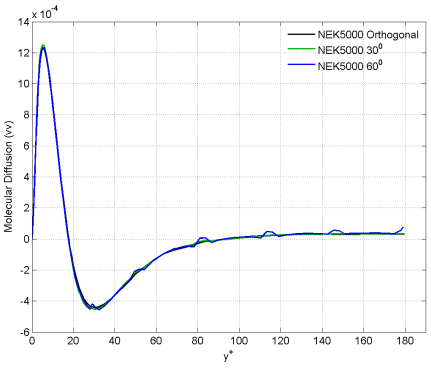

(f) Molecular diffusion

Figure 7.7: Budget quantities for the Reynolds stress term $\overline{v'v'}$; *black:* NEK5000 normal domain, *green:* NEK5000 small domain

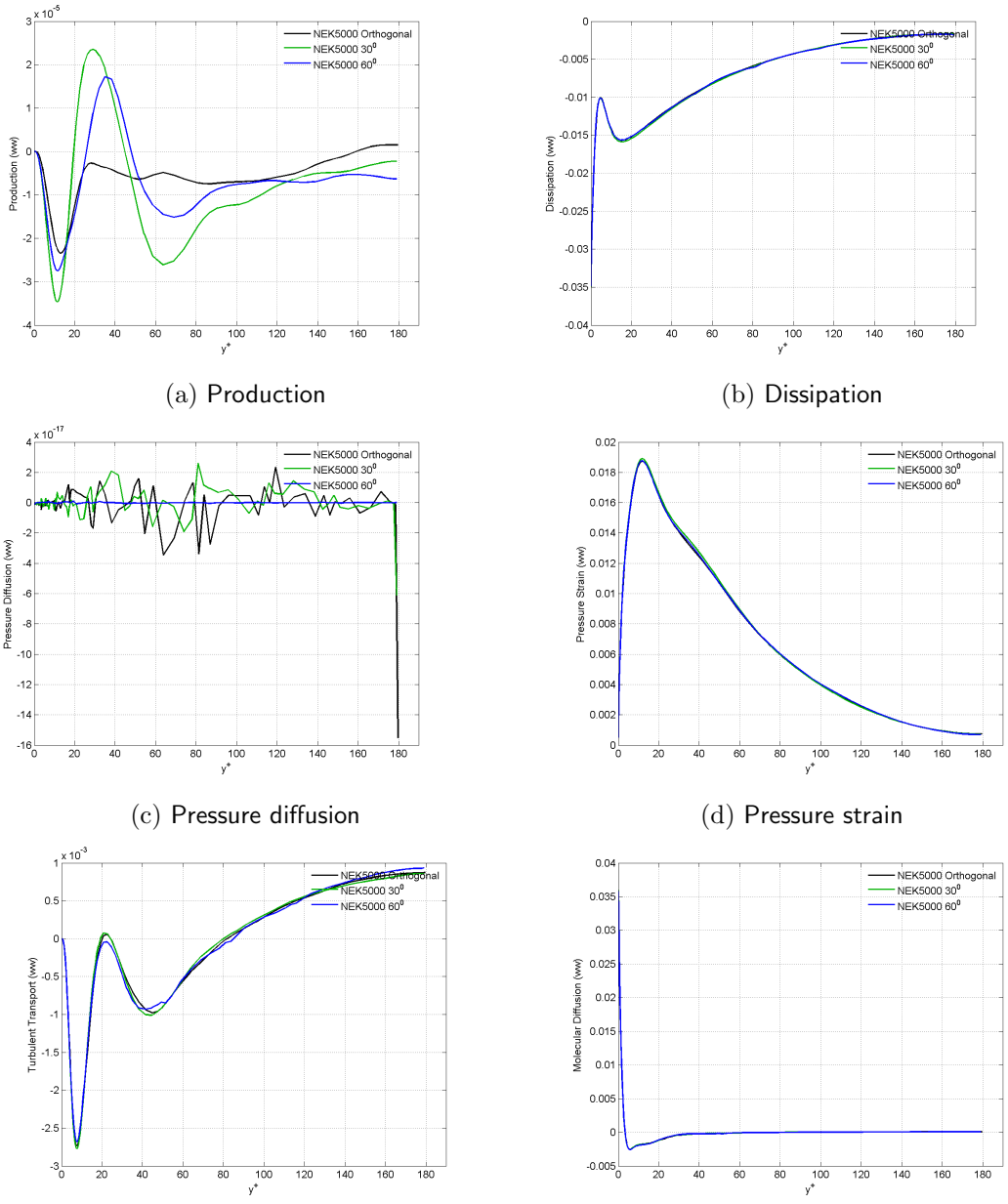

(a) Production

(b) Dissipation

(c) Pressure diffusion

(d) Pressure strain

(e) Turbulent transport

(f) Molecular diffusion

Figure 7.8: Budget quantities for the Reynolds stress term $\overline{w'w'}$; *black:* NEK5000 normal domain, *green:* NEK5000 small domain

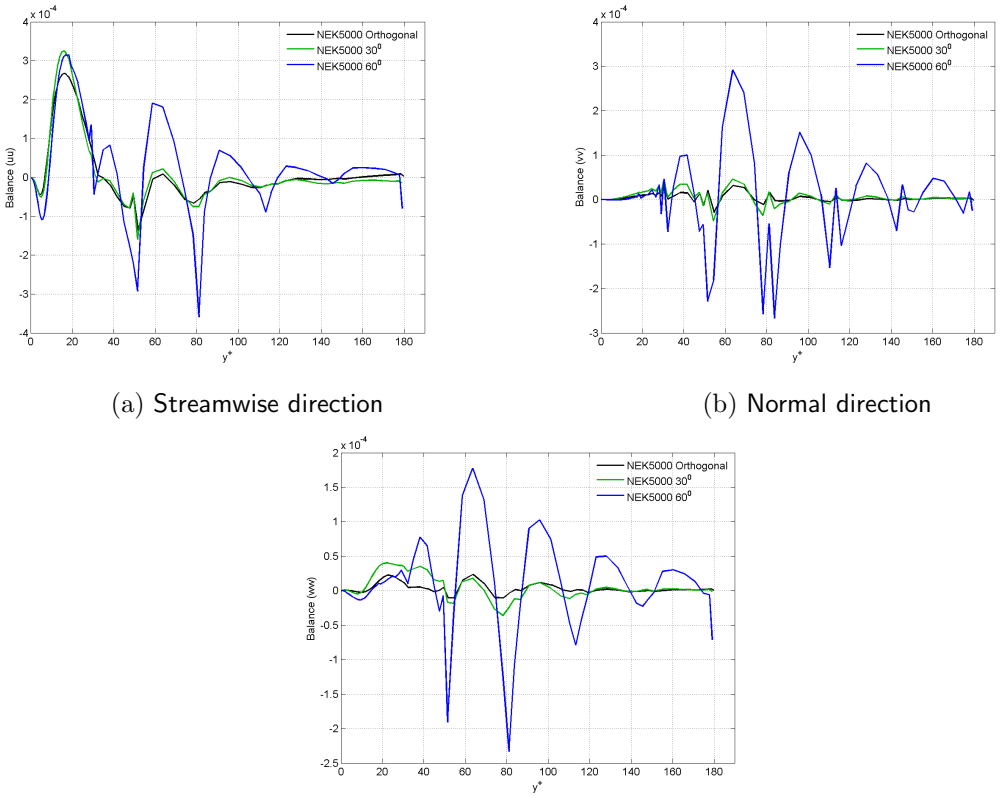

(a) Streamwise direction

(b) Normal direction

(c) Spanwise direction

Figure 7.9: Sum of the budget equation terms in the three coordinate directions; *black:* NEK5000 normal domain, *green:* NEK5000 small domain

The mean and the RMS of the velocity fluctuations for the distorted meshes, are in very good agreement with the orthogonal meshes. The discrepancies are seen for skewness in the spanwise direction but are mostly very small in terms of absolute values. The deciation in the results for the 30^0 and the 60^0, with respect to the orthogonal meshes are mostly comparable. This variation is seen in the figures for the Reynolds stresses.

7.4 Conclusions

The results of NEK5000 on sheared domains were compared to orthogonal domains and it was found that they are in good agreement. Thus we can conclude that NEK5000 may be used to produce high quality DNS results for the flow field for turbulent flows, with distortions and deviations upto 60^0.

Chapter 8

Assessment of NEK5000: Conjugate Heat Transfer

8.1 Objective

While the analysis of the fluid flow statistics and profiles forms an important part of the assessment of NEK5000, its capability to accurately and reliably predict the behavior of temperature fields and heat flow in a system is another equally important aspect. Since the intended application of the NEK solver is to compute a DNS quality database for the PTS scenario and to be able to use it as a reference for less expensive CFD computations, it is crucial that the solution of thermal fields in NEK5000 be very accurate. Therefore, a thorough assessment of the thermal solution capabilities in comparison with existing databases and, in case of presence of discrepancies, investigation of the possible reasons form the objectives for the research described in this chapter. The methodology adopted in achieving the objectives is outlined in the following sections.

8.2 Higher order assessment

In order to understand the solution capabilites of NEK5000 for thermal variables, a heat transfer simulation on a turbulent channel flow domain is conducted. To achieve DNS accuracy, a ninth order spectral element mesh is used on the *normal* domain. Insertion of artificial boundary conditions like isoflux (Neumann) or isothermal (dirichlet) boundary condition may not adequately describe the fluctuations and near wall phenomenon in the thermal field of the flow. Therefore to more accurately represent a realistic scenario, conjugate heat transfer boundary conditions are utilized. Also as discussed in chapter 3, NEK5000 deals with temperature as a passive scalar. This means that the value of the temperature does not affect the velocity or any other flow parameter. Thus the velocity and pressure can be computed independently of temperature and the energy and the Navier-Stokes (momentum) equation become decoupled. This reduces the complexity of

the solution and has the additional advantage that multiple passive transport scalars can be computed in the same simulation. For more details regarding the boundary conditions and literature on such a scenario, the reader may refer to chapter 3 on Turbulent Channel Flow and Conjugate Heat Transfer.

The configuration used for the conjugate heat transfer is shown in figure 8.1. For the governing equations and other details refer to section 3.2.

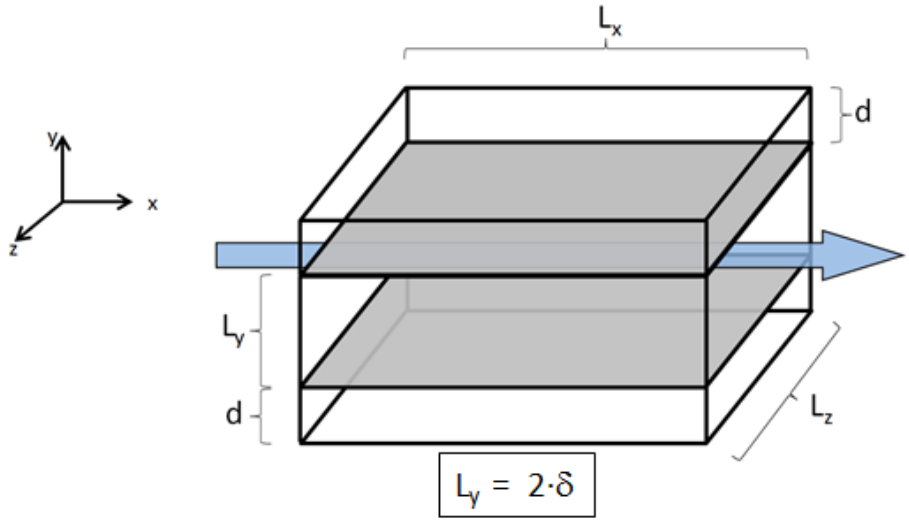

Figure 8.1: Conjugate Heat Transfer configuration

8.2.1 Definition of simulations

In order to be able to compare the temperature field solutions of NEK5000 without uncertainties about the involved flow field, the same setup of the simulation as discussed in section 5.2.2 is used. Two solid wall *boxes* are introduced to the configuration(as seen in figure 8.1) without affecting the flow-field (the boundary conditions of the fluid does not change). The mesh on the solid wall is set up mirroring the fluid mesh, so that this mesh is symmetrical to the fluid domain mesh about the wall-fluid interface. This serves the purpose of intensifying or damping effects at the interface.

As with the simulations with only the flow field computations (turbulent channel flow), the Re_τ is set to 180. The total grid count was 15.4 million grid points for each of the passive scalars, and 7.7 million grid points for the fluid only. The mesh grid spacing is given, in non-dimensional units as $(\Delta x^+, \Delta y^+_{wall} \rightarrow \Delta y^+_{center}, \Delta z^+) = (9.0, 0.28 \rightarrow 5.0, 4.5)$ Further details of the flow aspects of the simulation can be found by referring to the section 5.2.2. The thermal field in the entire domain is initialized with a uniform temperature. This temperature distribution evolves, due to the effect of the source and sink terms (in the fluid and solid respectively) and the turbulence of the flow itself. The simulation was performed on the Narodowe Centrum Badan Jadrowych (NCBJ) supercomputer in Poland, with 512 processors for a period of two months. Due to the demand of the computational capability, only two passive scalars were simulated, namely K = 1 and K

= 0.01 (although preliminary simulations were run for K = 10 case). Here, K indicates the ratio of thermal effusivities.

8.2.2 Results and analysis

The statistics of temperature are compared in the following discussion along with the data from the q-DNS by Komen et. al. [11] and Tiselj et. al. [21]. The database from C. Flageul et. al. is not used, as it is at a different Prandtl number. The temperature profiles for the mean are normalized after subtracting the wall temperature as follows:

$$\theta^+ = \frac{T - T_w}{T_\tau} \tag{8.1}$$

where the value of T_τ was given in section 3.2. This defines the value of θ^+_{wall} to be zero at the wall. The domain, in non-dimensionalized units, is given by $y^+ = 0$ at the wall to $y^+ = 180$ at the centerline of the fluid domain, and by $y^+ = 0$ at the wall interface to $y^+ = -180$ at the external wall boundary. The mean and RMS of the fluctuations of the temperature, higher order statistics: skewness and kurtosis and the turbulent heat flux terms are compared. Since the N = 9 simulation was conducted for K = 1 and K = 0.01, only these are presented here (refer figures **??** through 8.3).

All the databases are in excellent agreement for the mean temperature, for both K =1 and K = 0.01. With regards to the RMS, NEK5000 and Tiselj data agree only in the fluid domain, but deviation is seen in the solid domain. It can also be observed that this deviation is larger for K = 1 than K = 0.01. The q-DNS data is somewhat intermediate to the two other databases. Tiselj and NEK5000 agree quite well for the heat flux, and show a similar trend for the skewness. However for the kurtosis, large deviations are shown in between the databases. It can be observed that the skewness and kurtosis for both the databases have similar values in the wall vicinity, however near the cennter, NEK5000 overestimates the values. On the other hand, Tiselj et al. shows a constant kurtosis in the wall normal direction, which is only typical for a Gaussian distribution.

For the sake of completeness, RMS plots of temperature for the K = 10 case, with a coarser mesh of N = 3 is shown.

Despite excellent agreement in the flow related profiles, there are significant differences between Tiselj et al and NEK5000. These are already observable in the lower statistics such as RMS of the temperature profiles. The discrepancies seem to increase with increase in K, notwithstanding the averaging time. Therefore a further detailed analysis is carried out in order to understand the source of the discrepancies.

Intermediary conclusions

NEK5000 was used to compute the flow field and thermal fields in the conjugate heat transfer in a turbulent channel flow. The flow field results for such a configuration has shown excellent agreement in all results from lower to higher order statistics and turbulent kinetic energy budget terms. However with respect to the only other true DNS literature available on this simulation setup (Tiselj et. al [21]), shows some deviation. The deviations

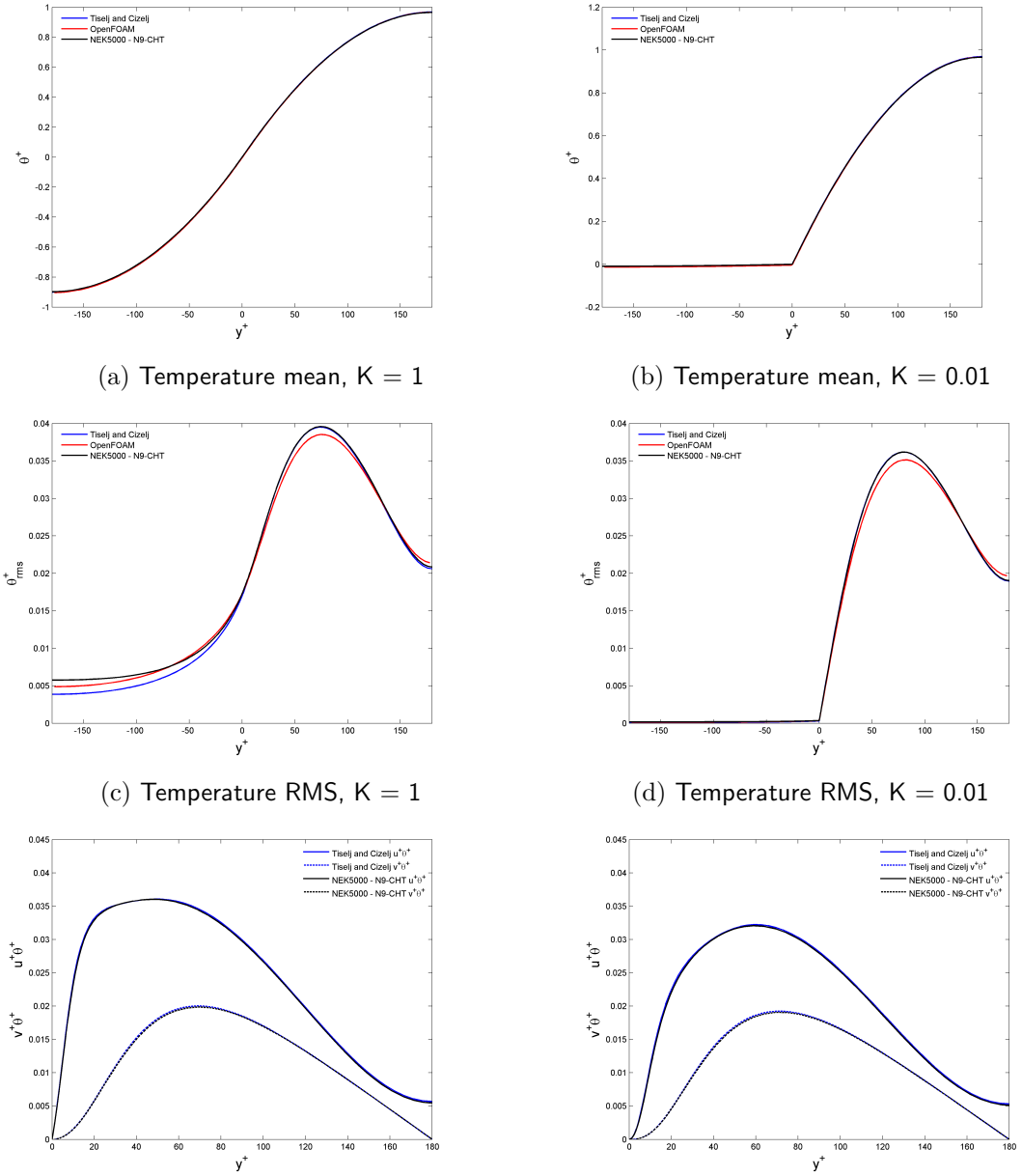

(a) Temperature mean, K = 1

(b) Temperature mean, K = 0.01

(c) Temperature RMS, K = 1

(d) Temperature RMS, K = 0.01

(e) Turbulent heat flux, K = 1

(f) Turbulent heat flux, K = 0.01

Figure 8.2: Mean, RMS of temperature fluctuations and Turbulent Heat Flux ($\overline{u^+\theta^+}$ and $\overline{v^+\theta^+}$) for two values of K = 1 and K = 0.01; *blue:* Tiselj et.al., *red:* OpenFOAM Komen et.al., *black:* NEK5000 9th order

are almost negligible for the mean temperature profiles, however are already noticeable to a significant degree in the RMS profiles. In the higher order statistics, there is no agreement between the two DNS databases. To understand this discrepancy, further simulations and analyses are necessary, which will form the next part of the objectives of the thesis research. This is explained in the subsequent sections.

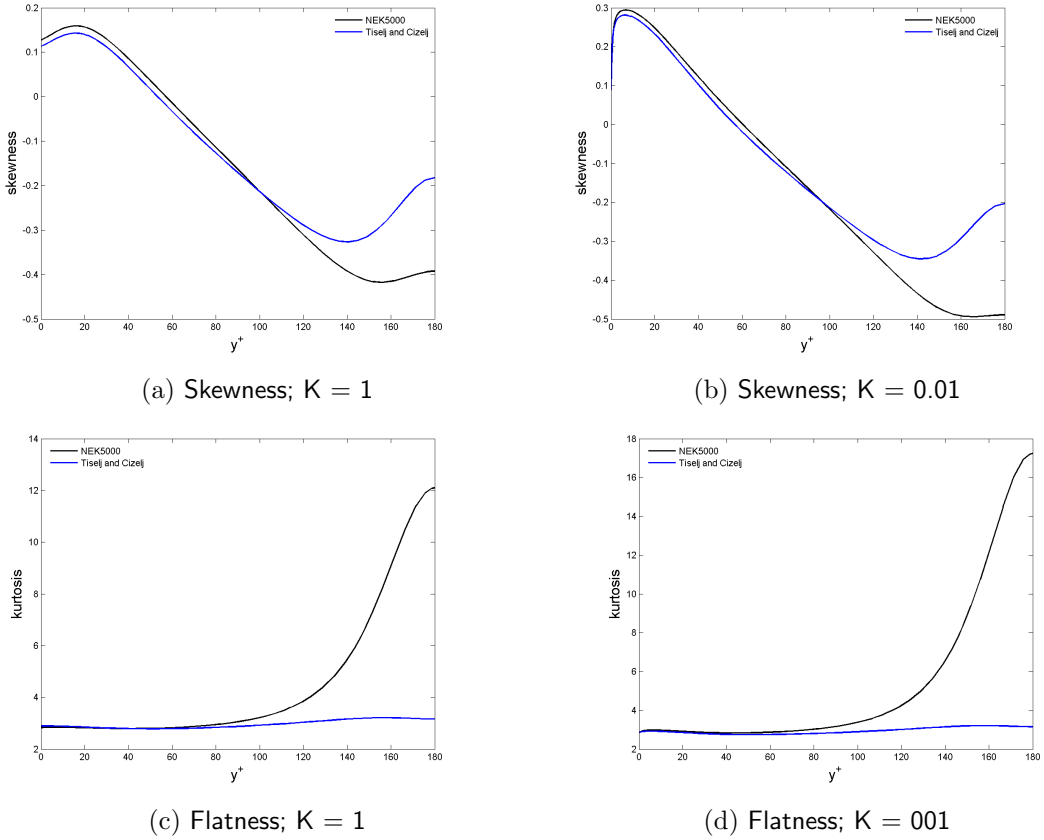

(a) Skewness; K = 1

(b) Skewness; K = 0.01

(c) Flatness; K = 1

(d) Flatness; K = 001

Figure 8.3: Skewness and flatness/kurtosis of the temperature fluctuations for K = 1 and K = 0.01; *black:* NEK5000, *blue:* Tiselj et.al.

8.3 Systematic analysis of discrepancies

There are several possible sources of error that could attribute to the differences in the results as explained in the previous sections. Such a factor would have to be different between the two DNS databases in consideration. To zero in on this factor, a detailed analysis has been conducted varying several parameters individually, maintaining the rest of the parameters a constant. The effect of these factors are all considered individually and certain important conclusions are drawn. The two simulation configurations (Tiselj et. al. and NEK5000) were considered and a range of such factors were listed, as given below.

- Effect of order of the simulation
- Effect of the domain size
- Effect of averaging time
- Effect of the start time of the averaging
- Effect of time step interval/ CFL

- Effect of the sample size of the post-processing (post-processing technique)
- Effect of numerical solution technique

For all these test simulations, fifth or third order spectral element discretization on the *small* domain has been employed in order to minimize the computational effort. Since the method of numerical solution by NEK5000 in solving the passive scalars is the same as that for the flow parameters, and since the latter has been extensively tested, as described in the previous chapters, this is not further tested at the moment. A step-by-step analyses is conducted to investigate the effect of the remaining reasons.

8.3.1 Effect of the order of the simulation

In spectral element solutions, every super-element consists of various points, each of which are involved in the solution process, and dictates the order of the solution. Seventh or ninth order simulations are necessary in NEK5000 to resolve all the necessary scales of turbulence (5.2). However running a ninth order simulation is costlier than a fifth order simulation by a factor of $9^3/5^3 \approx 6$ and is costlier than a third order simulation by a factor of $9^3/3^3 \approx 27$. This means that a simulation that would take five days for a third order simulation would take about 23 days for a fifth order resolution and more than four months (135 days) for ninth order! Therefore it is not practical to run a ninth order simulation for the purposes of analyzing discrepancies. Also, it was also known through experience and flow field simulations that a fifth or even third order simulation might be sufficient to sufficiently converge the lower order statistics. Therefore in order to scientifically test this, to be able to use this for future test simulations, the same case of the ninth order simulation as described in the previous section was conducted with third and fifth order resolution. Other simulation parameters were maintained the same. The results of the same are indicated in the figures.

It is seen in these figures 8.4 that the mean velocities for the various orders are almost perfectly coincidental for all the three orders of simulation. For the RMS of fluctuations of the temperature we can observe slight discrepancies, but the order of the difference is not very significant, especially compared to the difference with Tiselj et al as in figure **??**. Therefore it can be said that the order of simulation is not responsible for the discrepancy which we are attempting to investigate. Moreover this exercise also proves that it is enough to use fifth or even third order simulations to study the mean and RMS of fluctuations of temperature.

8.3.2 Effect of domain size

From figure 3.2, it was discussed that domain sizes in excess of $(L_x, L_y, L_z) = (2\pi\delta, 2\delta, \pi\delta)$, that we will now call the *small* domain, was sufficiently large to allow the two-point correlations near the ends be practically zero (practically uncorrelated). However since a lot of literature for the turbulent channel has been on the *normal* domain of $(L_x, L_y, L_z) = (4\pi\delta, 2\delta, (4/3)\pi\delta)$, that was chosen for the purposes of the turbulent channel flow and the higher order conjugate heat transfer simulation. However, the purposes of conducting multiple simulations, in order to reduce the computational cost, the use of a *small*

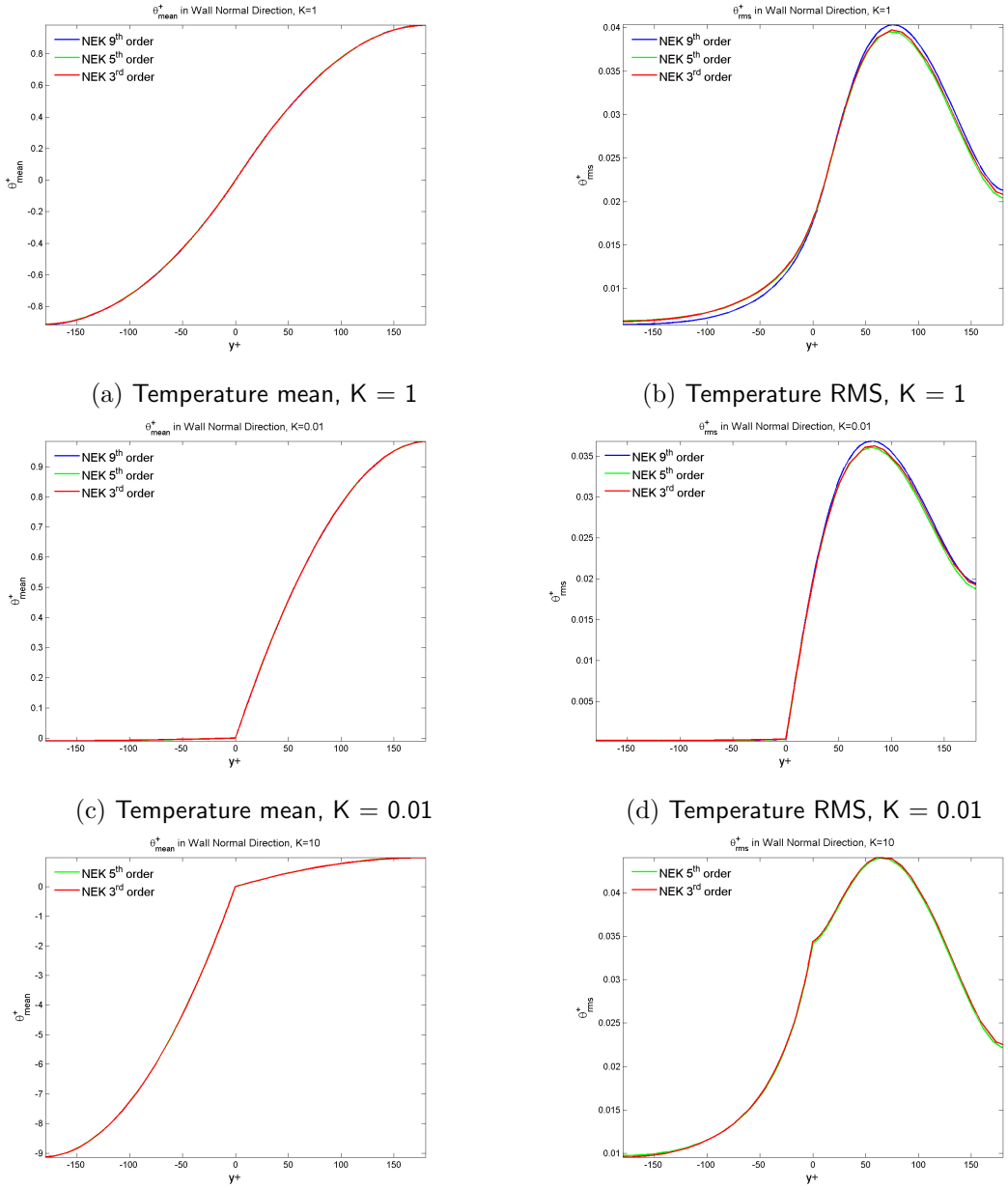

(a) Temperature mean, K = 1

(b) Temperature RMS, K = 1

(c) Temperature mean, K = 0.01

(d) Temperature RMS, K = 0.01

(e) Temperature mean, K = 10

(f) Temperature RMS, K = 10

Figure 8.4: Effect of order of simulation: Mean temperature and RMS of temperature fluctuations for various values of K = 1, 0.01 and 10; *blue:* NEK5000 9th order, *green:* NEK5000 5th order, *red:* NEK5000 3rd order

domain would be advantageous. A ninth order simulation on the *normal* domain with the discretization as described for the computations in section 8.2 would consist of 15 million points, while that on the *small* domain would only have 5.6 million points for a single field. If temperature and multiple passive scalar fields are used, this would further increase the computational cost gap. Therefore simulations on the small domain was desirable. However in order to ensure that the change of domain does not impact the

results, a thorough assessment of the differences in the results between the large and the small domain was conducted.

The results are discussed in this section. The mean velocities for all the three values of K used indicate a very good agreement and practically converge to each other (not shown here). There is good agreement for the RMS of temperature fluctuations as well, especially for K = 0.01. The discrepancy is slightly more for the values of K = 1 and 10, however is still well within acceptable limits (see figure 8.5). On the basis of this, we can conclude that the domain size is not significant, especially for the mean and RMS statistics, and can be used for the investigation of the discrepancies.

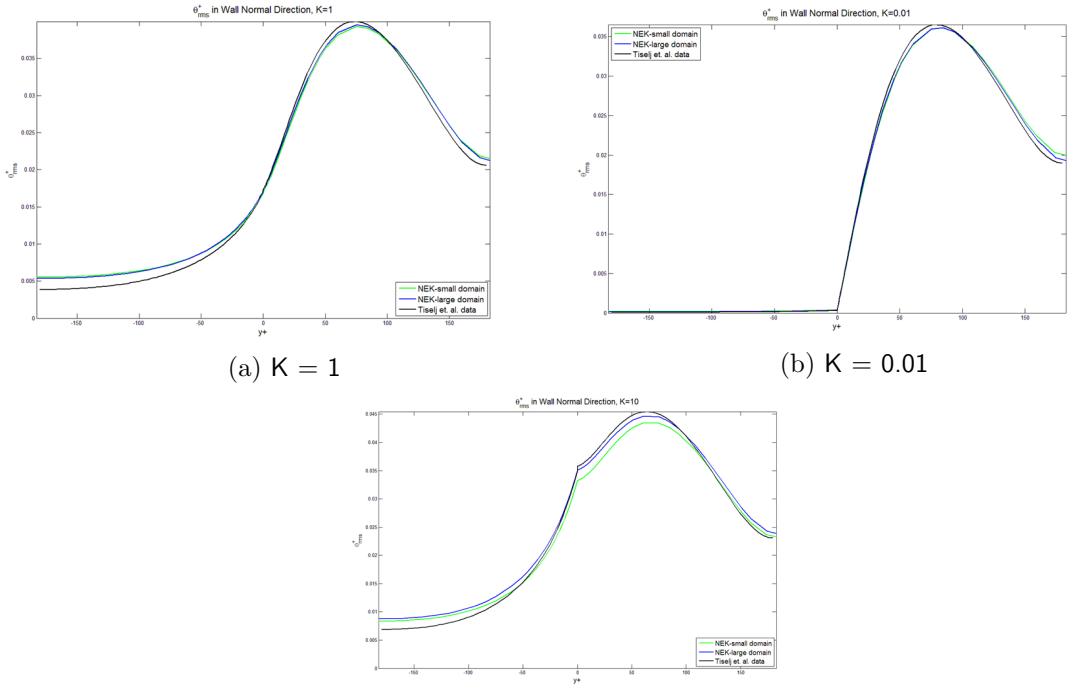

(a) K = 1

(b) K = 0.01

(c) K = 10

Figure 8.5: Effect of domain size: RMS of temperature fluctuation profiles for various values of K = 1, 0.01 and 10; *green:* Small domain, *blue:* Normal domain, *black:* Tiselj et.al.

8.3.3 Effect of averaging time and different start-times

The averaging time could be an important parameter, contributing to the accuracy of the results. Insufficient averaging time implies insufficient statistical samples in order to converge the statistics. Thus the goal of this particular exercise was to understand the effect of the averaging.

Even though it has been found for flow field simulations of the turbulent channel flow, that an averaging time over $\Delta t_a^+ vg = 9000$ is sufficient for averaging, it was necessary to verify that this was also the case in the solution of thermal fields for conjugate heat transfer. To understand the effect of this, two fifth order simulations were conducted with

all parameters other than averaging time the same. The statistics were computed for two separate averaging durations: $\Delta t_a^+ vg = 8000$ and $\Delta t_a^+ vg = 18000$.

Moreover, further simulations were conducted with different start times of the statistical averaging to understand if this had any effect. Since the boundary layers has to be fully developed before the flow can become statistically stationary, the start time could have an impact on the resultant statistics. Therefore two simulations with similar averaging times, but different start-times-for-integration of $t^+_{start} = 2300$ and $t^+_{start} = 15000$ were computed. The latter simulation was run for a total length of $t^+ = 25000$. Further to understand the evolution of temperature fields with time at various locations in the domain, several temperature monitors were placed in the numerical domain to record instantaneous temperatures. The results of this are shown in figure 8.7. It can be seen from this figure that the temperature fields seem to approach statistical steadiness quite early, somewhere around $t^+ = 1000$ (in the figures, time is represented in seconds. Non-dimensional time t^+ is given by $t^+ = tu_\tau^2/\nu$, which works out in this simulation to be $t^+ = 11.52t$). The statistics computed in each of these simulations agree very with each other (only the plots for different start times are given due to lack of space) and it could be concluded that the averaging times are not the reason for the discrepancy as well.

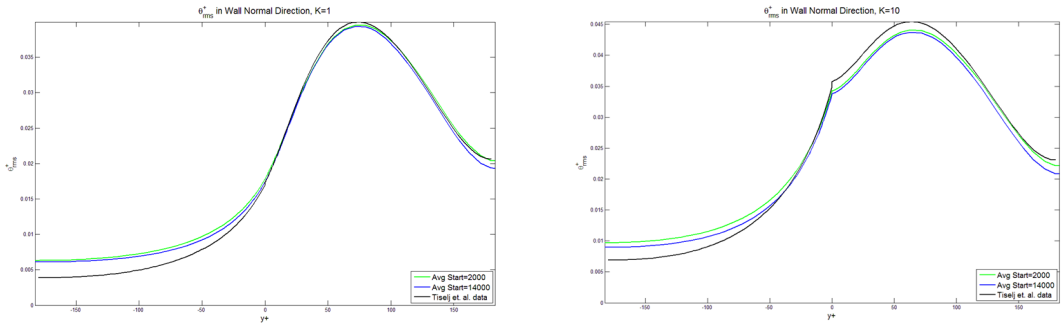

(a) K = 1 (b) K = 10

Figure 8.6: Effect of averaging start time: RMS of temperature fluctuation profiles for K = 1 and K = 10; *green:* $t^+_{start} = 2000$, *blue:* $t^+_{start} = 14000$, *black:* Tiselj et.al.

8.3.4 Effect of time step interval/ CFL

Several simulations were run on coarser grids, varying the time step in each to achieve different values of CFL numbers from 0.05 through 0.5, and the results are compared with Tiselj et. al. This is shown in figure 8.8

8.3.5 Effect of post-processing method (statistical sampling)

The start time for the collection of the samples and the quantity of samples collected from the simulation in order to perform the averaging could be important parameters which define the results obtained. Tiselj et. al [21] uses a post-processing method that involves collection of instantaneous field files at various time instants, and then using Python scripts performs an averaging operation of the collected samples. However, this

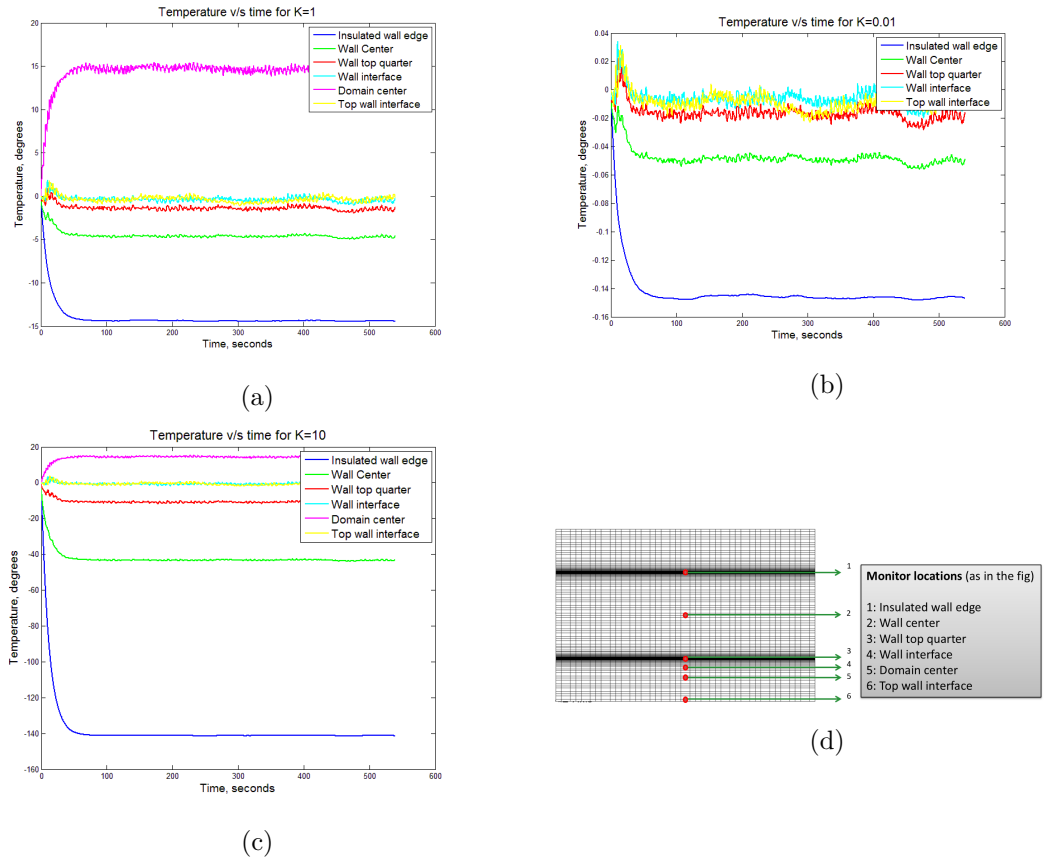

Figure 8.7: Evolution of instantaneous temperature profiles at various locations in the fluid and solid domains as indicated in part 8.7d

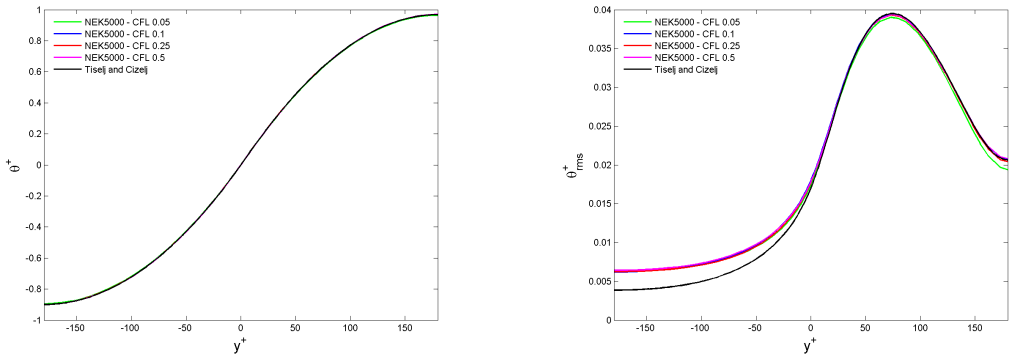

Figure 8.8: Effect of CFL/time step interval: Mean and RMS of temperature fluctuation profiles at K = 1 and various values of CFL; *black:* Tiselj et.al.

has the disadvantage that due to the bulk of the field files, the number of field files that can be collected can be limited. Indeed, in their simulation only 300 fields are captured for averaging, which could be an insufficient number with an impact on the results. To understand if this is actually the case, simulations were run on the small domain, with

various averaging methods as follows:

Simulation nr.	Averaging start time	Sample size	Sampling frequency	Remarks
1.	$t^+ = 2000$	300	30 time steps	Same starting time as NEK 9th order
2.	$t^+ = 2000$	1500	10 time steps	Same starting time as NEK 9th order
3.	$t^+ = 2000$	5000	1 time step	**Same starting time *and* sample size as NEK 9th order**
4.	$t^+ = 9000$	300	30 time steps	**Same starting time *and* sample size as Tiselj et. al.**
5.	$t^+ = 9000$	1500	10 time steps	Same starting time as Tiselj et. al.
6.	$t^+ = 9000$	15000	1 time step	Same starting time as Tiselj et. al.

In practice a few of these were computed with multiple averaging scripts in a single simulation to reduce computational demand. The results for these are presented in figure 8.9. The means for all the K values and the RMS for K = 0.01 practically collapse together. Only the RMS of the temperature fluctuations are shown, as only these displayed even the slightest discrepancy. It is evident from the figures that the order of difference of even the is much lesser than the Tiselj et. al. that we can conclude that the discrepancy between the databases is not due to this cause.

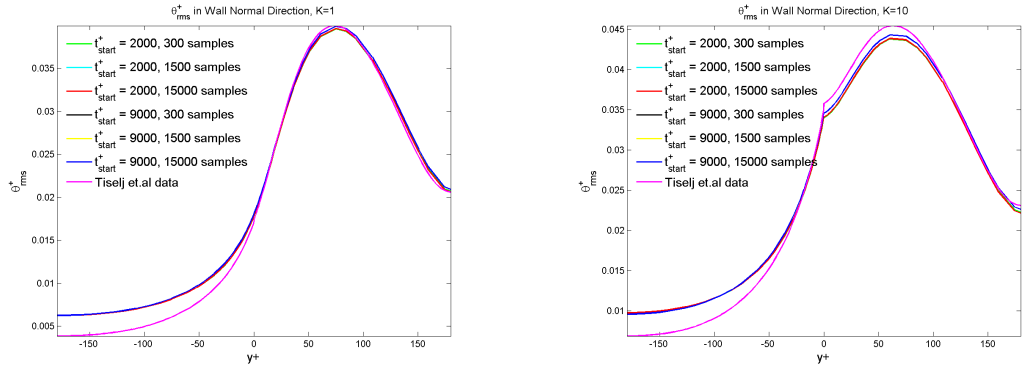

(a) RMS for K = 1 (b) RMS for K = 10

Figure 8.9: Effect of sampling size and frequency: RMS of temperature fluctuation profiles for K = 1 and 10; *magenta:* Tiselj et.al.

8.4 Conclusions

Ninth order DNS was conducted on the conjugate heat transfer for the turbulent channel flow domain on NEK5000 for different values of the effusivity ratio K (K = 1 and 0.01). The results were compared to Tiselj et.al and the quasi-DNS of Komen et.al. There was

excellent agreement in the mean profiles of the temperature. For the RMS of the temperature fluctuations for K = 0.01, there was some discrepancy, but for K = 1 and K = 10 (run with coarser meshes) there were significant discrepancies between the NEK5000 and the Tiselj et.al. RMS temperature profiles. For the skewness and kurtosis, no agreement was seen at all between these databases.

To understand these discrepancies, several lower-order simulations were conducted to systematically search and locate the source of the discrepancies. Several factors were considered, including the averaging duration, sampling size and frequency and CFL. However in spite of exhaustive simulations and analysis of the results, it was found that the source of the discrepancy could not be any of these analyzed parameters. The differences in between the computational methods of the two databases needs to be analyzed and other sources of discrepancies investigated, possibly in conjunction between the researchers.

Chapter 9

Conclusions and future work

The enhancement of safety of nuclear reactors requires the continual prediction and analysis of possibilities of threats. The analysis of Pressurized Thermal Shocks (PTS), a transient that poses significant threat to the integrity assessment of nuclear reactors, therefore can be seen as a very vital area of research. Due to the difficulty of obtaining experimental data for such extreme phenomenon, there remains a need for reliable references to validate CFD codes that are used to simulate such conditions. Thus the presence of suitable DNS data for similar (or simplified) scenarios presents a vital need.

Towards the creation of such a DNS database for simplified PTS scenarios, the spectral element solver NEK5000 has been chosen, due to its accuracy and scalability. However before the solver is used for the use of such a computation, there is a need to assess its accuracy.

The present thesis work was aimed at systematically setting up and achieving objectives that would holistically prove the reliance of the solver in the aforementioned scenarios. The objectives of the conducted research, and the conclusions gained from such research are discussed below.

- **Assessment of NEK5000 DNS on an incompressible turbulent channel flow**: 9th order fully resolved DNS was run on the normal domain of the turbulent channel. The results for the flow field variables, consisting of lower and higher order velocity and pressure statistics, and Reynolds stress budget terms agreed very well with the reference. *It can be concluded that the NEK5000 can produce reliable and accurate results for turbulent incompressible flow fields.*

- **Assessment of NEK5000 DNS on turbulent channels with distorted domains and mesh elements:** NEK5000 DNS was performed on distorted mesh grids with 30^0 and 60^0 shear in the mesh respectively. From the results, it was concluded that *NEK5000 can perform reliable and accurate computations on distorted elements and domains (verified up to* 60^0*).*

- **Assessment of NEK5000 DNS on conjugate heat transfer analysis for a turbulent channel flow:** NEK5000 was used to compute passive temperature fields on conjugate solid and fluid domains, intended to capture the realistic thermal interactions. Even though the mean of temperature fields matched well with the *one* other DNS database for the given Prandtl number, the RMS of the temperature fluctuations indicated recognizable deviation, while the higher order statistics of temperature fluctuations showed little agreement with the reference. An extensive analysis through the use of multiple simulations was conducted to isolate the source of the differences. However, all the sources of discrepancies postulated and tested did not prove to be the source of errors.

9.1 Future research

It is said that every good question asked, leads to more good questions than answers. Research, in my belief, can be quite similar. Even though all of the set objectives at the beginning of the thesis, were accomplished, it was found that given additional time or computational resources, many more investigations would have been possible. Some of the possibilities for such investigations are briefly discussed here:

- In the analysis of sources of discrepancies for conjugate heat transfer, the effect of the forcing term (to drive the flow) on the thermal field was not analyzed due to the lack of time. This remains one of the only possibilities for sources of differences, and could be investigated.
- Turbulent heat flux budget (similar to the Reynolds stress budget terms) can be evaluated for conjugate heat transfer. The post-processing tool for this for NEK5000 was also developed during the time of this thesis, but due to lack of time, could not be tested.
- Effect of mesh distortion on thermal fields can be evaluated.

9.2 Publications

The contents of this work will be partially published in two papers:

- A.Shams, P.M.K.Prasad, E.M.J Komen, *Towards the Direct Numerical Simulation of simplified Pressurized Thermal Shock*,(Under review) ERCOFTAC Direct and Large-Eddy Simulation (DLES) 11
- P.M.K.Prasad, A.Shams, E.M.J Komen, *Assessment of NEK5000 to perform a DNS of a single phase Pressurized Thermal Shock*, (Under review), 17th International Topical Meeting on Nuclear Reactor Thermal-Hydraulics (NURETH-17).

References

[1] *A first course in turbulence.*

[2] Cfd course notes, s j hulshoff, tu delft. US NRC http://www.nrc.gov/.

[3] Nuclear energy institute. http://www.nei.org.

[4] Standard review plan for the review of safety analysis reports for nuclear power plants: Lwr edition. US NRC http://www.nrc.gov/.

[5] World nuclear association. http://www.world-nuclear.org.

[6] World energy outlook, 2015.

[7] D. Rosa E.M.J. Komen A. Shams, G. Damiani. Design of a single-phase pts numerical experiment for a reference direct numerical simulation. *Nuclear Engineering and Design*, 300: 282296, 2015.

[8] R.B. Dean. Reynolds number dependence of skin friction and other bulk flow variables in two-dimensional rectangular duct flow. *Journal of Fluids Engineering*, 100:215, 1978.

[9] J. C. del Alamo and J. Jimenez. Spectra of the very large anisotropic scales in turbulent channels. *Physics of Fluids*, 15,L41L43, 2003.

[10] H. Eckelmann. Turbulence statistics in fully developed channel low at low reynolds number. *Journal of Fluid Mechanics*, 65, 439, 1974.

[11] Leonardo Camilo Barry Koren Ed Komen, Afaque Shams. Quasi-dns capabilities of openfoam for different mesh types. *Computers and Fluids*, 96(1):1–18, March 2014.

[12] P.F. Fischer. An overlapping schwarz method for spectral element solution of the incompressible navier-stokes equations. *Journal of Computational Physics*, (1), 1997.

[13] S. Hoyas and J. Jimenez. Reynolds number effects on the reynolds-stress budgets in turbulent channels. *Physics of Fluids*, 20, 2008.

[14] Borut Mavko Iztok Tiselj, Robert Bergant and Ivan Bajsic. Dns of turbulent heat transfer in channel flow with heat conduction in the solid wall. *Journal of Heat Transfer*, 2012.

[15] P. Moin J. Kim and R. Moser. Turbulence statistics in fully developed channel low at low reynolds number. *Journal of Fluid Mechanics*, 177:133-166(1), 1987.

[16] Shnel T. Rohde U. Hhne T. Prasser H.M. Weiss F.P. Kliem, S. Experiments at the mixing test facility rocom for benchmarking of cfd codes. *Nuclear Engineering and Design*, 238, 566576., 2008.

[17] P. Moin and K. Mahesh. Direct numerical simulation: A tool in turbulence research. *Annual review of fluid mechanics*, 30(1):539578(1), 1998.

[18] A. Toutant R. Monod, G. Brillant and F. Bataille. Dimensionless equations for conjugate heat transfer. *International Communications in Heat and Mass Transfer*, 2012.

[19] John Kim Robert D. Moser and Nagi N. Mansour. Direct numerical simulation of turbulent channel flow up to re =590. *Physics of Fluids*, 11,943, 1999.

[20] Hhne T. Kliem S. Hemstrm B. Scheuerer M. Toppila T. Aszodi A. Boros I. Farkas I. Mhlbauer P. Vyskocil L. Klepac J. Remis J. Dury T Rohde, U. Fluid mixing and flow distribution in a primary circuit of a nuclearpressurized water reactorvalidation of cfd codes. *Nuclear Engineering and Design*, 237,16391655.

[21] Iztok Tiselj and Leon Cizelj. Dns of turbulent channel flow with conjugate heat transfer at prandtl number 0.01. *Nuclear Engineering and Design*, 2012.

[22] A.W. Vreman and J.G.M. Kuerten. Comparison of direct numerical simulation databases of turbulent channel flow at $re_\tau = 180$. *Physics of Fluids*, 26, 015102, 2014.